nature portfolio

https://doi.org/10.1038/s41586-025-09570-2

Supplementary information

Heat-rechargeable computation in DNA logic circuits and neural networks

In the format provided by the authors and unedited

Heat-rechargeable computation in DNA logic circuits and neural networks

Supplementary information

Tianqi Song and Lulu Qian*

Contents

1 Materials and methods

1.1 Sequence design

A sequence design consideration for improving the performance of the logic circuits was to reduce toehold occlusion on the threshold molecules (Fig. S1). Because the mechanism of thresholding relies on the signal to react with the threshold much faster than it reacts with the restoration gate, the toehold on the threshold is longer. A longer toehold also means worse occlusion, especially via reversible binding to the fuel strands. In previous work,[1] for reducing undesired leak reactions between gates, a common clamp sequence was utilized at both the 5' and 3' of all long domains, and all toeholds on gates and thresholds were extended to include the clamp. Here, to reduce toehold occlusion on thresholds, we used two distinct clamp sequences (highlighted with gray and orange bars in Fig. S1) in all long domains associated with a hairpin gate (e.g. domain S4 on gate $G_{4,5}$). Thus, the clamp next to the toehold on a fuel strand (e.g. F_4) is different from the clamp within the open toehold on a threshold (e.g. $Th_{3,4}$), reducing the binding strength of occlusion from 7−10 base pairs to just 5 base pairs. As a result, thresholds become more available and thus perform better in large circuits.

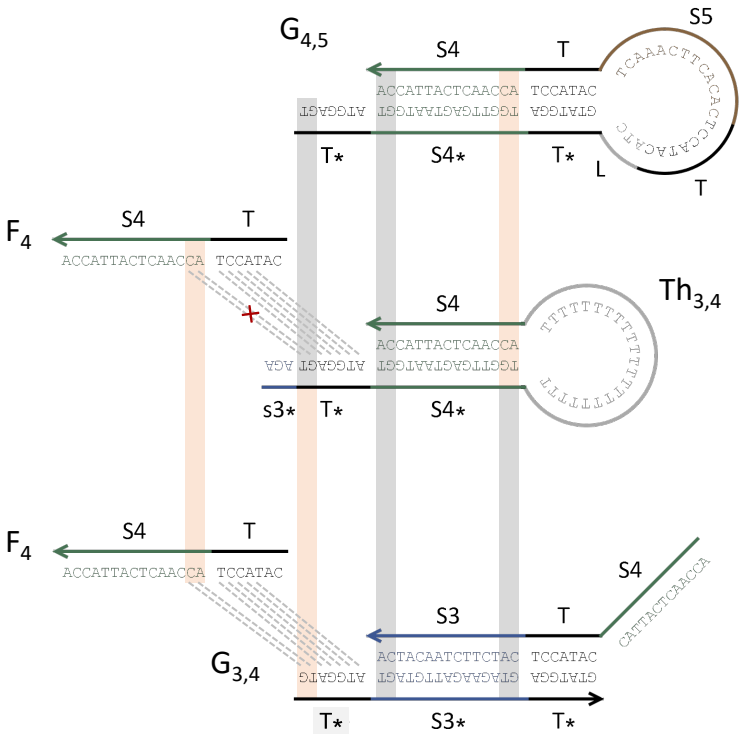

Fig. S1 | Sequence design criterion for reducing toehold occlusion in threshold molecules. Orange and gray bars highlight two distinct clamp sequences (AC at the 5' end and CA at the 3' end of domain S4 on hairpin gate $G_{4,5}$). Dashed lines indicate matching base pairs, whereas dashed lines with a red cross indicate mismatching base pairs. The occlusion between a fuel strand (F_4) and a threshold ($Th_{3,4}$) is reduced from 7−10 base pairs (depending on the similarity between sequences of the S3 and S4 domains, which will vary in a large circuit) to 5 base pairs, whereas the occlusion between a fuel strand and a two-stranded summation gate ($G_{3,4}$) remains unchanged at 7 base pairs.

1.2 Fluorescence kinetics experiments

The parallel procedure is illustrated in Fig. S2 and described as follows. For n rounds of computation, a sample that contains the circuit but no input is prepared (step 1) and distributed into n test tubes (step 2). Suppose each round of computation takes t hours. At time 0, the first input combination (e.g. five input strands composing a pattern L for testing the 9-bit neural network shown in Extended Data Fig. 8) will be added to the n-th test tube. At time t, the n-th test tube will be reset by adding input inhibitors of the same amount as the previous input strands, heating to 95 °C for five minutes, cooling to 20 °C in one minute, and staying at 20 °C for three minutes. The

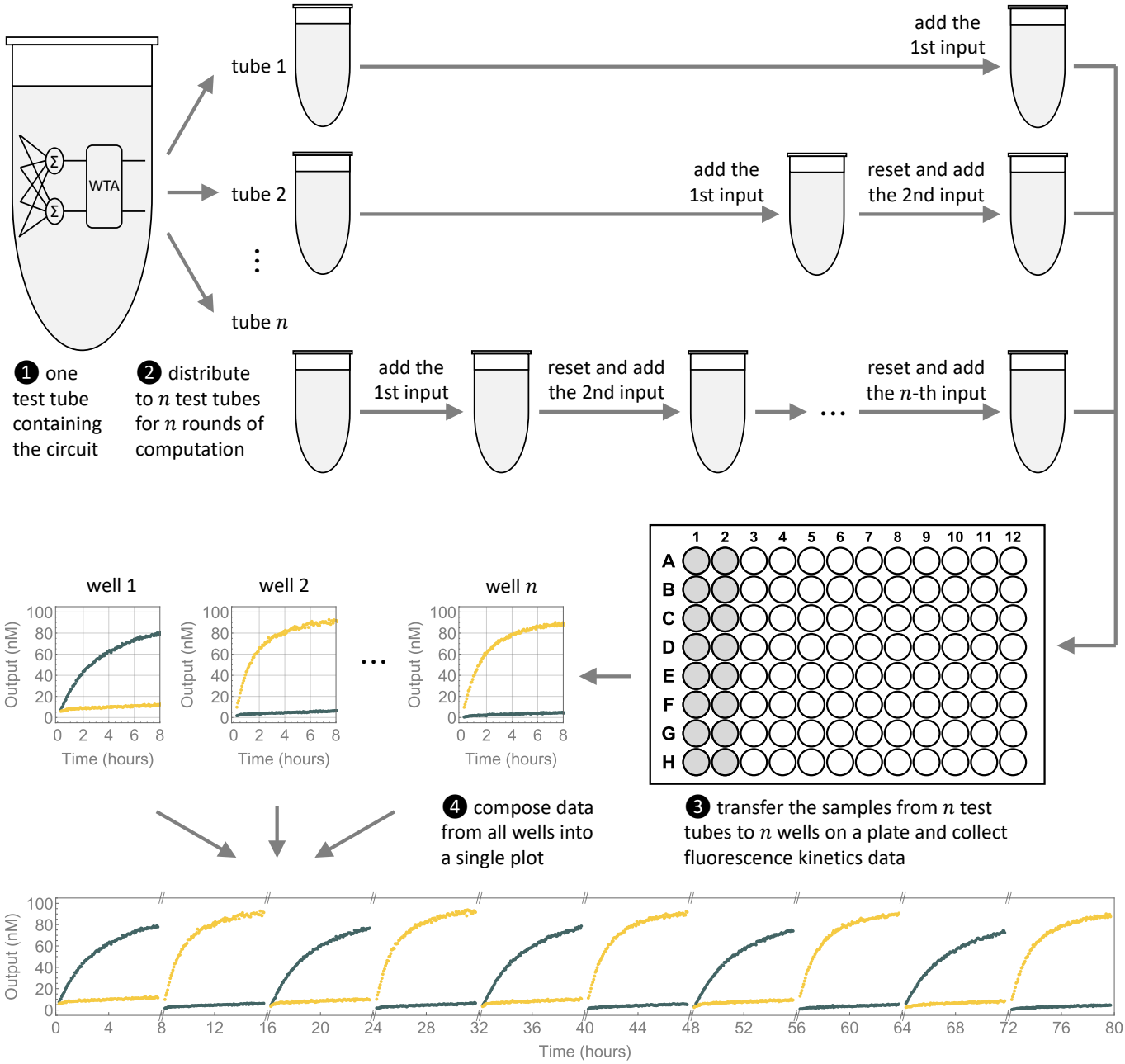

Fig. S2 | Procedure for efficient data collection using parallel samples.

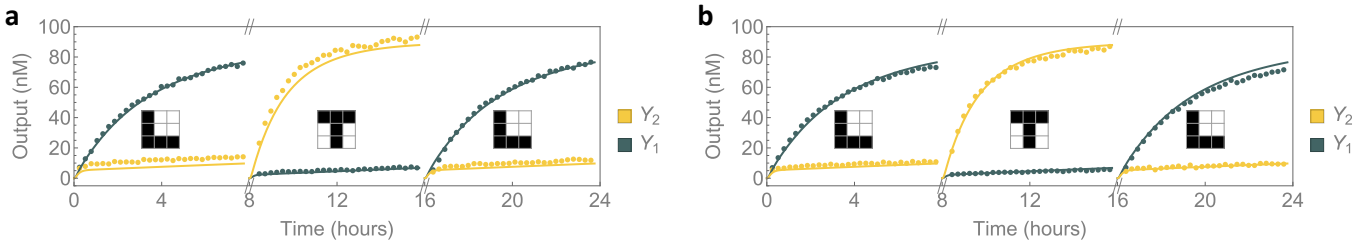

Fig. S3 | Evaluation of the wait time between resets. a,b, Simulations and fluorescence kinetics experiments of a 9-bit, two-memory winner-take-all neural network with alternating test patterns for three rounds of computation, with (**a**) and without (**b**) a 20-hour wait between resets.

second input combination will then be added to the n-th test tube while the first input combination will be added to the $(n-1)$-th test tube. At time $2t$, the n-th and $(n-1)$-th test tubes will be reset and the third, second, and first input combinations will be added to the n-th, $(n-1)$-th, and $(n-2)$-th test tubes, respectively. The same process repeats until time $(n-1)t$, when the first input is added to the first test tube and all other test tubes are reset with the i-th input added to the i-th test tube, where $i = 2$ to n. All samples will then be immediately transferred to n wells on

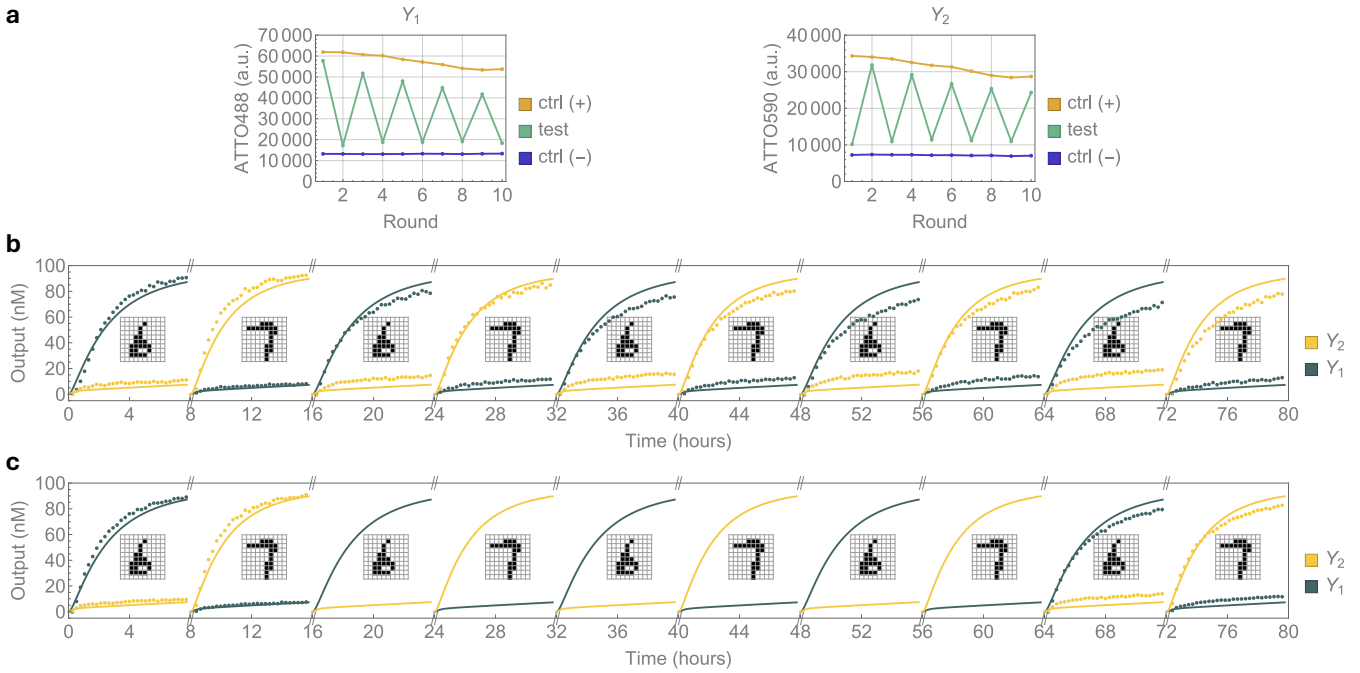

Fig. S4 | Comparing a single-sample procedure with parallel samples. a, Raw fluorescence data of a 100-bit, two-memory winner-take-all neural network with alternating test patterns for ten rounds of computation. The measurements are shown for a pair of output signals in two fluorescence channels (ATTO488 and ATTO590) at 8 hours after each subsequent test was added. Positive and negative control experiments were performed along with the test, where a trigger strand to the output gate in the neural network was added as a positive control, whereas the neural network without any inputs was used as a negative control. **b,c,** Simulations and fluorescence kinetics experiments using a single sample (**b**) or 4 parallel samples that corresponded to the first and last two rounds of computation (**c**). Simulations (solid trajectories) represent the ideal behavior of reset. Differences between experiments (dotted trajectories) and simulations indicate undesired behavior caused by experimental errors including the inevitable volume loss and thus excess input inhibitors using the single-sample procedure.

a plate before the data collection starts (step 3). After the data is obtained, fluorescence kinetics trajectories from the n wells will be combined into a single plot, in which the kinetics from time $(i-1) \times t$ to $i \times t$ corresponds to the i-th well, where $i = 1$ to n (step 4).

We evaluated the impact of the wait time between resets. Nearly no difference was observed between experiments in which the sample was reset right after a new input was added (Fig. S3a) and experiments in which there was a 20-hour wait between resets (Fig. S3b). This result makes sense because when the sample is heated up to 95 °C for five minutes, the molecules are expected to reach the same single-stranded states regardless of whether they were at the initial or final state of a circuit computation. With this observation, we further simplified the experimental procedure in Fig. S2: instead of waiting for t hours between resets and introductions of subsequent inputs, we performed all n rounds of computation (between steps 2 and 3) without any wait.

We further performed experiments of a 100-bit, two-memory winner-take-all neural network with ten rounds of computation using a single sample and compared the results with the same experiments using parallel samples (Fig. S4). The decrease in raw fluorescence for the positive control shown in Fig. S4a indicated the degree of material loss when the sample was transferred between a 96-well plate with clear and flat bottom for fluorescence kinetics measurements in a plate reader and a test tube with conical bottom for heat and cool in a thermal cycler. Because the signal level depends on both concentration and volume, even though the concentrations of molecules composing the neural network were expected to remain the same after each reset, the volume loss caused by each transfer event resulted in the decrease in raw fluorescence. Using the positive and negative controls, we normalized the raw fluorescence to output concentration (Fig. S4b). With this normalization method, the volume loss did not impact the interpretation of the output concentration. However, the volume loss impacted the ratio of inputs and input inhibitors. When inhibitors were added to inactivate the inputs from a previous round of computation, the volume loss of inputs led to excess inhibitors that would inactivate a small fraction of the inputs for the next round of computation. This problem explains the increasing difference between simulations and experiments with more rounds of computation shown in Fig. S4b. Reduced difference was observed with parallel samples (Fig. S4c), suggesting the effectiveness of the procedure for reducing inevitable experimental errors that interfere with the quantification of the system behavior.

1.3 Data normalization

Besides the internal control discussed in Methods, an alternative data normalization method is to use a calibration curve: an output strand with varying concentration is used to react with a reporter, and the best linear fit to the data is used to derive a function that converts raw fluorescence to output concentration. We call this method an external control and typically use it for initial experiments that investigate the basic functions of a new gate motif. The advantage of the external control is that it helps evaluate the amount of output produced by the gate motif without any assumption of how well the gate responds to an input signal. However, the external control has several major limitations. First, fluorescence signals measured by BioTek Synergy H1, the plate reader used for this work, depend on both the concentration and the volume of the sample. While the dependence to concentration is a linear function, the dependence to volume is not, especially with small volumes. Thus, the external control cannot be applied to samples with various volumes. In some cases, the sample volume may even change within an experiment, due to evaporation over a long period of time and multi-step procedures where materials are added (for example, the addition of inputs and input

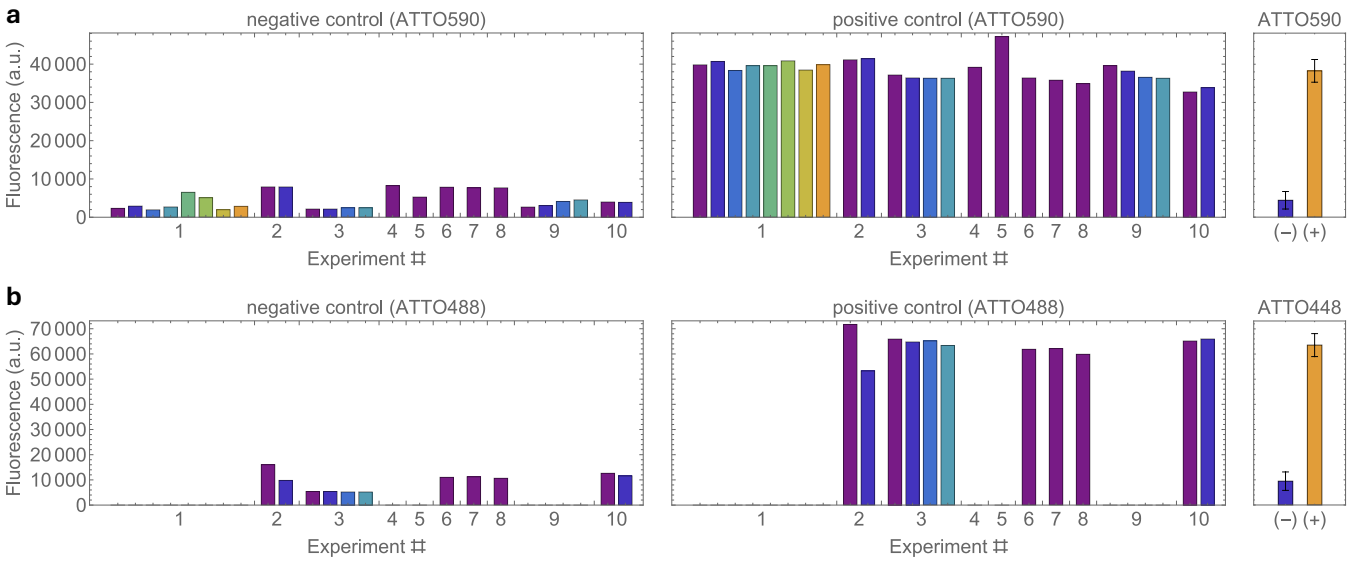

Fig. S5 | Variations in internal controls. a,b, Raw fluorescence data of negative and positive controls for a representative set of experiments, some of which had a single output and measurements of ATTO590 fluorescence (**a**) and others had two outputs including additional measurements of ATTO488 fluorescence (**b**). Normalized data of Experiments 1 through 10 are shown in Figs. 2c-d, 3b-c, Extended Data Fig. 6, Figs. 3f, 3g, Extended Data Figs. 8e-f, 8b-c, Figs. S3, 5c-d, and 6c, respectively. Other experiments were done on different plate readers and the raw fluorescence signal cannot be directly compared. Error bars indicate standard deviation of the mean for the negative and positive controls across 10 sets of experiments.

inhibitors in our experiments). Second, fluorescence signals also depend on the conditions of the plate reader, including age of the flash lamp and contamination on the light path. These conditions may result in noticeable fluorescence changes over the course of a few months. The external control becomes inaccurate over time even for samples with a fixed volume. Third, fluorescence signals are sensitive to molecular interactions with the fluorophore-labeled strand. For example, compared to being single-stranded, fluorescence change occurs when the strand becomes fully or partially bound to another strand. Thus, we specifically used a reporting mechanism where the fluorophore-labeled strand remains double-stranded before and after detecting an output signal. Even in that case, considering possible spurious interactions with the fluorescent product, we expect the signal to be affected by the complexity of the circuit.

Compared to the external control, the internal control provides more accurate references that are robust to sample volume, equipment conditions, and circuit complexity. Fig. S5 illustrates the variations in internal controls for 10 representative sets of experiments, from a single reusable catalyst (Experiment 1) to winner-take-all neural networks (Experiments 6 to 8) and logic circuits (Experiments 9 and 10). In addition to the above factors, variations in the negative controls also include a varying degree of instantaneous leak due to synthesis errors. As we use unpurified strands purchased from IDT, synthesis errors play a major role in the strand quality. Truncations, deletions, and mismatches could result in undesired output release without the presence of inputs. Moreover, distinct batches of IDT orders often result in variations in strand quality. As discussed in Methods, we annealed each hairpin gate and double-stranded complex and then PAGE purified them in the lab. This in-house purification procedure reduces malformed structures and stoichiometric errors, but the resolution of the gel is not high enough to eliminate synthesis errors. The quality of the

PAGE purified complexes also varies from batch to batch, as the size and position of the excised band cannot be precisely controlled. Despite these issues, the standard deviation of raw fluorescence signals for the negative controls remained relatively low at 6% of the average raw fluorescence signal for the positive controls. The standard deviation for the positive controls was slightly higher at 8% of the average raw fluorescence signal.

1.4 Quantification of effective concentration

Assuming that the input concentration is accurate and the inhibitor concentration is off by a factor of α, the value of α can be estimated by fluorescence experiments with a fixed amount of the input and varying amount of the inhibitor. A translator can be used to detect the leftover amount of input and produce an equal amount of output for readout through an existing reporter. Generally, inaccurate input concentration would not affect the demonstration of reusability as long as the inhibitor is added at the same concentration. We tested three scenarios where errors were introduced intentionally to create $\alpha = 0.9$, 1, and 1.1 (Fig. S6a). To distinguish from the measured value of α, the set value is shown as α^*. A linear fit was applied to the output concentration versus the input inhibitor concentration, excluding data points with output concentration at zero

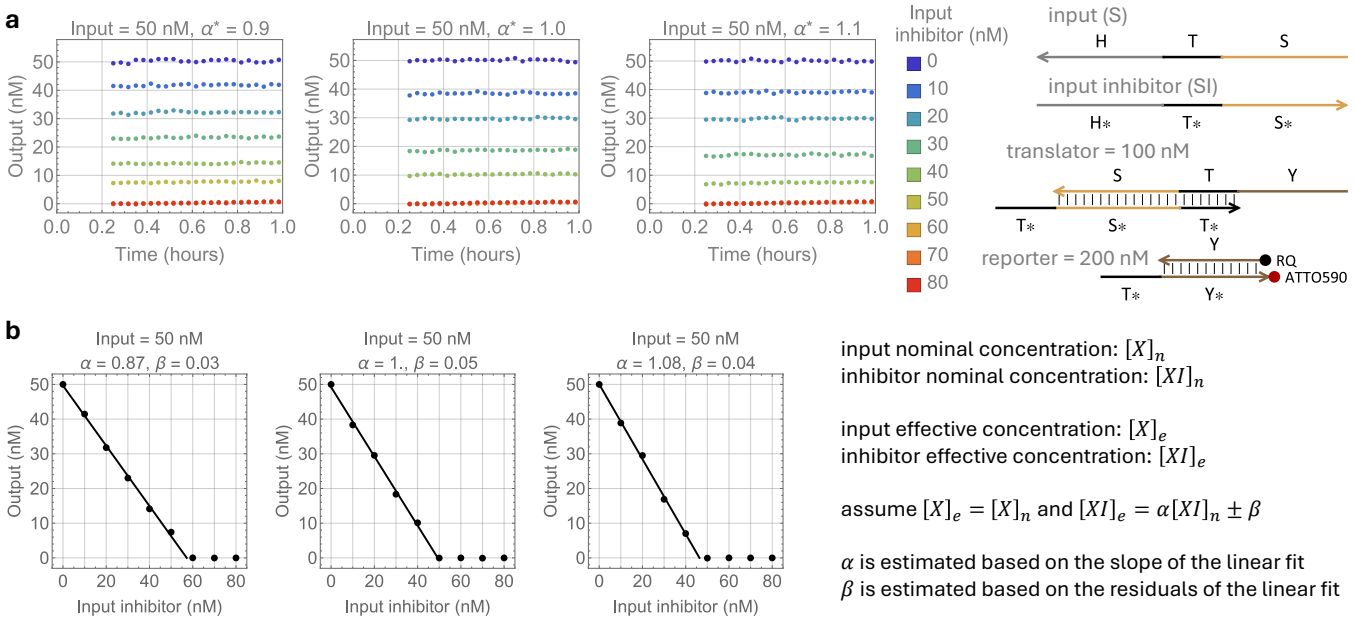

Fig. S6 | Quantification of effective concentration. a, Fluorescence experiments with a fixed amount (50 nM) of an input strand and varying amount (0 to 80 nM) of a complementary strand serving as the input inhibitor. Three scenarios were investigated, where the effective concentration of the input inhibitor was lower (left plot), the same (middle plot), and higher (right plot) than its nominal concentration. Raw fluorescence signals with 0 and 80 nM input inhibitor were used as the internal control for 50 and 0 nM output concentration, respectively, for data normalization. Data points that appear missing (for example, for 50 to 70 nM inhibitor in the right plot) are underneath the data points for 80 nM inhibitor. **b,** Best linear fit to the experimental data of measured output concentration versus input inhibitor concentration for each set of experiments shown in (a). Data points with approximately 0 nM output concentration (the last 3, 4, and 4 data points in each of the three plots, respectively) were excluded from the linear fit. α^* and α above each plot indicate the set value and measured value of the effective concentration of the inhibitor relative to that of the input. β indicates pipette error.

(Fig. S6b). The slope of the linear fit was used to estimate the value of α, whereas the residuals were used to estimate the pipette error β. In all three cases, the estimated value of α agreed with the set value within two digits of precision when rounded. The pipette errors were all within 5% of the input concentration.

Using this quantification method, we sampled a few input inhibitor concentrations and found them to be consistent with the nominal concentrations for IDT purified input and inhibitor strands, which were used for the reusable logic circuits demonstrated in this work. Winner-take-all neural networks are naturally robust to small noise in the inputs, and thus unpurified input and inhibitor strands were used.

1.5 Data reproducibility

Fluorescence kinetics data naturally has better validity than experimental methods with single data points, for example including steady-state fluorescence data and formation gel data. Comparing kinetics simulations with fluorescence kinetics data further improves validity by illustrating the difference between expected and observed system behavior. In this work, data reproducibility is further supported by up to 100 rounds of repeated circuit computation and reset (Figs. S18 and S19). Moreover, we investigated data reproducibility through three repeats of the fluorescence kinetics experiments for eight distinct designs of a reusable DNA catalyst (Figs. S14 and S16). These experiments were performed roughly two years later from the experiments shown in Figs. S13 and S15, using distinct batches of strands ordered from IDT. Error bars shown in Figs. 2c and 2d indicate standard deviations of the mean for all repeated experiments performed two years apart. On average, a 13% standard deviation compared to the mean was observed for the 90% reaction completion time. In the worst case, the standard deviation was 35% of the mean.

The following factors contributed to the observed variations. First, strand quality ordered from IDT varies from batch to batch, especially for unpurified strands. Second, complex quality PAGE purified in the lab varies from batch to batch, mainly because the size and position of the excised band cannot be precisely controlled. Third, effective concentrations of strands and complexes change over time due to evaporation and degradation. Finally, some amount of experimental errors including human and instrument errors are inevitable.

2 Modeling and simulations

2.1 A biophysical model for reset by heating and cooling

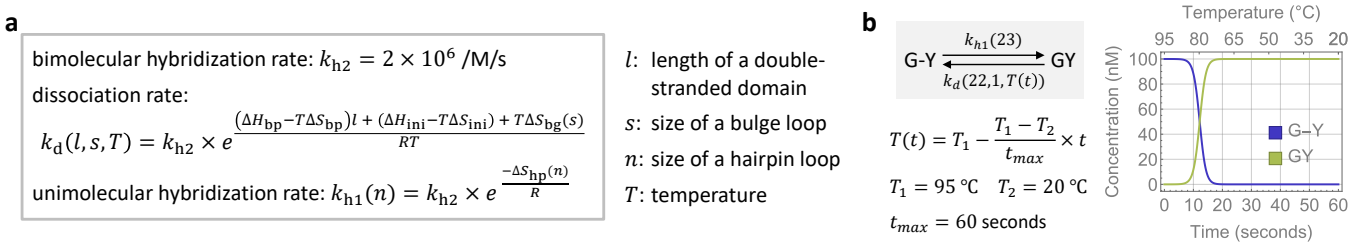

Fig. S7 | Modeling of reset by heating and cooling. **a,** A biophysical model for estimating temperature-dependent hybridization and dissociation rates. The unit of k_{h2} is per molar per second, and the unit of k_d and k_{h1} is per second. ΔH_{bp} and ΔS_{bp} are the enthalpy and entropy of forming a base pair, respectively. $\Delta H_{ini} - T\Delta S_{ini}$ is the initiation penalty of hybridization. ΔS_{bg} and ΔS_{hp} are the entropy of opening a bulge loop and a hairpin loop, respectively. $R = 1.9872$ is the gas constant. **b,** Reaction and simulation of resetting a hairpin gate.

An example simulation of resetting a single hairpin gate is shown in Fig. S7b. The unimolecular hybridization rate was estimated as $k_{h1}(23)$ based on the size of the hairpin loop (Y, T, and L). The dissociation rate was estimated as $k_d(22, 1, T(t))$ based on the length of the double-stranded domain (S and T), the size of the bulge (B), and the temperature T which is a linear function of time t. For example, $T(0) = 95$ and $T(60) = 20$ correspond to a cooling schedule of 95 to 20 °C in 60 seconds.

Specific thermodynamic parameters are taken from SantaLucia and Hicks, 2004[2] and listed as follows. Adjustments on bulge energy and unimolecular hybridization rate were made to better explain experimental data, which will be discussed in Supplementary Note 2.2.

Entropy of forming a bulge of size s:

$$\Delta S_{bg}(1) = (\Delta G_{37,bg}(1) + \Delta G_{37,bp}) \times 1000/310.15$$
$$\Delta S_{bg}(s) = \Delta G_{37,bg}(s) \times 1000/310.15$$

where $\Delta G_{37,bg}(s)$ (unit: kcal per mol) is the free energy of forming a bulge at 37°C:

$$\Delta G_{37,bg}(s) = \{4, 2.9, 3.1, 3.2, 3.3, 3.5, 3.7, 3.9, 4.1, 4.3\} \text{ for } s = 1 \text{ to } 10$$

and $\Delta G_{37,bp}$ (unit: kcal per mol) is the average free energy of forming a base pair at 37°C:

$$\Delta G_{37,bp} = \text{Mean}[\{-1, -0.88, -0.58, -1.45, -1.44, -1.28, -1.3, -2.17, -2.24, -1.84\}]$$

Entropy of forming a hairpin loop of size n:

$$\Delta S_{hp}(n) = \Delta G_{37,hp}(n) \times 1000/310.15$$

where $\Delta G_{37,hp}(n)$ (unit: kcal per mol) is the free energy of forming a hairpin loop at 37°C, based on the longest loop of size 30 for which there are experimental data:

$$\Delta G_{37,hp}(n) = 6.3 + 2.44 \times R/1000 \times 310.15 \times \ln(n/30) \text{ for } n > 4$$

Equilibrium constant for bimolecular hybridization:

$$\frac{k_{\mathrm{h2}}}{k_{\mathrm{d}}} = e^{-\frac{(\Delta H_{\mathrm{bp}} - T\Delta S_{\mathrm{bp}}) \times l + (\Delta H_{\mathrm{ini}} - T\Delta S_{\mathrm{ini}}) + T\Delta S_{\mathrm{bg}}(s)}{RT}}$$

and thus

$$k_{\mathrm{d}}(l, s, T) = k_{\mathrm{h2}} \times e^{\frac{(\Delta H_{\mathrm{bp}} - T\Delta S_{\mathrm{bp}}) \times l + (\Delta H_{\mathrm{ini}} - T\Delta S_{\mathrm{ini}}) + T\Delta S_{\mathrm{bg}}(s)}{RT}}$$

where ΔH_{bp} (unit: cal per mol) is the average enthalpy of forming a base pair:

$$\Delta H_{\mathrm{bp}} = \mathrm{Mean}[\{-7.6, -7.2, -7.2, -8.5, -8.4, -7.8, -8.2, -10.6, -9.8, -8.0\}] \times 1000$$

ΔS_{bp} (unit: cal per K per mol) is the average entropy of forming a base pair:

$$\Delta S_{\mathrm{bp}} = \mathrm{Mean}[\{-21.3, -20.4, -21.3, -22.7, -22.4, -21, -22.2, -27.2, -24.4, -19.9\}]$$

and $\Delta H_{\mathrm{ini}} - T\Delta S_{\mathrm{ini}}$ is the initiation penalty of hybridization:

$$\Delta H_{\mathrm{ini}} = 0.2 \times 1000$$
$$\Delta S_{\mathrm{ini}} = -5.7$$

To convert the unit of temperature from K to °C, the dissociation rate can be revised as follows:

$$k_{\mathrm{d}}(l, s, T) = k_{\mathrm{h2}} \times e^{\frac{(\Delta H_{\mathrm{bp}} - (273.15+T)\Delta S_{\mathrm{bp}}) \times l + (\Delta H_{\mathrm{ini}} - (273.15+T)\Delta S_{\mathrm{ini}}) + (273.15+T)\Delta S_{\mathrm{bg}}(s)}{R(273.15+T)}}$$

Equilibrium constant for unimolecular hybridization:

$$\frac{k_{\mathrm{h1}}}{k_{\mathrm{d}}} = e^{-\frac{(\Delta H_{\mathrm{bp}} - T\Delta S_{\mathrm{bp}}) \times l + (\Delta H_{\mathrm{ini}} - T\Delta S_{\mathrm{ini}}) + T\Delta S_{\mathrm{bg}}(s) + T\Delta S_{\mathrm{hp}}(n)}{RT}}$$

and thus

$$\begin{aligned} k_{\mathrm{h1}}(n) &= k_{\mathrm{d}} \times e^{-\frac{(\Delta H_{\mathrm{bp}} - T\Delta S_{\mathrm{bp}}) \times l + (\Delta H_{\mathrm{ini}} - T\Delta S_{\mathrm{ini}}) + T\Delta S_{\mathrm{bg}}(s) + T\Delta S_{\mathrm{hp}}(n)}{RT}} \\ &= k_{\mathrm{h2}} \times e^{\frac{(\Delta H_{\mathrm{bp}} - T\Delta S_{\mathrm{bp}}) \times l + (\Delta H_{\mathrm{ini}} - T\Delta S_{\mathrm{ini}}) + T\Delta S_{\mathrm{bg}}(s)}{RT}} \times e^{-\frac{(\Delta H_{\mathrm{bp}} - T\Delta S_{\mathrm{bp}}) \times l + (\Delta H_{\mathrm{ini}} - T\Delta S_{\mathrm{ini}}) + T\Delta S_{\mathrm{bg}}(s) + T\Delta S_{\mathrm{hp}}(n)}{RT}} \\ &= k_{\mathrm{h2}} \times e^{-\frac{\Delta S_{\mathrm{hp}}(n)}{R}} \end{aligned}$$

2.2 Modeling the reset of a DNA catalyst

The following set of reactions was used for modeling the reset of a DNA catalyst with eight distinct designs (Fig. S15).

$$\text{G-Y} \underset{k_{\mathrm{d}}(n_{\mathrm{S}}+n_{\mathrm{T}}+1,n_{\mathrm{B}},T(t))}{\overset{k_{\mathrm{h1}}(n_{\mathrm{Y}}-2+n_{\mathrm{LT}}+n_{\mathrm{L}}+10)}{\rightleftharpoons}} \text{GY}$$

$$\text{G-Y} + \text{F} \underset{k_{\mathrm{d}}(n_{\mathrm{S}}+n_{\mathrm{B}}+n_{\mathrm{T}},0,T(t))}{\overset{k_{\mathrm{h2}}}{\rightleftharpoons}} \text{GF-Y}$$

$$\text{G-Y} + \text{R} \underset{k_{\mathrm{d}}(n_{\mathrm{Y}}+n_{\mathrm{T}}+n_{\mathrm{LT}},n_{\mathrm{RB}},T(t))}{\overset{k_{\mathrm{h2}}}{\rightleftharpoons}} \text{G-YR}$$

$$\text{G-YR} + \text{F} \underset{k_{\mathrm{d}}(n_{\mathrm{S}}+n_{\mathrm{B}}+n_{\mathrm{T}},0,T(t))}{\overset{k_{\mathrm{h2}}}{\rightleftharpoons}} \text{GF-YR}$$

$$\text{GF-Y} + \text{R} \underset{k_{\mathrm{d}}(n_{\mathrm{Y}}+n_{\mathrm{T}}+n_{\mathrm{LT}},n_{\mathrm{RB}},T(t))}{\overset{k_{\mathrm{h2}}}{\rightleftharpoons}} \text{GF-YR}$$

$$\text{R} + \text{Q} \underset{k_{\mathrm{d}}(n_{\mathrm{Y}}+n_{\mathrm{RT}}-1,0,T(t))}{\overset{k_{\mathrm{h2}}}{\rightleftharpoons}} \text{RQ}$$

where $n_{\mathrm{S}} = 15$ (15-nt S domain), $n_{\mathrm{T}} = 6.3$ (7-nt toehold whose binding energy is similar to 6.3 average base pairs based on experimental data), $n_{\mathrm{B}} = 0$ or 1 (no bulge or a 1-nt bulge), $n_{\mathrm{Y}} = 13$ (15-nt Y domain whose binding energy is similar to 13 average base pairs), $n_{\mathrm{L}} = 3$ (3-nt linker domain), $n_{\mathrm{LT}} = 0$, 5.3, or 6.3 (0, 6, or 7-nt loop toehold), $n_{\mathrm{RT}} = 0$, 5.3, or 6.3 (0, 6, or 7-nt reporter toehold), and $n_{\mathrm{RB}} = 0$ or 2 (no bulge or a 1-nt bulge whose entropy is similar to a 2-nt bulge when the reporter strand R is bound to the output Y).

The length of the hybridization domain in GY was calculated as $n_{\mathrm{S}} + n_{\mathrm{T}} + 1$. The additional nucleotide was to account for the dangle effect due to the hairpin loop.

The loop size in GY was calculated as $n_{\mathrm{Y}} - 2 + n_{\mathrm{LT}} + n_{\mathrm{L}} + 10$. The subtraction of two nucleotides was because the 2-nt clamp domain at the 3' end of the Y domain was bound to the T$*$ domain on the gate strand. The addition of 10 nucleotides was necessary to better explain the experimental data shown in Fig. S15. The 10-nt adjustment decreases the unimolecular hybridization rate by 2.5 to 35.8-fold depending on the loop size. We suspect the slower unimolecular hybridization rate is due to sequence-dependent spurious interaction, as the thermodynamic parameters for hairpin loops in SantaLucia and Hicks, 2004[2] were measured using different sequences and also different salt conditions and temperature compared to our experiments.

For similar reasons, the free energy of forming a 1-nt bulge, $\Delta G_{37,\mathrm{bg}}(1)$, was adjusted from 4 to 2.2–2.3 kcal per mol, and that of forming a 2-nt bulge, $\Delta G_{37,\mathrm{bg}}(2)$, was adjusted from 2.9 to 2.3–2.9 kcal per mol in our simulations. These two parameters were used for the gate bulge (size n_{B}) and reporter-output bulge (size n_{RB}) respectively, where distinct sequences were involved within and adjacent to the bulge.

The length of the hybridization domain in reporter RQ was calculated as $n_{\mathrm{Y}} + n_{\mathrm{RT}} - 1$. The subtraction of one nucleotide was because there was a 1-nt truncation at the 3' end of the quencher strand in the reporters (Fig. S13). This truncation reduces the impact of the binding energy between a fluorophore and a quencher and thus allows for the reporting reaction to be more irreversible.

Toeless leak reactions are not modeled here even though they can occur at a lower temperature during cooling; the impact is expected to be negligible given the entropic penalty of fewer free molecules, especially at a higher temperature.

2.3 Modeling the kinetics of a reusable DNA catalyst

The following set of reactions was used for modeling the kinetics of a reusable DNA catalyst with eight distinct designs (Fig. S13), an example of which is shown in Fig. S8.

$$\mathrm{S} + \mathrm{GY} \underset{k_\mathrm{d}}{\overset{k_\mathrm{h2}}{\rightleftharpoons}} \mathrm{sGY}$$

$$\mathrm{sGY} \underset{k_\mathrm{b1}}{\overset{k_\mathrm{b}}{\rightleftharpoons}} \mathrm{SGy}$$

$$\mathrm{SGy} \underset{k_\mathrm{h1}(n_\mathrm{Y}-2+n_\mathrm{LT}+n_\mathrm{L}+10)}{\overset{k_\mathrm{d1}}{\rightleftharpoons}} \mathrm{SG\text{-}Y}$$

$$\mathrm{SG\text{-}Y} \underset{k_\mathrm{d2}}{\overset{k_\mathrm{h1}(n_\mathrm{L}+10)}{\rightleftharpoons}} \mathrm{SG\text{-}y}$$

$$\mathrm{SG\text{-}y} + \mathrm{RQ} \underset{k_\mathrm{r}}{\overset{k_\mathrm{f}}{\rightleftharpoons}} \mathrm{SG\text{-}yR} + \mathrm{Q}$$

$$\mathrm{SG\text{-}yR} \underset{k_\mathrm{e}(k_\mathrm{b2},0,n_\mathrm{L},-n_\mathrm{RB})}{\overset{k_\mathrm{b2}}{\rightleftharpoons}} \mathrm{SG\text{-}YR}$$

$$\mathrm{SG\text{-}Y} + \mathrm{F} \underset{k_\mathrm{f}}{\overset{k_\mathrm{f}}{\rightleftharpoons}} \mathrm{S} + \mathrm{GF\text{-}Y}$$

$$\mathrm{SG\text{-}YR} + \mathrm{F} \underset{k_\mathrm{f}}{\overset{k_\mathrm{f}}{\rightleftharpoons}} \mathrm{S} + \mathrm{GF\text{-}YR}$$

$$\mathrm{SG\text{-}Y} + \mathrm{RQ} \xrightarrow{k_\mathrm{f}} \mathrm{SG\text{-}YR} + \mathrm{Q}$$

$$\mathrm{GF\text{-}Y} + \mathrm{RQ} \xrightarrow{k_\mathrm{f}} \mathrm{GF\text{-}YR} + \mathrm{Q}$$

$$\mathrm{GY} + \mathrm{F} \underset{k_\mathrm{e}(k_\mathrm{l},-1,n_\mathrm{Y}+n_\mathrm{LT}+n_\mathrm{L},n_\mathrm{B})}{\overset{k_\mathrm{l}}{\rightleftharpoons}} \mathrm{GF\text{-}Y}$$

where $k_\mathrm{h2} = 2 \times 10^6$ per molar per second is bimolecular hybridization rate,
$k_\mathrm{h1}(n_\mathrm{Y} - 2 + n_\mathrm{LT} + n_\mathrm{L} + 10)$ is unimolecular hybridization rate with a large hairpin loop,
$k_\mathrm{h1}(n_\mathrm{L} + 10)$ is unimolecular hybridization rate with a small hairpin loop,
$k_\mathrm{d} = 0.5$ per second is dissociation rate of a 7-nt toehold ($k_\mathrm{d} \approx 10^{(6-L)} = 0.5$ where $L = 6.3$),
$k_\mathrm{d1} = 0.02$–0.1 per second is dissociation rate of a 7-nt toehold while opening a large 16 to 23-nt hairpin loop (k_d1 is slower than k_d to account for spurious binding within the large loop),
$k_\mathrm{d2} = 10$–30 per second is dissociation rate of a 6 or 7-nt toehold while opening a small 3-nt hairpin loop (k_d2 for a 7-nt toehold is faster than k_d1 to account for increased base pair breathing near the small loop; $k_\mathrm{d2} = 10^6$ per second is used when no loop toehold is present,
$k_\mathrm{b} = 1$ per second is branch migration rate,
$k_\mathrm{b1} = 1$ and 0.01 per second for 0 and 1-nt bulge, respectively, is branch migration rate with possible addition of a bulge in the gate GY,
$k_\mathrm{b2} = 1$ and 0.01 per second for 0 and 1-nt bulge, respectively, is branch migration rate with possible addition of a bulge in the reporter-output complex SG-GY,
$k_\mathrm{e}(k_\mathrm{b2}, 0, n_\mathrm{L}, -n_\mathrm{RB})$ is branch migration rate with removal of a bulge and addition of a hairpin,
$k_\mathrm{f} = 2 \times 10^6$ per molar per second is effective rate of strand displacement with a 7-nt toehold,
$k_\mathrm{l} = 5$–10 per molar per second is effective strand displacement rate of toeless leak reaction between fuel F and hairpin gate GY,

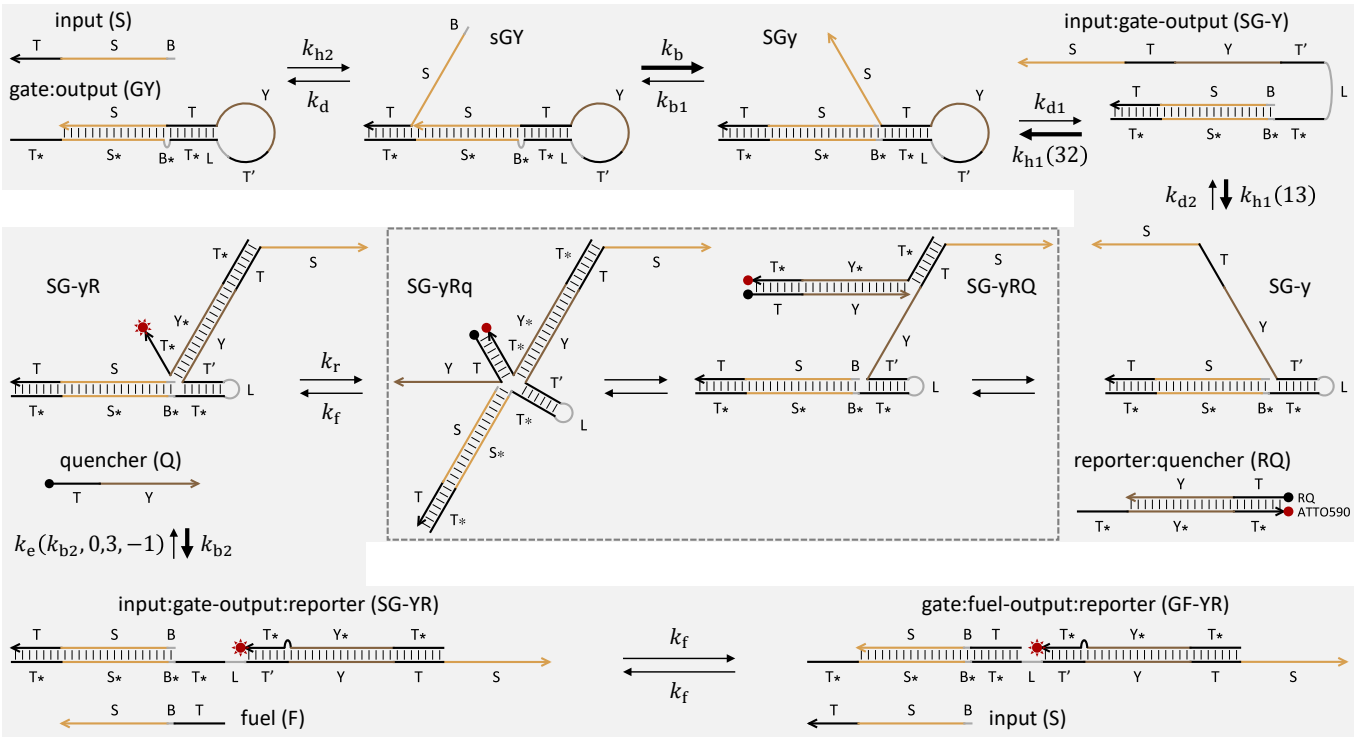

Fig. S8 | Reaction steps and rate constants for modeling a reusable DNA catalyst GY-B1T6 with reporter RQ-T7. The reporting step is simplified by using effective strand displacement rates while skipping the intermediate states shown in the dotted box. $k_{h2} = k_f = 2 \times 10^6$ and $k_r = 10^5$ per molar per second. $k_{h1}(32) = 62$, $k_{h1}(13) = 560$, $k_d = 0.5$, $k_{d1} = 0.1$, $k_{d2} = 30$, $k_b = 1$, $k_{b1} = k_{b2} = 0.01$, and $k_e(k_{b2}, 0, 3, -1) = 3.6 \times 10^{-4}$ per second.

$k_e(k_l, -1, n_Y + n_{LT} + n_L, n_B)$ is reverse rate of the leak reaction,
$k_r = 10$, 10^5, and 2×10^5 per molar per second for reporter with a 0, 6, and 7-nt dissociation toehold, respectively, is reverse rate of reporting reaction when the small hairpin loop is closed and thus the toehold T∗ on reporter strand is open in SG-yR (k_r for a 7-nt toehold is 10 times slower than k_f because the 1-nt truncation on the quencher strand results in the loss of a strong G-C base pair), $n_B = 0$ or 1, $n_Y = 15$, $n_L = 3$, $n_{LT} = 0$, 6, or 7, and $n_{RB} = 0$ or 1.

The same formula of unimolecular hybridization rate $k_{h1}(n)$ for modeling reset was applied here for modeling kinetics.

The forward rate of a reaction with known reverse rate k, a total of l nucleotides gained, a hairpin loop of size n formed, and a bulge loop of size s formed was estimated as follows and applied to derive two of the above rate constants with temperature $T = 298.15$ K (25 °C):

$$k_e(k, l, n, s) = k \times e^{-\frac{(\Delta H_{bp} - T\Delta S_{bp}) \times l + T\Delta S_{hp}(n) + T\Delta S_{bg}(s)}{RT}}$$

Note that for an arbitrary reversible reaction, either direction can be referred to as the "forward" direction. Here for the purpose of rate estimation, whichever direction has a known rate is referred to as the "reverse" direction. By contrast, the "forward" and "reverse" rates of specific reactions listed above indicate their roles in the context of a reaction pathway and do not necessarily agree with the "forward" and "reverse" rates referred to in this formula.

We investigated the impact of key rate constants involved in the reaction steps (Fig. S9). Three criteria were established for evaluating the circuit performance of a reusable DNA catalyst: reac-

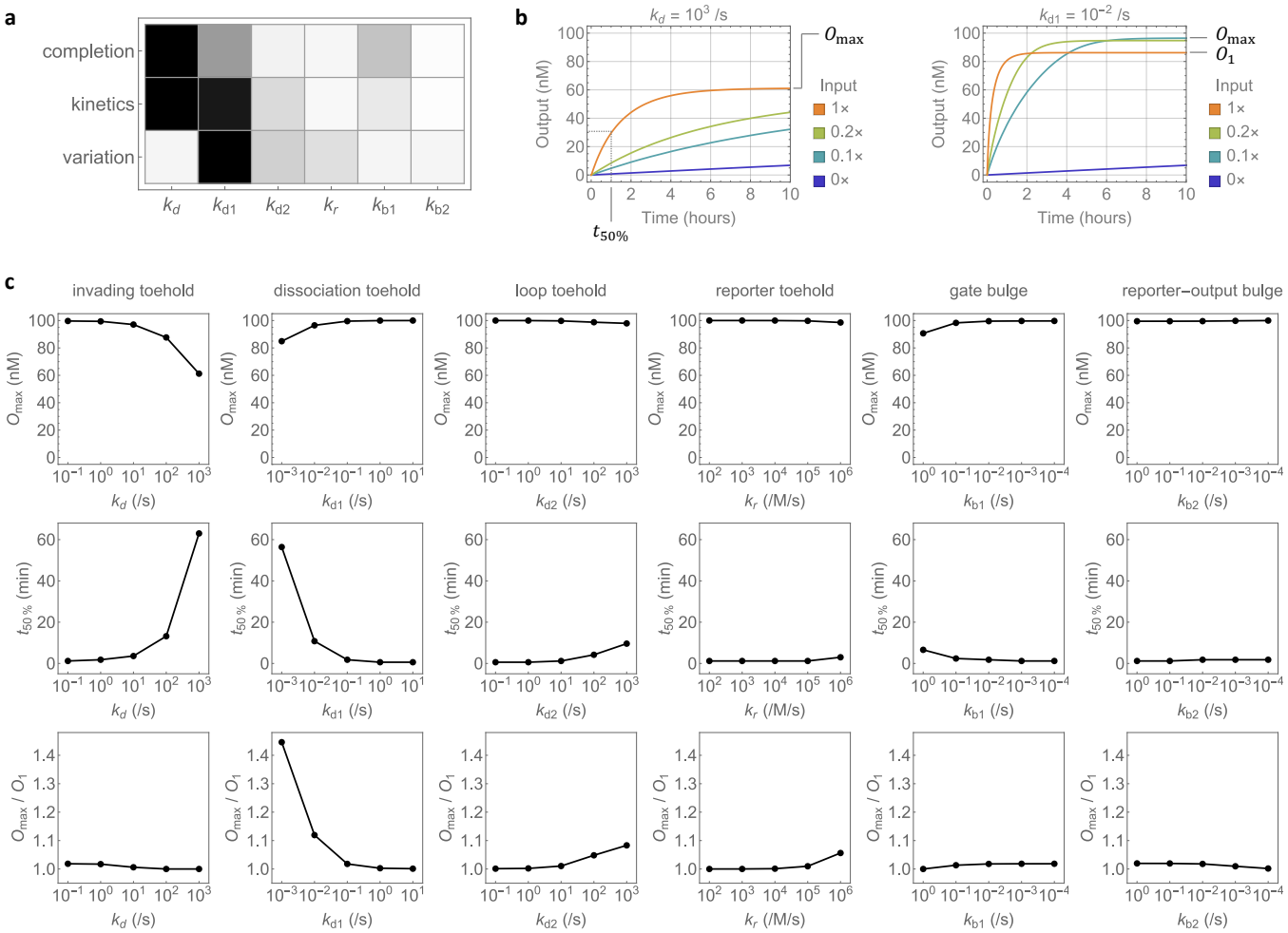

Fig. S9 | Impact of key rate constants on reaction completion, kinetics, and variation. a, Comparison across six rate constants. The level of changes in completion, kinetics, and variation in response to the change of each rate constant are shown in gray scale. Darker color indicates a larger change whereas lighter color indicates a smaller change. **b,** Definition of parameters. Standard concentration 1× = 100 nM. **c,** Values of completion, kinetics, and variation across 4 orders of magnitude change in each rate constant in simulations. The range for each rate constant is chosen based on practical design considerations.

tion completion, kinetics, and variation. Reaction completion is represented by $O_{\max}$, the maximum steady-state output concentration for all input concentrations between 0 and 1×. Kinetics is represented by $t_{50\%}$, the 50% reaction completion time with 1× input. Variation is represented by $O_{\max}/O_1$, the ratio between maximum steady-state output concentration and the steady-state output concentration with 1× input. When O_1 is below $O_{\max}$, it suggests that the input is not effectively released by the fuel, resulting in a fraction of input-bound gate where the output remains sequestered (SGy shown in Fig. S8) at equilibrium.

Through simulations, we found that reaction completion is most strongly affected by k_{d}, dissociation rate of the toehold that allows the input to bind to the gate and initiates strand displacement (Fig. S9a, top row). Because k_{d} depends on the length and sequence of the invading toehold that is initially open on the gate, synthesis errors including truncations within this toehold will affect the rate. DNA synthesis starts from the 3' end of the strand, and thus truncations are expected at the

5' end where the toehold locates, especially for unpurified strands. With a 99.4% nucleotide coupling efficiency by IDT, only 64% full-length product is expected for the 74-nt hairpin gate strand GY shown in Fig. S8. Simulations suggested that reaction completion would decrease from 100 to 60 nM if a 3 to 4-nt truncation occurs (Fig. S9c, first row, first column). Experiments in Fig. S13 suggested an average of 10% signal decrease in reaction completion comparing the steady-state raw fluorescence output for 1× input with the positive control where a trigger strand was used to irreversibly trigger the hairpin gate. With these findings, we consistently applied a factor of 0.9 to the output concentration in simulations when compared with experiments, except in a few cases where the observed reaction completion was higher. The variations in observed reaction completion could be due to variations in strand quality provided by IDT and complex quality after in-house PAGE purification (Supplementary Note 1.5). In addition to reaction completion, truncations in the invading toehold would also strongly affect the kinetics, resulting in over 50-fold slowdown if a 3 to 4-nt truncation occurs (Fig. S9c, second row, first column).

Completion is also affected by k_{d1}, dissociation rate of the toehold that opens the hairpin loop when the input is fully branch migrated on the gate (Fig. S9a, top row). k_{d1} depends on spurious interactions between the loop and the dissociation toehold on the gate, and thus could change with sequence of the loop and with synthesis errors within the loop and the dissociation toehold. For six of the eight designs shown in Fig. S13, $k_{\mathrm{d1}} = 0.05$ and 0.1 per second quantitatively agreed with the experimental data without and with a bulge in the gate, respectively. We speculated that the change in k_{d1} was caused by the nucleotide sequence adjacent to the dissociation toehold. Without a bulge, the adjacent two nucleotides are CA, whereas the nucleotides become AA with a bulge. The weaker sequence might have resulted in more breathing near the end of the double-stranded S domain, reducing the stacking energy that contributes to the dissociation rate of the toehold. For the other two cases, k_{d1} was slower at 0.02 and 0.05 per second, presumably due to variations in strand and complex quality. The change in k_{d1} affects kinetics and variation more strongly than it affects completion (Fig. S9a, middle and bottom rows). Simulations suggested that half completion time would increase by over 30-fold if a 2-nt spurious binding within the loop adjacent to the dissociation toehold occurs (Fig. S9c, second row, second column). Similarly, steady-state output concentration with 1× input would become 30% lower than the maximum output concentration if a 2-nt spurious binding occurs (Fig. S9c, third row, second column).

The length and synthesis errors in the loop toehold determines k_{d2}, which has an impact on both kinetics and variation. A 4-nt shorter loop toehold would lead to a 16-fold slowdown in kinetics (Fig. S9c, second row, third column) and an 8% lower steady-state output concentration with 1× input compared to the maximum (Fig. S9c, third row, third column). The length of the dissociation toehold on the reporter determines k_{r}, which has an impact on variation. A 7-nt full toehold without any truncations shown in Fig. S13 would result in a 5% lower steady-state output concentration with 1× input compared to the maximum (Fig. S9c, third row, fourth column). The reverse branch migration rate of displacing the input, k_{b1}, depends on the size of the bulge on the gate. Simulations suggested that a 1-nt bulge is sufficient for achieving desired reaction completion and kinetics, whereas a larger bulge would no longer improve the performance (Fig. S9c, first and second rows, fifth column). The bulge has an impact on the variation, but is small enough (less than 2%) to be neglected (Fig. S9c, third row, fifth column). Finally, k_{b2} determined by the size of the bulge on the reporter-output complex has the least impact on all three aspects of the operation performance (Fig. S9c, last column), making it a good choice for engineering the reset performance of a reusable DNA catalyst.

2.4 Modeling the reset of a two-input winner-take-all circuit

Simulation of reset predicted that 87–98% of the annihilator would reset successfully, depending on different assumptions of hybridization rate and input removal (Fig. S10). Because the annihilator is in excess, imperfect reset would not have much impact on the circuit performance.

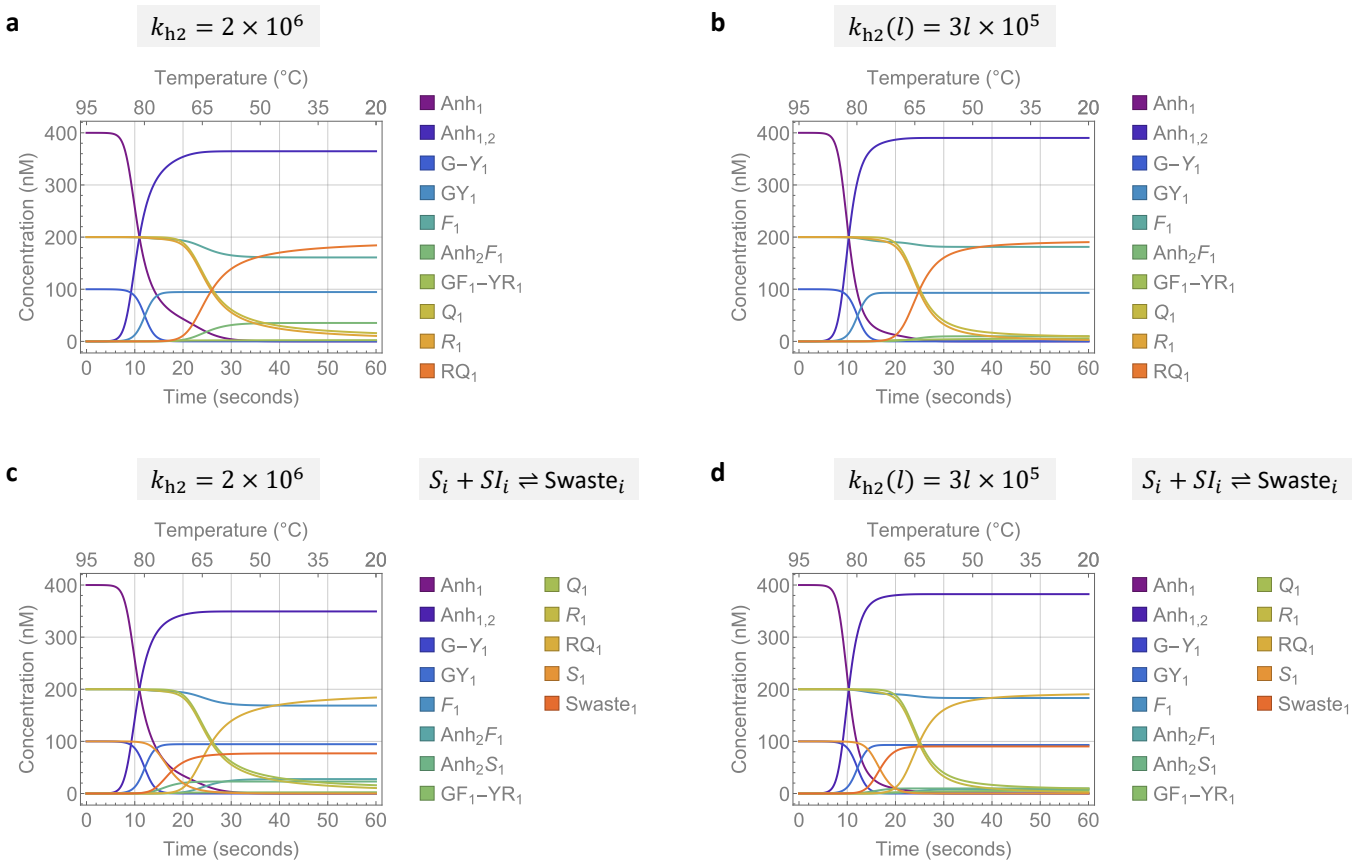

Fig. S10 | Simulations of resetting a two-input winner-take-all circuit. a, If bimolecular hybridization rate does not depend on the length of the hybridization domain, the annihilator reset success rate is 91.2%. **b,** If bimolecular hybridization rate depends on the length of the hybridization domain, the annihilator reset success rate is higher, for example at 97.6% using the length-dependent hybridization rate reported in Badelt et al., 2020.[3] **c,** Considering the presence of input strands S_i and input inhibitors SI_i, if bimolecular hybridization rate does not depend on the length of the hybridization domain, the annihilator reset success rate is 87.3%. **d,** Considering the presence of input strands S_i and input inhibitors SI_i, if bimolecular hybridization rate depends on the length of the hybridization domain, the annihilator reset success rate is 95.6%.

The following set of reactions was used for modeling the reset of a two-input winner-take-all circuit (Fig. S10a):

$$\mathrm{Anh}_i + \mathrm{Anh}_j \underset{k_\mathrm{d}(2n_\mathrm{S}+2n_\mathrm{B},0,T(t))}{\overset{k_\mathrm{h2}}{\rightleftharpoons}} \mathrm{Anh}_{i,j}$$

$$\mathrm{Anh}_i + \mathrm{F}_j \underset{k_\mathrm{d}(n_\mathrm{S}+n_\mathrm{B},0,T(t))}{\overset{k_\mathrm{h2}}{\rightleftharpoons}} \mathrm{Anh}_i\mathrm{F}_j$$

$$\mathrm{Anh}_j + \mathrm{F}_i \underset{k_\mathrm{d}(n_\mathrm{S}+n_\mathrm{B},0,T(t))}{\overset{k_\mathrm{h2}}{\rightleftharpoons}} \mathrm{Anh}_j\mathrm{F}_i$$

$$\mathrm{Anh}_i + \mathrm{G\text{-}Y}_i \underset{k_\mathrm{d}(n_\mathrm{S}+n_\mathrm{B},0,T(t))}{\overset{k_\mathrm{h2}}{\rightleftharpoons}} \mathrm{AnhG\text{-}Y}_i$$

$$\mathrm{Anh}_j + \mathrm{G\text{-}Y}_j \underset{k_\mathrm{d}(n_\mathrm{S}+n_\mathrm{B},0,T(t))}{\overset{k_\mathrm{h2}}{\rightleftharpoons}} \mathrm{AnhG\text{-}Y}_j$$

$$\mathrm{G\text{-}Y}_i \underset{k_\mathrm{d}(n_\mathrm{S}+n_\mathrm{T}+1,n_\mathrm{B},T(t))}{\overset{k_\mathrm{h1}(n_\mathrm{Y}-2+n_\mathrm{LT}+n_\mathrm{L}+10)}{\rightleftharpoons}} \mathrm{GY}_i$$

$$\mathrm{G\text{-}Y}_i + \mathrm{F}_i \underset{k_\mathrm{d}(n_\mathrm{S}+n_\mathrm{B}+n_\mathrm{T},0,T(t))}{\overset{k_\mathrm{h2}}{\rightleftharpoons}} \mathrm{GF\text{-}Y}_i$$

$$\mathrm{G\text{-}Y}_i + \mathrm{R}_i \underset{k_\mathrm{d}(n_\mathrm{Y}+n_\mathrm{T}+n_\mathrm{LT},n_\mathrm{RB},T(t))}{\overset{k_\mathrm{h2}}{\rightleftharpoons}} \mathrm{G\text{-}YR}_i$$

$$\mathrm{G\text{-}YR}_i + \mathrm{F}_i \underset{k_\mathrm{d}(n_\mathrm{S}+n_\mathrm{B}+n_\mathrm{T},0,T(t))}{\overset{k_\mathrm{h2}}{\rightleftharpoons}} \mathrm{GF\text{-}YR}_i$$

$$\mathrm{GF\text{-}Y}_i + \mathrm{R}_i \underset{k_\mathrm{d}(n_\mathrm{Y}+n_\mathrm{T}+n_\mathrm{LT},n_\mathrm{RB},T(t))}{\overset{k_\mathrm{h2}}{\rightleftharpoons}} \mathrm{GF\text{-}YR}_i$$

$$\mathrm{R}_i + \mathrm{Q}_i \underset{k_\mathrm{d}(n_\mathrm{Y}+n_\mathrm{RT}-1,0,T(t))}{\overset{k_\mathrm{h2}}{\rightleftharpoons}} \mathrm{RQ}_i$$

The following set of reactions was added for simulations shown in Figs. S10c and S10d:

$$\mathrm{Anh}_i + \mathrm{S}_j \underset{k_\mathrm{d}(n_\mathrm{T}+n_\mathrm{S}+n_\mathrm{B},0,T(t))}{\overset{k_\mathrm{h2}}{\rightleftharpoons}} \mathrm{Anh}_i\mathrm{S}_j$$

$$\mathrm{Anh}_j + \mathrm{S}_i \underset{k_\mathrm{d}(n_\mathrm{T}+n_\mathrm{S}+n_\mathrm{B},0,T(t))}{\overset{k_\mathrm{h2}}{\rightleftharpoons}} \mathrm{Anh}_j\mathrm{S}_i$$

$$\mathrm{S}_i + \mathrm{SI}_i \underset{k_\mathrm{d}(n_\mathrm{T}+n_\mathrm{S}+n_\mathrm{B},0,T(t))}{\overset{k_\mathrm{h2}}{\rightleftharpoons}} \mathrm{Swaste}_i$$

$$\mathrm{S}_j + \mathrm{SI}_j \underset{k_\mathrm{d}(n_\mathrm{T}+n_\mathrm{S}+n_\mathrm{B},0,T(t))}{\overset{k_\mathrm{h2}}{\rightleftharpoons}} \mathrm{Swaste}_j$$

In Figs. S10b and S10d, bimolecular hybridization rate was revised to $k_\mathrm{h2}(l) = 3l \times 10^5$ per molar per second[3] to evaluate the impact of hybridization domain length on the rate, given that the annihilator has a hybridization domain that is roughly twice as long as the other complexes.

2.5 Modeling the reset of a winner-take-all neural network

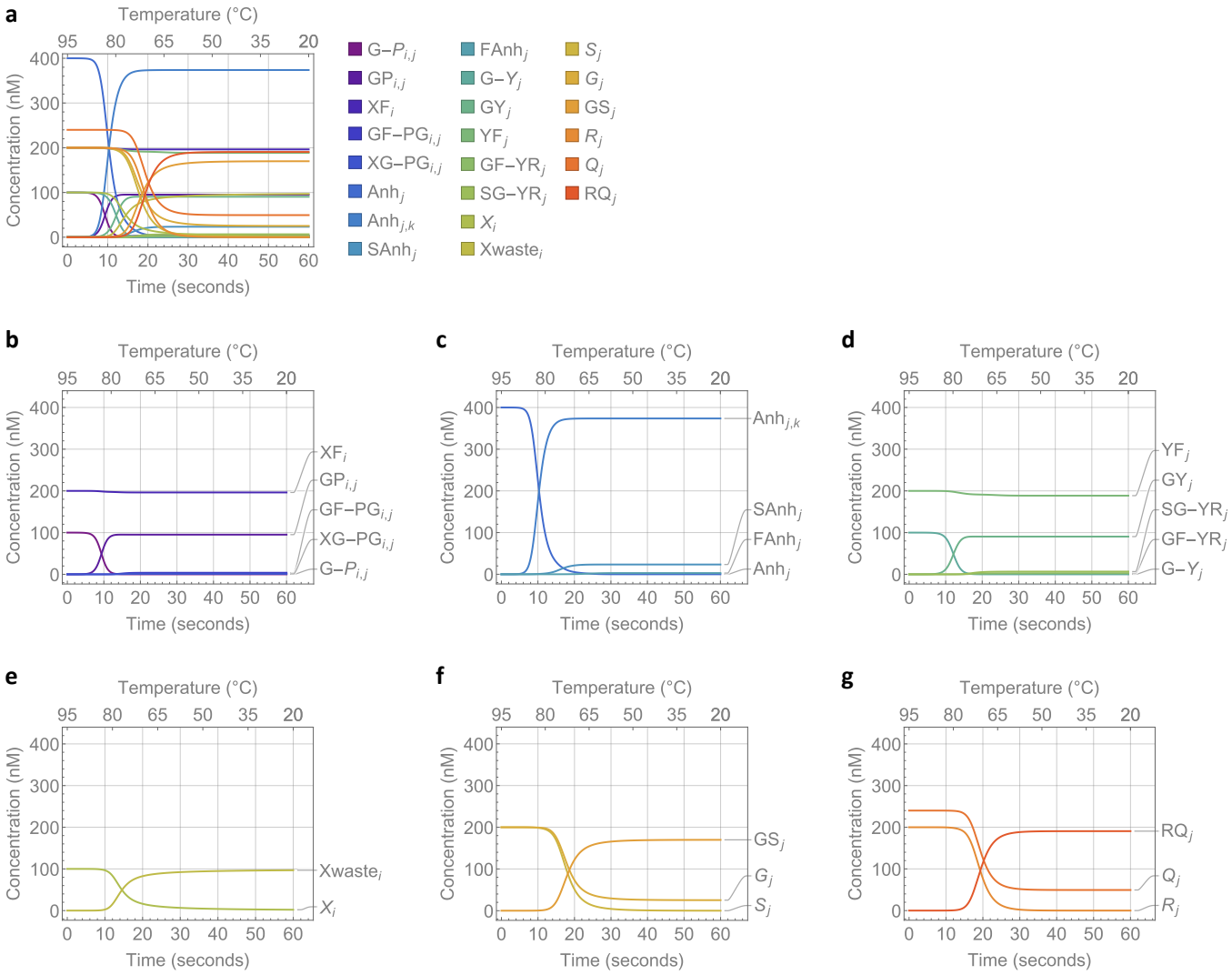

Fig. S11 | Simulations of resetting a winner-take-all neural network. a, Plot of simulation that includes all representative species. **b-g,** Plot of simulation that includes a subset of representative species involved in the weight gate (**b**), annihilator (**c**), restoration gate (**d**), input (**e**), summation gate (**f**), and reporter (**g**). When input inhibitors XI_i are added to inactivate the inputs X_i, they form double-stranded wastes at a temperature slightly higher than two-stranded gates and reporters, because they have longer domains for enabling a larger sequence design space for a hundred unique inputs.

In addition to the reactions for resetting a two-input winner-take-all circuit, the following set of reactions was added for simulations of resetting a winner-take-all neural network (Fig. S11):

$$\mathrm{X}_i + \mathrm{XI}_i \underset{k_{\mathrm{d}}(n_{\mathrm{T}}+n_{\mathrm{X}}+n_{\mathrm{B}},0,T(t))}{\overset{k_{\mathrm{h2}}(n_{\mathrm{T}}+n_{\mathrm{X}}+n_{\mathrm{B}})}{\rightleftharpoons}} \mathrm{Xwaste}_i$$

$$\mathrm{G\text{-}P}_{i,j} \underset{k_{\mathrm{d}}(n_{\mathrm{X}}+n_{\mathrm{T}}+1,n_{\mathrm{B}},T(t))}{\overset{k_{\mathrm{h1}}(n_{\mathrm{P}}-2+n_{\mathrm{LT}}+n_{\mathrm{L}}+10)}{\rightleftharpoons}} \mathrm{GP}_{i,j}$$

$$\text{G-P}_{i,j} + \text{X}_i \underset{k_\text{d}(n_\text{T}+n_\text{X}+n_\text{B},0,T(t))}{\overset{k_\text{h2}(n_\text{T}+n_\text{X}+n_\text{B})}{\rightleftharpoons}} \text{XG-P}_{i,j}$$

$$\text{G-P}_{i,j} + \text{XF}_i \underset{k_\text{d}(n_\text{X}+n_\text{B}+n_\text{T},0,T(t))}{\overset{k_\text{h2}(n_\text{X}+n_\text{B}+n_\text{T})}{\rightleftharpoons}} \text{GF-P}_{i,j}$$

$$\text{G-P}_{i,j} + \text{G}_j \underset{k_\text{d}(n_\text{P}+n_\text{T}+n_\text{LT},n_\text{B},T(t))}{\overset{k_\text{h2}(n_\text{P}+n_\text{T}+n_\text{LT})}{\rightleftharpoons}} \text{G-PG}_{i,j}$$

$$\text{G-PG}_{i,j} + \text{X}_i \underset{k_\text{d}(n_\text{T}+n_\text{X}+n_\text{B},0,T(t))}{\overset{k_\text{h2}(n_\text{T}+n_\text{X}+n_\text{B})}{\rightleftharpoons}} \text{XG-PG}_{i,j}$$

$$\text{G-PG}_{i,j} + \text{XF}_i \underset{k_\text{d}(n_\text{X}+n_\text{B}+n_\text{T},0,T(t))}{\overset{k_\text{h2}(n_\text{X}+n_\text{B}+n_\text{T})}{\rightleftharpoons}} \text{GF-PG}_{i,j}$$

$$\text{XG-P}_{i,j} + \text{G}_j \underset{k_\text{d}(n_\text{P}+n_\text{T}+n_\text{LT},n_\text{B},T(t))}{\overset{k_\text{h2}(n_\text{P}+n_\text{T}+n_\text{LT})}{\rightleftharpoons}} \text{XG-PG}_{i,j}$$

$$\text{GF-P}_{i,j} + \text{G}_j \underset{k_\text{d}(n_\text{P}+n_\text{T}+n_\text{LT},n_\text{B},T(t))}{\overset{k_\text{h2}(n_\text{P}+n_\text{T}+n_\text{LT})}{\rightleftharpoons}} \text{GF-PG}_{i,j}$$

$$\text{S}_j + \text{G}_j \underset{k_\text{d}(n_\text{P}+n_\text{T},0,T(t))}{\overset{k_\text{h2}(n_\text{P}+n_\text{T})}{\rightleftharpoons}} \text{GS}_j$$

2.6 Modeling the kinetics of a reusable winner-take-all neural network

The following set of reactions was used for modeling the kinetics of a reusable winner-take-all neural network (Fig. 4e). S and G represent total signal and total gate, respectively, for modeling toehold occlusion that occurs between any pair of signal and gate species (Supplementary Note S13 in Qian and Winfree, 2011[1]).

Weight multiplication (mulCRN$[i, j]$):

$$\mathrm{X}_i + \mathrm{GP}_{i,j} \underset{k_\mathrm{d}}{\overset{k_\mathrm{h2}}{\rightleftharpoons}} \mathrm{xGP}_{i,j}$$

$$\mathrm{xGP}_{i,j} \underset{k_\mathrm{b1}}{\overset{k_\mathrm{b}}{\rightleftharpoons}} \mathrm{XGp}_{i,j}$$

$$\mathrm{XGp}_{i,j} \underset{k_\mathrm{h1}(32)}{\overset{k_\mathrm{d1}}{\rightleftharpoons}} \mathrm{XG\text{-}P}_{i,j}$$

$$\mathrm{XG\text{-}P}_{i,j} \underset{k_\mathrm{d2}}{\overset{k_\mathrm{h1}(13)}{\rightleftharpoons}} \mathrm{XG\text{-}p}_{i,j}$$

$$\mathrm{XG\text{-}P}_{i,j} + \mathrm{XF}_i \underset{k_\mathrm{f}}{\overset{k_\mathrm{f}}{\rightleftharpoons}} \mathrm{X}_i + \mathrm{GF\text{-}P}_{i,j}$$

$$\mathrm{XG\text{-}PG}_{i,j} + \mathrm{XF}_i \underset{k_\mathrm{f}}{\overset{k_\mathrm{f}}{\rightleftharpoons}} \mathrm{X}_i + \mathrm{GF\text{-}PG}_{i,j}$$

$$\mathrm{GP}_{i,j} + \mathrm{XF}_i \underset{k_\mathrm{e}(k_\mathrm{l},-1,22,1)}{\overset{k_\mathrm{l}}{\rightleftharpoons}} \mathrm{GF\text{-}P}_{i,j} \text{ (leak)}$$

$$\mathrm{XG\text{-}P}_{i,j} + \mathrm{S} \underset{k_\mathrm{d}}{\overset{k_\mathrm{h2}}{\rightleftharpoons}} \mathrm{XGs\text{-}P}_{i,j} \text{ (occlusion)}$$

$$\mathrm{XG\text{-}PG}_{i,j} + \mathrm{S} \underset{k_\mathrm{d}}{\overset{k_\mathrm{h2}}{\rightleftharpoons}} \mathrm{XGs\text{-}PG}_{i,j} \text{ (occlusion)}$$

$$\mathrm{X}_i + \mathrm{G} \underset{k_\mathrm{d}}{\overset{k_\mathrm{h2}}{\rightleftharpoons}} \mathrm{xG}_i \text{ (occlusion)}$$

$$\mathrm{XG\text{-}P}_{i,j} + \mathrm{G} \underset{k_\mathrm{d}}{\overset{k_\mathrm{h2}}{\rightleftharpoons}} \mathrm{XG\text{-}pG}_{i,j} \text{ (occlusion)}$$

$$\mathrm{XG\text{-}p}_{i,j} + \mathrm{G} \underset{k_\mathrm{d}}{\overset{k_\mathrm{h2}}{\rightleftharpoons}} \mathrm{XG\text{-}pG}_{i,j} \text{ (occlusion)}$$

$$\mathrm{GF\text{-}P}_{i,j} + \mathrm{G} \underset{k_\mathrm{d}}{\overset{k_\mathrm{h2}}{\rightleftharpoons}} \mathrm{GF\text{-}pG}_{i,j} \text{ (occlusion)}$$

Summation (sumCRN$[i, j]$):

$$\mathrm{XG\text{-}p}_{i,j} + \mathrm{GS}_j \underset{k_\mathrm{r}}{\overset{k_\mathrm{f}}{\rightleftharpoons}} \mathrm{XG\text{-}pG}_{i,j} + \mathrm{S}_j$$

$$\mathrm{XG\text{-}pG}_{i,j} \underset{k_\mathrm{e}(k_\mathrm{b2},0,3,-1)}{\overset{k_\mathrm{b2}}{\rightleftharpoons}} \mathrm{XG\text{-}PG}_{i,j}$$

$$\mathrm{XG\text{-}P}_{i,j} + \mathrm{GS}_j \xrightarrow{k_\mathrm{f}} \mathrm{XG\text{-}PG}_{i,j} + \mathrm{S}_j$$

$$\mathrm{GF\text{-}P}_{i,j} + \mathrm{GS}_j \xrightarrow{k_\mathrm{f}} \mathrm{GF\text{-}PG}_{i,j} + \mathrm{S}_j$$

$$\mathrm{GS}_j + \mathrm{S} \underset{k_\mathrm{d}}{\overset{k_\mathrm{h2}}{\rightleftharpoons}} \mathrm{sGS}_j \text{ (occlusion)}$$

Annihilation (anhCRN$[j,k]$):

$$\mathrm{Anh}_{j,k} + \mathrm{S}_j \underset{k_\mathrm{d}}{\overset{k_\mathrm{f}}{\rightleftharpoons}} \mathrm{SAnh}_{j,k}$$

$$\mathrm{Anh}_{j,k} + \mathrm{S}_k \underset{k_\mathrm{d}}{\overset{k_\mathrm{f}}{\rightleftharpoons}} \mathrm{AnhS}_{j,k}$$

$$\mathrm{SAnh}_{j,k} + \mathrm{S}_k \xrightarrow{k_\mathrm{f}} \text{waste}$$

$$\mathrm{AnhS}_{j,k} + \mathrm{S}_j \xrightarrow{k_\mathrm{f}} \text{waste}$$

$$\mathrm{Anh}_{j,k} + \mathrm{S} \underset{k_\mathrm{d}}{\overset{k_\mathrm{h2}}{\rightleftharpoons}} \mathrm{SAnh}_k \text{ (occlusion)}$$

$$\mathrm{Anh}_{j,k} + \mathrm{S} \underset{k_\mathrm{d}}{\overset{k_\mathrm{h2}}{\rightleftharpoons}} \mathrm{AnhS}_j \text{ (occlusion)}$$

$$\mathrm{SAnh}_k + \mathrm{S} \underset{k_\mathrm{d}}{\overset{k_\mathrm{h2}}{\rightleftharpoons}} \mathrm{SAnhS} \text{ (occlusion)}$$

$$\mathrm{AnhS}_j + \mathrm{S} \underset{k_\mathrm{d}}{\overset{k_\mathrm{h2}}{\rightleftharpoons}} \mathrm{SAnhS} \text{ (occlusion)}$$

$$\mathrm{SAnh}_{j,k} + \mathrm{S} \underset{k_\mathrm{d}}{\overset{k_\mathrm{h2}}{\rightleftharpoons}} \mathrm{SAnhS}_j \text{ (occlusion)}$$

$$\mathrm{AnhS}_{j,k} + \mathrm{S} \underset{k_\mathrm{d}}{\overset{k_\mathrm{h2}}{\rightleftharpoons}} \mathrm{SAnhS}_k \text{ (occlusion)}$$

$$\mathrm{SAnh}_k + \mathrm{S}_k \underset{k_\mathrm{d}}{\overset{k_\mathrm{f}}{\rightleftharpoons}} \mathrm{SAnhS}_k \text{ (reaction on half occluded annihilator)}$$

$$\mathrm{AnhS}_j + \mathrm{S}_j \underset{k_\mathrm{d}}{\overset{k_\mathrm{f}}{\rightleftharpoons}} \mathrm{SAnhS}_j \text{ (reaction on half occluded annihilator)}$$

Restoration (resCRN$[j]$):

$$\mathrm{S}_i + \mathrm{GY}_j \underset{k_\mathrm{d}}{\overset{k_\mathrm{h2}}{\rightleftharpoons}} \mathrm{sGY}_j$$

$$\mathrm{sGY}_j \underset{k_\mathrm{b1}}{\overset{k_\mathrm{b}}{\rightleftharpoons}} \mathrm{SGy}_j$$

$$\mathrm{SGy}_j \underset{k_\mathrm{h1}(32)}{\overset{k_\mathrm{d1}}{\rightleftharpoons}} \mathrm{SG\text{-}Y}_j$$

$$\mathrm{SG\text{-}Y}_j \underset{k_\mathrm{d2}}{\overset{k_\mathrm{h1}(13)}{\rightleftharpoons}} \mathrm{SG\text{-}y}_j$$

$$\mathrm{SG\text{-}Y}_j + \mathrm{YF}_j \underset{k_\mathrm{f}}{\overset{k_\mathrm{f}}{\rightleftharpoons}} \mathrm{S}_j + \mathrm{GF\text{-}Y}_j$$

$$\mathrm{SG\text{-}YR}_j + \mathrm{YF}_j \underset{k_\mathrm{f}}{\overset{k_\mathrm{f}}{\rightleftharpoons}} \mathrm{S}_j + \mathrm{GF\text{-}YR}_j$$

$$\mathrm{GY}_j + \mathrm{YF}_j \underset{k_\mathrm{e}(k_\mathrm{l},-1,22,1)}{\overset{k_\mathrm{l}}{\rightleftharpoons}} \mathrm{GF\text{-}Y}_j \text{ (leak)}$$

$$\mathrm{SG\text{-}Y}_j + \mathrm{S} \underset{k_\mathrm{d}}{\overset{k_\mathrm{h2}}{\rightleftharpoons}} \mathrm{SGs\text{-}Y}_j \text{ (occlusion)}$$

$$\text{SG-YR}_j + \text{S} \underset{k_\text{d}}{\overset{k_\text{h2}}{\rightleftharpoons}} \text{SGs-YR}_j \text{ (occlusion)}$$

$$\text{S}_j + \text{G} \underset{k_\text{d}}{\overset{k_\text{h2}}{\rightleftharpoons}} \text{sG}_j \text{ (occlusion)}$$

$$\text{SG-Y}_j + \text{G} \underset{k_\text{d}}{\overset{k_\text{h2}}{\rightleftharpoons}} \text{SG-yG}_j \text{ (occlusion)}$$

$$\text{SG-y}_j + \text{G} \underset{k_\text{d}}{\overset{k_\text{h2}}{\rightleftharpoons}} \text{SG-yG}_j \text{ (occlusion)}$$

$$\text{GF-Y}_j + \text{G} \underset{k_\text{d}}{\overset{k_\text{h2}}{\rightleftharpoons}} \text{GF-yG}_j \text{ (occlusion)}$$

Reporting (repCRN[j]):

$$\text{SG-y}_j + \text{RQ}_j \underset{k_\text{r}}{\overset{k_\text{f}}{\rightleftharpoons}} \text{SG-yR}_j + \text{Q}_j$$

$$\text{SG-yR}_j \underset{k_\text{e}(k_\text{b2},0,3,-1)}{\overset{k_\text{b2}}{\rightleftharpoons}} \text{SG-YR}_j$$

$$\text{SG-Y}_j + \text{RQ}_j \xrightarrow{k_\text{f}} \text{SG-YR}_j + \text{Q}_j$$

$$\text{GF-Y}_j + \text{RQ}_j \xrightarrow{k_\text{f}} \text{GF-YR}_j + \text{Q}_j$$

$$\text{RQ}_j + \text{S} \underset{k_\text{d}}{\overset{k_\text{h2}}{\rightleftharpoons}} \text{sRQ}_j \text{ (occlusion)}$$

A winner-take-all neural network with n inputs and m outputs:

$$\text{mulCRN}[i,j] \text{ for all } i \in \{1,\ldots,n\} \text{ and } j \in \{1,\ldots,m\}$$
$$\text{sumCRN}[i,j] \text{ for all } i \in \{1,\ldots,n\} \text{ and } j \in \{1,\ldots,m\}$$
$$\text{anhCRN}[j,k] \text{ for all } j \in \{1,\ldots,m-1\} \text{ and } k \in \{j+1,\ldots,m\}$$
$$\text{resCRN}[j] \text{ for all } j \in \{1,\ldots,m\}$$
$$\text{repCRN}[j] \text{ for all } j \in \{1,\ldots,m\}$$

For the 100-bit, two-memory winner-take-all neural network simulations shown in Fig. 4e, $k_\text{d} = 20$ per second was used for restoration gates, whereas $k_\text{d} = 0.5$ per second was used for all other gates including weights (multiplication gates), summation gates, annihilators, and reporters. The difference in k_d is due to the length of the invading toehold: restoration gates have a shorter 5-nt toehold to allow for faster annihilation that selects a winner before the signal is amplified, whereas all other gates have a 7-nt toehold. $k_\text{d1} = 0.1$ per second was used for all weights, whereas $k_\text{d1} = 0.025$ and 0.04 per second were used for the two restoration gates, respectively. The difference in k_d1 is due to variations in sequence-dependent spurious binding between the loop and the dissociation toehold. The following rates were used for all reactions: $k_\text{d2} = 30$, $k_\text{b} = 1$, $k_\text{b1} = 0.01$, and $k_\text{b2} = 0.01$ per second; $k_\text{h2} = 2 \times 10^6$, $k_\text{f} = 2 \times 10^6$, $k_\text{r} = 10^5$, and $k_\text{l} = 10$ per molar per second. Formulas for deriving the values of k_h1 and k_e are specified in Supplementary Note 2.3. The total signal S was at 9× (including 1× inputs, 4× input fuels, and 4× output fuels) and the total gate G at 14× (including 2× weights, 4× summation gates, 4× annihilators, and 4× reporters), where standard concentration 1× = 100 nM. Restoration gates were not included in the total gate because they had a shorter toehold, resulting in negligible impact on toehold occlusion.

2.7 Modeling the reset of a logic gate

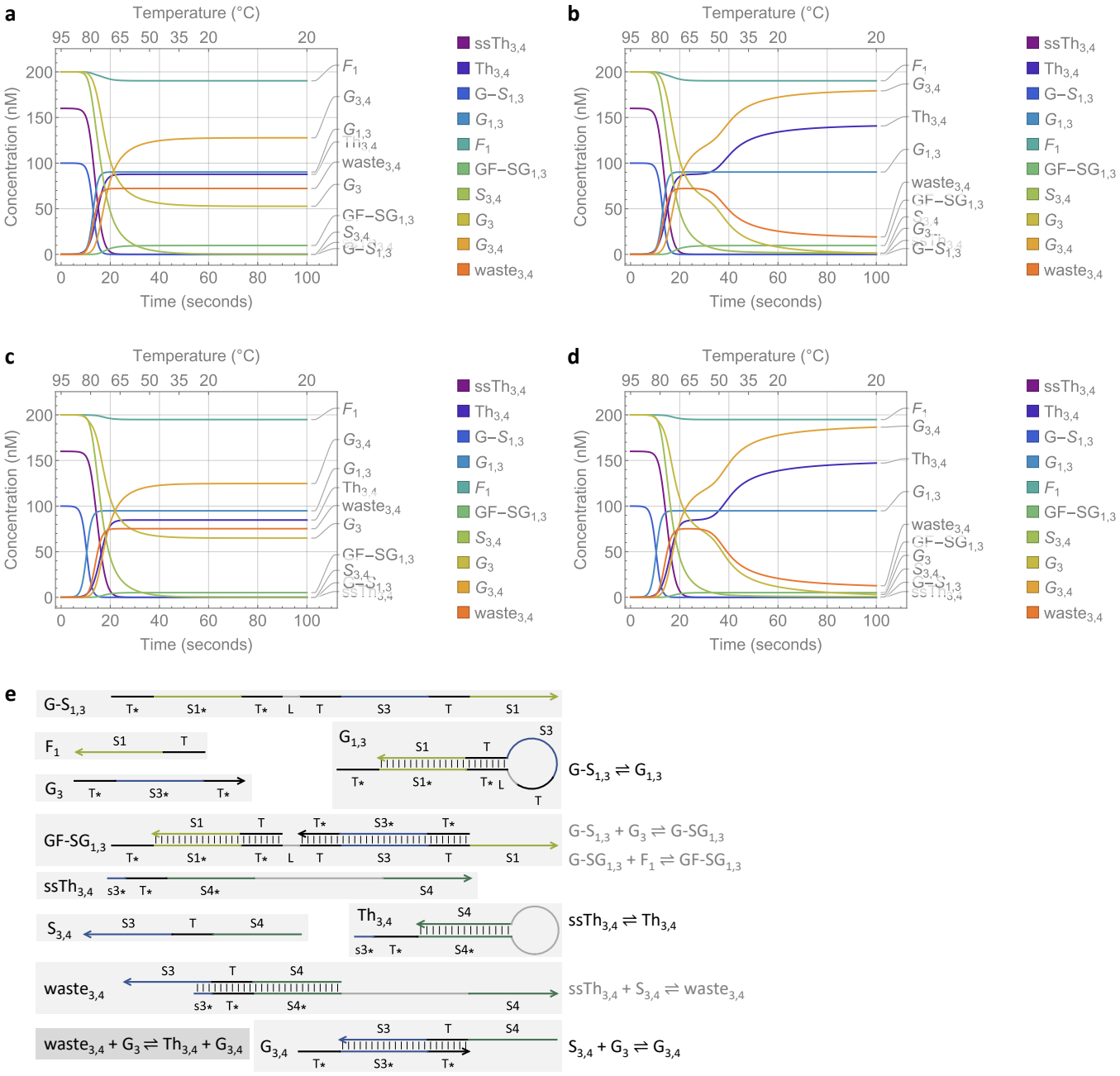

Fig. S12 | Simulations of resetting a logic gate. a,b, Simulations using the 1-nt bulge and 6-nt loop toehold design, without (**a**) and with (**b**) strand displacement that allows the gate strand to react with the waste product while producing the desired hairpin threshold and two-stranded summation gate ($waste_{3,4} + G_3 \rightleftharpoons Th_{3,4} + G_{3,4}$). The threshold reset success rates are 54.9% and 88.7%, respectively. **c,d,** Simulations using the no bulge and 7-nt loop toehold design, without (**c**) and with (**d**) the strand displacement reaction. The threshold reset success rates are 53.0% and 93.6%, respectively. **e,** A representative set of species and reactions for the no bulge and 7-nt loop toehold design (same as shown in Fig. 5b). Reactions in black and gray indicate desired and undesired reactions, respectively. Dark gray box highlights the strand displacement reaction that helps restore the threshold and summation gate.

We expected the design with no bulge to improve the reset of the threshold for the following reason. In a two-input logic gate, an undesired reaction that competes with the reset of the threshold during heating and cooling is the hybridization between the threshold, when it is single-stranded, and the summation signal ($\mathrm{ssTh}_{3,4} + \mathrm{S}_{3,4} \rightleftharpoons \mathrm{waste}_{3,4}$ in Fig. S12e). This hybridization forms a waste product that has 10 more base pairs than the hairpin threshold and thus occurs before the threshold is fully restored. This would also result in partial reset of the summation gate ($\mathrm{G}_{3,4}$) and leftover gate strand (G_3). Fortunately, strand displacement can take place at a lower temperature during cooling, allowing the gate strand to react with the waste product while producing the desired hairpin threshold and two-stranded summation gate ($\mathrm{waste}_{3,4} + \mathrm{G}_3 \rightleftharpoons \mathrm{Th}_{3,4} + \mathrm{G}_{3,4}$). However, with a 1-nt bulge in the upstream hairpin gate (for example, $\mathrm{G}_{1,3}$), the gate would reset at a lower temperature close to when the waste product forms. At this lower temperature, the undesired competing reaction ($\mathrm{G\text{-}S}_{1,3} + \mathrm{G}_3 \rightleftharpoons \mathrm{G\text{-}SG}_{1,3}$) would consume the summation gate strand (G_3) and reduce the amount of threshold that can be restored by strand displacement requiring the summation gate strand. Simulation predicted that 94% of the threshold would reset successfully using the design with no bulge (Fig. S12d), 5% higher than using the design with 1-nt bulge loop (Fig. S12b).

The following set of reactions was used for simulations of resetting a logic gate (Fig. S12):

$$\mathrm{X}_1 + \mathrm{XI}_1 \underset{k_\mathrm{d}(n_\mathrm{T}+n_\mathrm{S}+n_\mathrm{B},0,T(t))}{\overset{k_\mathrm{h2}}{\rightleftharpoons}} \mathrm{Xwaste}_1$$

$$\mathrm{X}_2 + \mathrm{XI}_2 \underset{k_\mathrm{d}(n_\mathrm{T}+n_\mathrm{S}+n_\mathrm{B},0,T(t))}{\overset{k_\mathrm{h2}}{\rightleftharpoons}} \mathrm{Xwaste}_2$$

$$\mathrm{G\text{-}S}_{1,3} \underset{k_\mathrm{d}(n_\mathrm{S}+n_\mathrm{T}+1,n_\mathrm{B},T(t))}{\overset{k_\mathrm{h1}(n_\mathrm{S}-2+n_\mathrm{LT}+n_\mathrm{L}+10)}{\rightleftharpoons}} \mathrm{G}_{1,3}$$

$$\mathrm{G\text{-}S}_{2,3} \underset{k_\mathrm{d}(n_\mathrm{S}+n_\mathrm{T}+1,n_\mathrm{B},T(t))}{\overset{k_\mathrm{h1}(n_\mathrm{S}-2+n_\mathrm{LT}+n_\mathrm{L}+10)}{\rightleftharpoons}} \mathrm{G}_{2,3}$$

$$\mathrm{G\text{-}S}_{1,3} + \mathrm{X}_1 \underset{k_\mathrm{d}(n_\mathrm{T}+n_\mathrm{S}+n_\mathrm{B},0,T(t))}{\overset{k_\mathrm{h2}}{\rightleftharpoons}} \mathrm{XG\text{-}S}_{1,3}$$

$$\mathrm{G\text{-}S}_{2,3} + \mathrm{X}_2 \underset{k_\mathrm{d}(n_\mathrm{T}+n_\mathrm{S}+n_\mathrm{B},0,T(t))}{\overset{k_\mathrm{h2}}{\rightleftharpoons}} \mathrm{XG\text{-}S}_{2,3}$$

$$\mathrm{G\text{-}S}_{1,3} + \mathrm{F}_1 \underset{k_\mathrm{d}(n_\mathrm{S}+n_\mathrm{T}+n_\mathrm{B},0,T(t))}{\overset{k_\mathrm{h2}}{\rightleftharpoons}} \mathrm{GF\text{-}S}_{1,3}$$

$$\mathrm{G\text{-}S}_{2,3} + \mathrm{F}_2 \underset{k_\mathrm{d}(n_\mathrm{S}+n_\mathrm{T}+n_\mathrm{B},0,T(t))}{\overset{k_\mathrm{h2}}{\rightleftharpoons}} \mathrm{GF\text{-}S}_{2,3}$$

$$\mathrm{G\text{-}S}_{1,3} + \mathrm{G}_3 \underset{k_\mathrm{d}(n_\mathrm{S}+2n_\mathrm{T},0,T(t))}{\overset{k_\mathrm{h2}}{\rightleftharpoons}} \mathrm{G\text{-}SG}_{1,3}$$

$$\mathrm{G\text{-}S}_{2,3} + \mathrm{G}_3 \underset{k_\mathrm{d}(n_\mathrm{S}+2n_\mathrm{T},0,T(t))}{\overset{k_\mathrm{h2}}{\rightleftharpoons}} \mathrm{G\text{-}SG}_{2,3}$$

$$\mathrm{G\text{-}SG}_{1,3} + \mathrm{X}_1 \underset{k_\mathrm{d}(n_\mathrm{T}+n_\mathrm{S}+n_\mathrm{B},0,T(t))}{\overset{k_\mathrm{h2}}{\rightleftharpoons}} \mathrm{XG\text{-}SG}_{1,3}$$

$$\mathrm{G\text{-}SG}_{2,3} + \mathrm{X}_2 \underset{k_\mathrm{d}(n_\mathrm{T}+n_\mathrm{S}+n_\mathrm{B},0,T(t))}{\overset{k_\mathrm{h2}}{\rightleftharpoons}} \mathrm{XG\text{-}SG}_{2,3}$$

$$\text{G-SG}_{1,3} + \text{F}_1 \underset{k_\text{d}(n_\text{S}+n_\text{T}+n_\text{B},0,T(t))}{\overset{k_\text{h2}}{\rightleftharpoons}} \text{GF-SG}_{1,3}$$

$$\text{G-SG}_{2,3} + \text{F}_2 \underset{k_\text{d}(n_\text{S}+n_\text{T}+n_\text{B},0,T(t))}{\overset{k_\text{h2}}{\rightleftharpoons}} \text{GF-SG}_{2,3}$$

$$\text{GF-S}_{1,3} + \text{G}_3 \underset{k_\text{d}(n_\text{S}+2n_\text{T},0,T(t))}{\overset{k_\text{h2}}{\rightleftharpoons}} \text{GF-SG}_{1,3}$$

$$\text{GF-S}_{2,3} + \text{G}_3 \underset{k_\text{d}(n_\text{S}+2n_\text{T},0,T(t))}{\overset{k_\text{h2}}{\rightleftharpoons}} \text{GF-SG}_{2,3}$$

$$\text{G}_3 + \text{S}_{3,4} \underset{k_\text{d}(n_\text{S}+n_\text{T},0,T(t))}{\overset{k_\text{h2}}{\rightleftharpoons}} \text{G}_{3,4}$$

$$\text{ssTh}_{3,4} \underset{k_\text{d}(n_\text{S}+n_\text{B},0,T(t))}{\overset{k_\text{h1}(n_\text{ThL})}{\rightleftharpoons}} \text{Th}_{3,4}$$

$$\text{ssTh}_{3,4} + \text{S}_{3,4} \underset{k_\text{d}(3+n_\text{T}+n_\text{S}+n_\text{B},0,T(t))}{\overset{k_\text{h2}}{\rightleftharpoons}} \text{waste}_{3,4}$$

$$\text{G-S}_{4,5} \underset{k_\text{d}(n_\text{S}+n_\text{T}+1,n_\text{B},T(t))}{\overset{k_\text{h1}(n_\text{S}-2+n_\text{LT}+n_\text{L}+10)}{\rightleftharpoons}} \text{G}_{4,5}$$

$$\text{G-S}_{4,5} + \text{S}_{3,4} \underset{k_\text{d}(n_\text{T}+n_\text{S}+n_\text{B},0,T(t))}{\overset{k_\text{h2}}{\rightleftharpoons}} \text{SG-S}_{3,4,5}$$

$$\text{G-S}_{4,5} + \text{F}_4 \underset{k_\text{d}(n_\text{S}+n_\text{T}+n_\text{B},0,T(t))}{\overset{k_\text{h2}}{\rightleftharpoons}} \text{GF-S}_{4,5}$$

$$\text{G-S}_{4,5} + \text{R}_5 \underset{k_\text{d}(n_\text{S}+2n_\text{T},0,T(t))}{\overset{k_\text{h2}}{\rightleftharpoons}} \text{G-SR}_{4,5}$$

$$\text{G-SR}_{4,5} + \text{S}_{3,4} \underset{k_\text{d}(n_\text{T}+n_\text{S}+n_\text{B},0,T(t))}{\overset{k_\text{h2}}{\rightleftharpoons}} \text{SG-SR}_{3,4,5}$$

$$\text{G-SR}_{4,5} + \text{F}_4 \underset{k_\text{d}(n_\text{S}+n_\text{T}+n_\text{B},0,T(t))}{\overset{k_\text{h2}}{\rightleftharpoons}} \text{GF-SR}_{4,5}$$

$$\text{GF-S}_{4,5} + \text{R}_5 \underset{k_\text{d}(n_\text{S}+2n_\text{T},0,T(t))}{\overset{k_\text{h2}}{\rightleftharpoons}} \text{GF-SR}_{4,5}$$

$$\text{R}_5 + \text{Q}_5 \underset{k_\text{d}(n_\text{S}+n_\text{T}-1,0,T(t))}{\overset{k_\text{h2}}{\rightleftharpoons}} \text{RQ}_5$$

The following set of reactions was added for simulations shown in Figs. S12b and S12d:

$$\text{waste}_{3,4} + \text{G}_3 \underset{k_\text{d}(n_\text{S}-5,0,T(t))}{\overset{k_\text{h2}}{\rightleftharpoons}} \text{wasteG}_{3,4}$$

$$\text{wasteG}_{3,4} \underset{k_\text{e}(k_\text{b},-2,-n_\text{ThL},0,T(t))}{\overset{k_\text{b}}{\rightleftharpoons}} \text{Th}_{3,4} + \text{G}_{3,4}$$

where $n_\text{ThL} = 22$ is the loop size in the threshold, $k_\text{b} = 1$ per second is branch migration rate, and $k_\text{e}(k, l, n, s)$ is defined in Supplementary Note 2.3.

2.8 Modeling the kinetics of a reusable logic circuit

The following set of reactions was used for simulating the kinetics of a reusable logic circuit (Fig. 5b). W, A, and H represent total signal, total gate, and total threshold, respectively, for modeling toehold occlusion that occurs between any pair of signal and gate or threshold species.

ampCRN[$concTh, concG, i, j, k_{\text{list}}$] represents an amplification gate with threshold concentration $concTh$, gate concentration $concG$, gate identity i, a single input j, and a list of outputs k_{list}, where each of the following reaction with a k applies to all $k \in k_{\text{list}}$:

$$\mathrm{S}_{j,i} + \mathrm{Th}_{j,i} \underset{k_{\mathrm{e}}(k_{\mathrm{f}},-10,22,0)}{\overset{k_{\mathrm{f}}}{\rightleftharpoons}} \mathrm{waste}_{j,i}$$

$$\mathrm{S}_{j,i} + \mathrm{G}_{i,k} \underset{k_{\mathrm{d}}}{\overset{k_{\mathrm{h2}}}{\rightleftharpoons}} \mathrm{sG}_{j,i,k}$$

$$\mathrm{sG}_{j,i,k} \underset{k_{\mathrm{b1}}}{\overset{k_{\mathrm{b}}}{\rightleftharpoons}} \mathrm{Gs}_{j,i,k}$$

$$\mathrm{Gs}_{j,i,k} \underset{k_{\mathrm{h1}}(33)}{\overset{k_{\mathrm{d1}}}{\rightleftharpoons}} \mathrm{G\text{-}S}_{j,i,k}$$

$$\mathrm{G\text{-}S}_{j,i,k} \underset{k_{\mathrm{d2}}}{\overset{k_{\mathrm{h1}}(13)}{\rightleftharpoons}} \mathrm{G\text{-}s}_{j,i,k}$$

$$\mathrm{G\text{-}S}_{j,i,k} + \mathrm{F}_i \underset{k_{\mathrm{f}}}{\overset{k_{\mathrm{f}}}{\rightleftharpoons}} \mathrm{S}_{j,i} + \mathrm{GF\text{-}S}_{i,k}$$

$$\mathrm{G\text{-}G}_{i,j,k} + \mathrm{F}_i \underset{k_{\mathrm{f}}}{\overset{k_{\mathrm{f}}}{\rightleftharpoons}} \mathrm{S}_{j,i} + \mathrm{GF\text{-}G}_{i,k}$$

$$\mathrm{G}_{i,k} + \mathrm{F}_i \underset{k_{\mathrm{e}}(k_{\mathrm{l}},0,23,0)}{\overset{k_{\mathrm{l}}}{\rightleftharpoons}} \mathrm{GF\text{-}S}_{i,k} \text{ (leak)}$$

$$\mathrm{Th}_{j,i} + \mathrm{W} \underset{k_{\mathrm{o2}}}{\overset{k_{\mathrm{h2}}}{\rightleftharpoons}} \mathrm{wTh}_{j,i} \text{ (occlusion)}$$

$$\mathrm{G}_{i,k} + \mathrm{W} \underset{k_{\mathrm{o1}}}{\overset{k_{\mathrm{h2}}}{\rightleftharpoons}} \mathrm{wG}_{i,k} \text{ (occlusion)}$$

$$\mathrm{GF\text{-}S}_{i,k} + \mathrm{W} \underset{k_{\mathrm{o1}}}{\overset{k_{\mathrm{h2}}}{\rightleftharpoons}} \mathrm{wGF\text{-}S}_{i,k} \text{ (occlusion)}$$

$$\mathrm{GF\text{-}G}_{i,k} + \mathrm{W} \underset{k_{\mathrm{o1}}}{\overset{k_{\mathrm{h2}}}{\rightleftharpoons}} \mathrm{wGF\text{-}G}_{i,k} \text{ (occlusion)}$$

$$\mathrm{G\text{-}S}_{j,i,k} + \mathrm{W} \underset{k_{\mathrm{o1}}}{\overset{k_{\mathrm{h2}}}{\rightleftharpoons}} \mathrm{Gw\text{-}S}_{j,i,k} \text{ (occlusion)}$$

$$\mathrm{G\text{-}G}_{j,i,k} + \mathrm{W} \underset{k_{\mathrm{o1}}}{\overset{k_{\mathrm{h2}}}{\rightleftharpoons}} \mathrm{Gw\text{-}G}_{j,i,k} \text{ (occlusion)}$$

$$\mathrm{S}_{j,i} + \mathrm{A} \underset{k_{\mathrm{o1}}}{\overset{k_{\mathrm{h2}}}{\rightleftharpoons}} \mathrm{sA}_{j,i} \text{ (occlusion)}$$

$$\mathrm{S}_{j,i} + \mathrm{H} \underset{k_{\mathrm{o2}}}{\overset{k_{\mathrm{h2}}}{\rightleftharpoons}} \mathrm{sH}_{j,i} \text{ (occlusion)}$$

intCRN[$concG, i, j_{\text{list}}, k$] represents an integration gate with concentration $concG$, identity i, a list of inputs j_{list}, and a single output k, where each of the following reaction with a j_0, the upstream node of j, and j applies to all pairs of $\{j_0, j\} \in j_{\text{list}}$:

$$\text{G-s}_{j_0,j,i} + \text{G}_{i,k} \underset{k_\text{r}}{\overset{k_\text{f}}{\rightleftharpoons}} \text{G-sG}_{j_0,j,i} + \text{S}_{i,k}$$

$$\text{G-sG}_{j_0,j,i} \underset{k_\text{e}(k_\text{b2},0,3,0)}{\overset{k_\text{b2}}{\rightleftharpoons}} \text{G-G}_{j_0,j,i}$$

$$\text{G-S}_{j_0,j,i} + \text{G}_{i,k} \xrightarrow{k_\text{f}} \text{G-G}_{j_0,j,i} + \text{S}_{i,k}$$

$$\text{GF-S}_{j,i} + \text{G}_{i,k} \xrightarrow{k_\text{f}} \text{GF-G}_{j,i} + \text{S}_{i,k}$$

$$\text{G}_{i,k} + \text{W} \underset{k_\text{o1}}{\overset{k_\text{h2}}{\rightleftharpoons}} \text{wG}_{i,k} \text{ (occlusion)}$$

$$\text{G-S}_{j_0,j,i} + \text{A} \underset{k_\text{o1}}{\overset{k_\text{h2}}{\rightleftharpoons}} \text{G-sA}_{j_0,j,i} \text{ (occlusion)}$$

$$\text{G-s}_{j_0,j,i} + \text{A} \underset{k_\text{o1}}{\overset{k_\text{h2}}{\rightleftharpoons}} \text{G-sA}_{j_0,j,i} \text{ (occlusion)}$$

$$\text{GF-S}_{j,i} + \text{A} \underset{k_\text{o1}}{\overset{k_\text{h2}}{\rightleftharpoons}} \text{GF-sA}_{j,i} \text{ (occlusion)}$$

$$\text{G-S}_{j_0,j,i} + \text{H} \underset{k_\text{o2}}{\overset{k_\text{h2}}{\rightleftharpoons}} \text{G-sH}_{j_0,j,i} \text{ (occlusion)}$$

$$\text{G-s}_{j_0,j,i} + \text{H} \underset{k_\text{o2}}{\overset{k_\text{h2}}{\rightleftharpoons}} \text{G-sH}_{j_0,j,i} \text{ (occlusion)}$$

$$\text{GF-S}_{j,i} + \text{H} \underset{k_\text{o2}}{\overset{k_\text{h2}}{\rightleftharpoons}} \text{GF-sH}_{j,i} \text{ (occlusion)}$$

repCRN$[concRep, i, \{j_0, j\}]$ represents a reporter with concentration $concRep$, identity i, and a single input j with upstream node j_0 (the last six occlusion reactions are the same as an integration gate, which were modeled but omitted from the list below):

$$\text{G-s}_{j_0,j,i} + \text{RQ}_i \underset{k_\text{r}}{\overset{k_\text{f}}{\rightleftharpoons}} \text{G-sG}_{j_0,j,i} + \text{Q}_i$$

$$\text{G-sG}_{j_0,j,i} \underset{k_\text{e}(k_\text{b2},0,3,0)}{\overset{k_\text{b2}}{\rightleftharpoons}} \text{G-G}_{j_0,j,i}$$

$$\text{G-S}_{j_0,j,i} + \text{RQ}_i \xrightarrow{k_\text{f}} \text{G-G}_{j_0,j,i} + \text{Q}_i$$

$$\text{GF-S}_{j,i} + \text{RQ}_i \xrightarrow{k_\text{f}} \text{GF-R}_{j,i} + \text{Q}_i$$

$$\text{RQ}_i + \text{W} \underset{k_\text{o1}}{\overset{k_\text{h2}}{\rightleftharpoons}} \text{wRQ}_i \text{ (occlusion)}$$

logic$[logic, i_1, i_2, j_\text{list}, k_\text{list}]$ represents a logic gate with function $logic$ = AND or OR, composed of two nodes i_1 and i_2, a list of inputs j_list, and a list of outputs k_list:

$$concInt = \text{length}(j_\text{list})$$

$$\text{If } logic = \text{OR}, concTh = 0.8, \text{otherwise } concTh = 0.6 + \text{length}(j_\text{list}) - 1$$

$$concAmp = 1$$

$$\text{intCRN}[concInt, i_1, j_\text{list}, i_2]$$

$$\text{ampCRN}[concTh, concAmp, i_2, i_1, k_\text{list}]$$

inputfanout$[i, k_{\text{list}}]$ represents an input fan-out gate with identity i and a list of outputs k_{list} (h indicates a history domain that can be omitted in input strands):

$$\text{ampCRN}[0, 1, i, \text{h}, k_{\text{list}}]$$

The Fibonacci logic circuit shown in Fig. 6 was modeled as follows.

$$\begin{gathered}
\text{inputfanout}[9, \{34, 36\}] \quad (x_2^0) \\
\text{inputfanout}[11, \{32, 38\}] \quad (x_2^1) \\
\text{inputfanout}[13, \{34\}] \quad (x_3^0) \\
\text{inputfanout}[15, \{32\}] \quad (x_3^1) \\
\text{inputfanout}[17, \{32, 38\}] \quad (x_4^0) \\
\text{inputfanout}[19, \{34, 36\}] \quad (x_4^1) \\
\text{logic}[\text{OR}, 32, 33, \{\{h, 15\}, \{h, 17\}, \{h, 11\}\}, \{40\}] \\
\text{logic}[\text{AND}, 34, 35, \{\{h, 13\}, \{h, 19\}, \{h, 9\}\}, \{42\}] \\
\text{logic}[\text{OR}, 36, 37, \{\{h, 19\}, \{h, 9\}\}, \{40\}] \\
\text{logic}[\text{AND}, 38, 39, \{\{h, 17\}, \{h, 11\}\}, \{42\}] \\
\text{logic}[\text{AND}, 40, 41, \{\{32, 33\}, \{36, 37\}\}, \{44\}] \\
\text{logic}[\text{OR}, 42, 43, \{\{34, 35\}, \{38, 39\}\}, \{46\}] \\
\text{repCRN}[2, 44, \{40, 41\}] \quad (y^0) \\
\text{repCRN}[2, 46, \{42, 43\}] \quad (y^1)
\end{gathered}$$

The following rates were used for all reactions: $k_{\text{d}} = 0.5$, $k_{\text{d1}} = 0.05$, $k_{\text{d2}} = 10$, $k_{\text{b}} = 1$, $k_{\text{b1}} = 1$, and $k_{\text{b2}} = 1$ per second; $k_{\text{h2}} = 2 \times 10^6$, $k_{\text{f}} = 2 \times 10^6$, $k_{\text{r}} = 10^5$, and $k_{\text{l}} = 5$ per molar per second. $k_{\text{o1}} = 5$ per second was used for occlusion between any signal and gate, whereas $k_{\text{o2}} = 0.5$ per second was used for occlusion between any signal and threshold. The difference between k_{o1} and k_{o2} is due to the length of the toehold: threshold molecules have a longer 10-nt toehold to allow for faster thresholding that consumes an input below the threshold concentration before any leftover input is amplified by the downstream gate. Strongly occlusion is expected for a longer toehold even though the common sequence remains at 7 nucleotides, because some sequence complementary may be present within the 3-nt extended toehold domain when there are many distinct signal strands in a large circuit. Formulas for deriving the values of k_{h1} and k_{e} are specified in Supplementary Note 2.3. The total signal W was at 32×, including 2× or 4× fuel for each of the six input fan-out gates and 2× fuel for each of the six logic gates. The total gate A was at 34×, including 1× or 2× gate for each of the six input fan-out gates, 2× or 3× integration gate and 1× amplification gate for each of the six logic gates, and 4× reporters. The total threshold H was at 8.2×, including 0.8× threshold for each of the three OR gates and 1.6× or 2.6× threshold for each of the three AND gates. The standard concentration 1× was at 100 nM.

Note that in order to explain the experimental data shown in Fig. 6c, occlusion between signal and gate in the logic circuit was modeled to be 10 times weaker than that in the winner-take-all neural network. We suspect this is due to the inaccuracy of the approximation for modeling occlusion grows larger with a higher total concentration of all species. In practice, the concentrations of total signal, gate, and threshold will be smaller, as some of the molecules will become consumed in circuit computation.

3 Supplementary data and analysis

3.1 Kinetics of a DNA catalyst

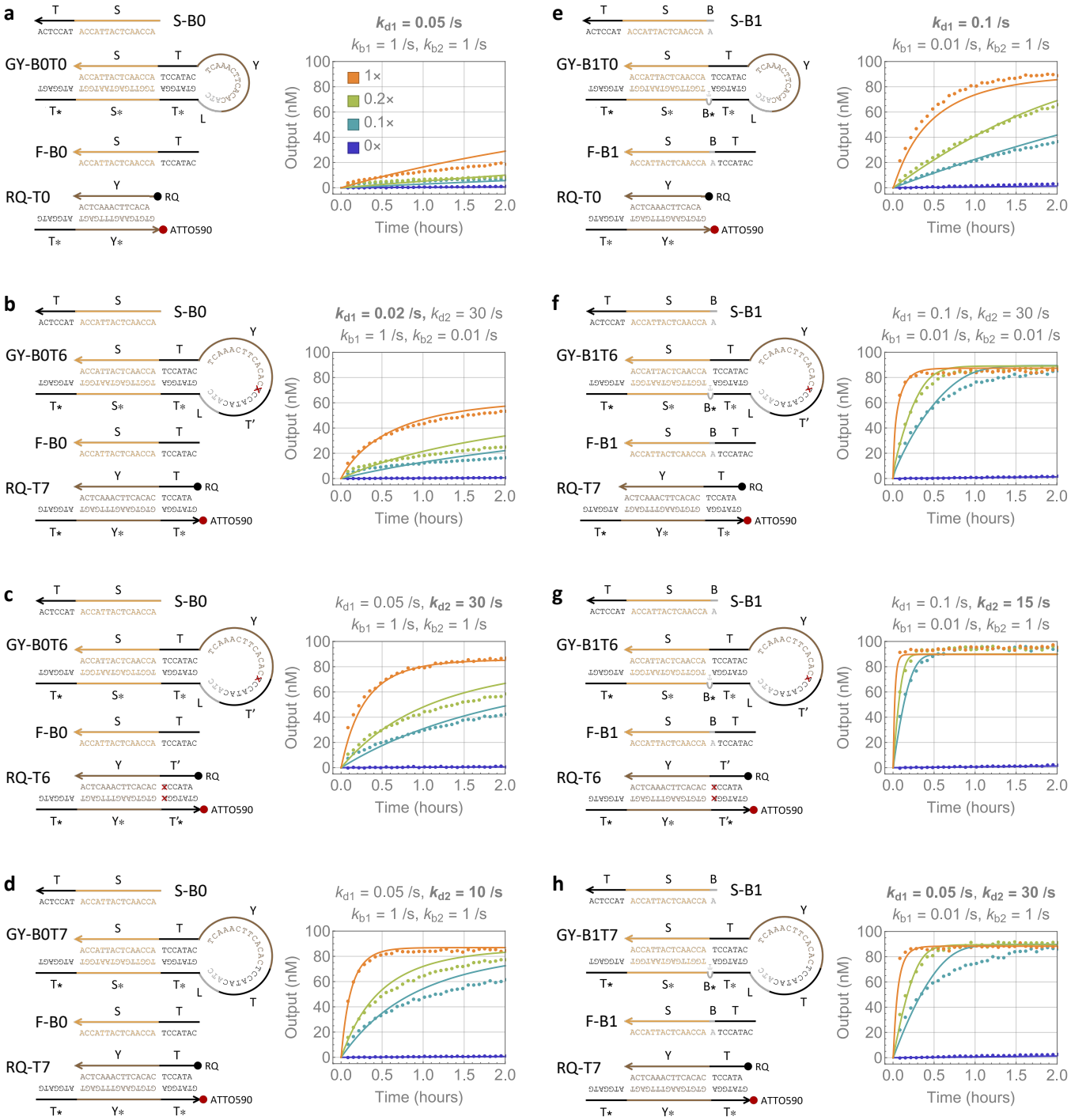

Fig. S13 | Simulations and fluorescence kinetics experiments of eight distinct designs of a DNA catalyst. BxTy in the gate names (e.g. GY-B0T0) indicates a x-nt bulge and a y-nt additional toehold in the hairpin loop. Bx in the input and fuel names (e.g. S-B0 and F-B0) match the bulge size in the gate that they react with. Ty in the reporter names (e.g. RQ-T0) indicate a y-nt additional toehold near the fluorophore and quencher.

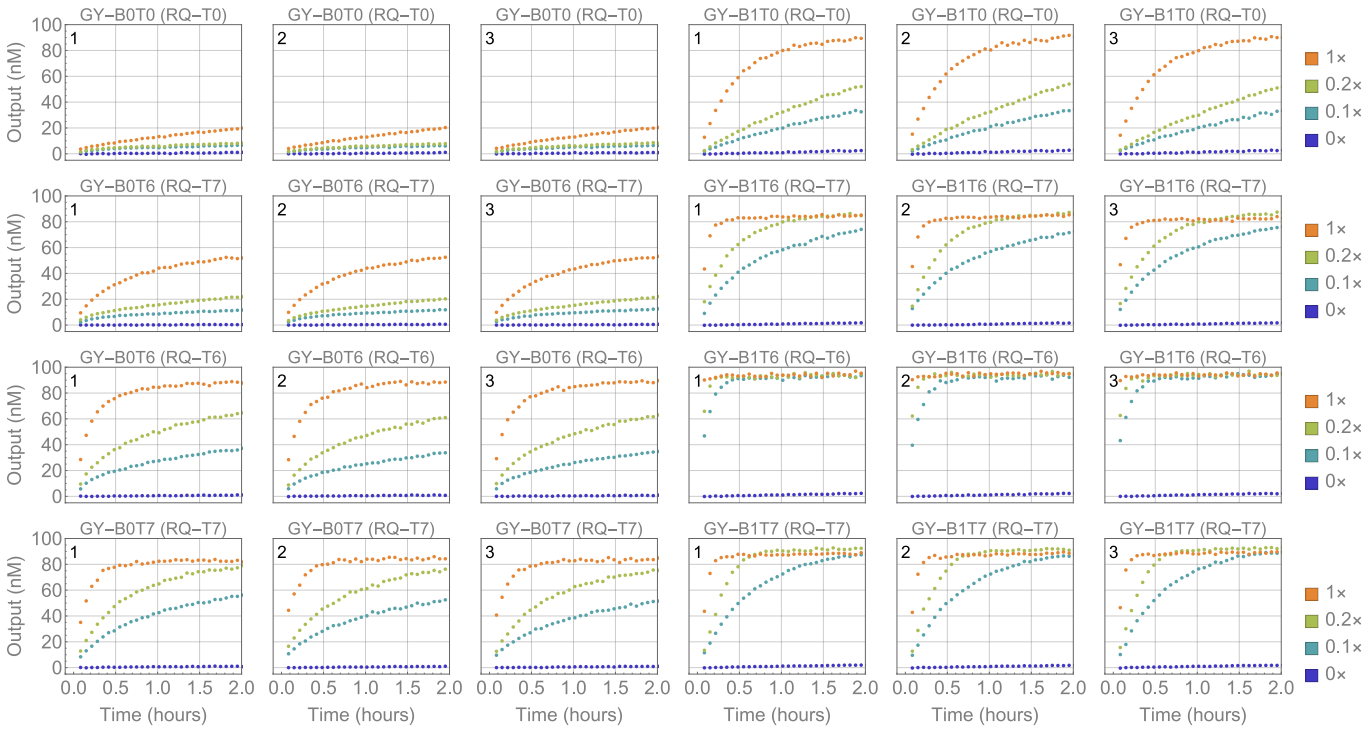

Fig. S14 | Reproducibility of kinetics of the DNA catalyst. Each of the experiments shown in Fig. S13 was repeated three times.

Modeling of the DNA catalyst is explained in Supplementary Note 2.3. Below we discuss how the key rate constants, k_{d1}, k_{d2}, k_{b1}, k_{b2}, and k_l, were estimated based on experimental data. The other rate constants were previously established (k_{h2}, k_d, k_b, k_f, k_r), or estimated based on thermodynamic parameters (k_{h1}) and equilibrium constants (reverse rates for k_{b2} and k_l).

Experiments for GY-B0T0 (Fig. S13a) was used to derive k_{d1}, the dissociation rate of a 7-nt toehold that opens a large 16 to 23-nt hairpin loop, because all other rates shown in Fig. S8 are either known or irrelevant for this design. Applying the value of k_{d1}, experiments for GY-B0T6 and GY-B0T7 (Figs. S13c and S13d) were then used to derive k_{d2}, the dissociation rate of a 6 or 7-nt toehold while opening a small 3-nt hairpin loop. The difference between k_{d2} and k_{d1} for a 7-nt toehold with the same sequence can be explained by the increased base pair breathing near the small loop. The difference between k_{d2} for a 6-nt and 7-nt toehold can be explained by the removal of a weak A-T base pair.

Applying the value of k_{d1} and k_{d2}, simulations for GY-B0T6 with a mismatched reporter RQ-T7 did not result in quantitative agreement with the experiments shown in Fig. S13b, when $k_{b2} = 0.01$ per second was utilized for branch migration rate with the addition of a 1-nt bulge in the reporter-output complex (SG-YR shown in Fig. S8). Changing k_{b2} to 0.001 per second resulted in better agreement, but conflicted with the value of k_{b1} and k_{b2} that explained all other experiments well. As both $k_{b1} = 0.01$ and $k_{b2} = 0.01$ per second were used for the rate of branch migration with the addition of a 1-nt bulge, in the gate or the reporter-output complex, respectively, we decided to keep these rates consistent across all simulations. We thus explored alternative values of k_{d1} for explaining the experiments shown in Fig. S13b. A 2.5-fold decrease in k_{d1} resulted in quantitative agreement between simulations and experiments. This change is relatively small and can be explained by

synthesis errors within the toehold domain. Given the variations in strand and complex purity (Supplementary Note 1.5), we concluded that the adjusted value was reasonable.

Compared to GY-B0T0, a 2-fold increase in k_{d1} was necessary to explain the experiments for GY-B1T0 (Fig. S13e). This increase is reasonable considering the stacking bond adjacent to the dissociation toehold. When a bulge in the hairpin gate was introduced, the two-nucleotide sequence next to the toehold changed from AC to AA, resulting in more fraying near the end of the S domain (on SGy shown in Fig. S8) that could weaken the stacking bond. Applying the value of k_{d1} derived from the experiments for GY-B1T0, quantitative agreement between simulations and experiments for GY-B1T6 with both reporters RQ-T7 and RQ-T6 were achieved with a small adjustment in k_{d2} for RQ-T6 (Figs. S13f and S13g). However, an exception was observed in experiments for GY-B1T7 (Fig. S13h), where the original k_{d1} value used for GY-B0T0 through GY-B0T7 fitted the experimental data better than the increased value.

Overall, $k_{d1} = 0.02$–0.1 per second and $k_{d2} = 10$–30 per second explained all kinetics experiments for the eight distinct designs of a reusable DNA catalyst. Given that the circuit performance, including reaction completion, kinetics, and variation, is sensitive to these rate constants (Fig. S9), a 5-fold and 3-fold range of adjustment are unsurprising.

Branch migration rate with the addition of a 1-nt bulge, $k_{b1} = 0.01$ per second, was estimated based on the experiments for the four designs with a bulge (Figs. S13e to S13h). $k_{b2} = 0.01$ per second was estimated based on the experiments for the two designs with a mismatched reporter (Figs. S13b and S13f), with the assumption that it should agree with k_{b1}.

Leak rate between the gate and the fuel, $k_l = 5$ and 10 per molar per second, was estimated based on the $0\times$ input trajectories in the experiments for the designs without (Figs. S13a to S13d) and with a bulge (Figs. S13e to S13h), respectively. These values are consistent with the previously established rate of toeless strand displacement in a use-once DNA catalyst.[1] The 2-fold increase in leak with a bulge can be explained by the additional base pair gained via removal of the bulge in the leak product.

For simplification, the input strands shown in Fig. S13 omitted a history domain that was present in the experiments shown in Figs. 2c, 2d, 2f, S13–S16. The sequences of the input strands including the history domain are shown in Table S2. We expect the history domain to have a very minor impact on the kinetics of a reusable DNA catalyst. The history domain could have a larger impact on the reset behavior when the input is inactivated using an inhibitor strand with complementary sequence (Fig. 2f, middle plot)—more base pairs for the input-inhibitor binding during heating and cooling could result in more effective input inactivation. However, the amount of input-bound gate should not exceed the amount of fuel-bound gate during reset (the latter is quantified in Fig. S15), and thus is expected to have a minor impact on the performance of subsequent computation when new input is introduced (Fig. 2f, right plot).

3.2 Reset of a DNA catalyst

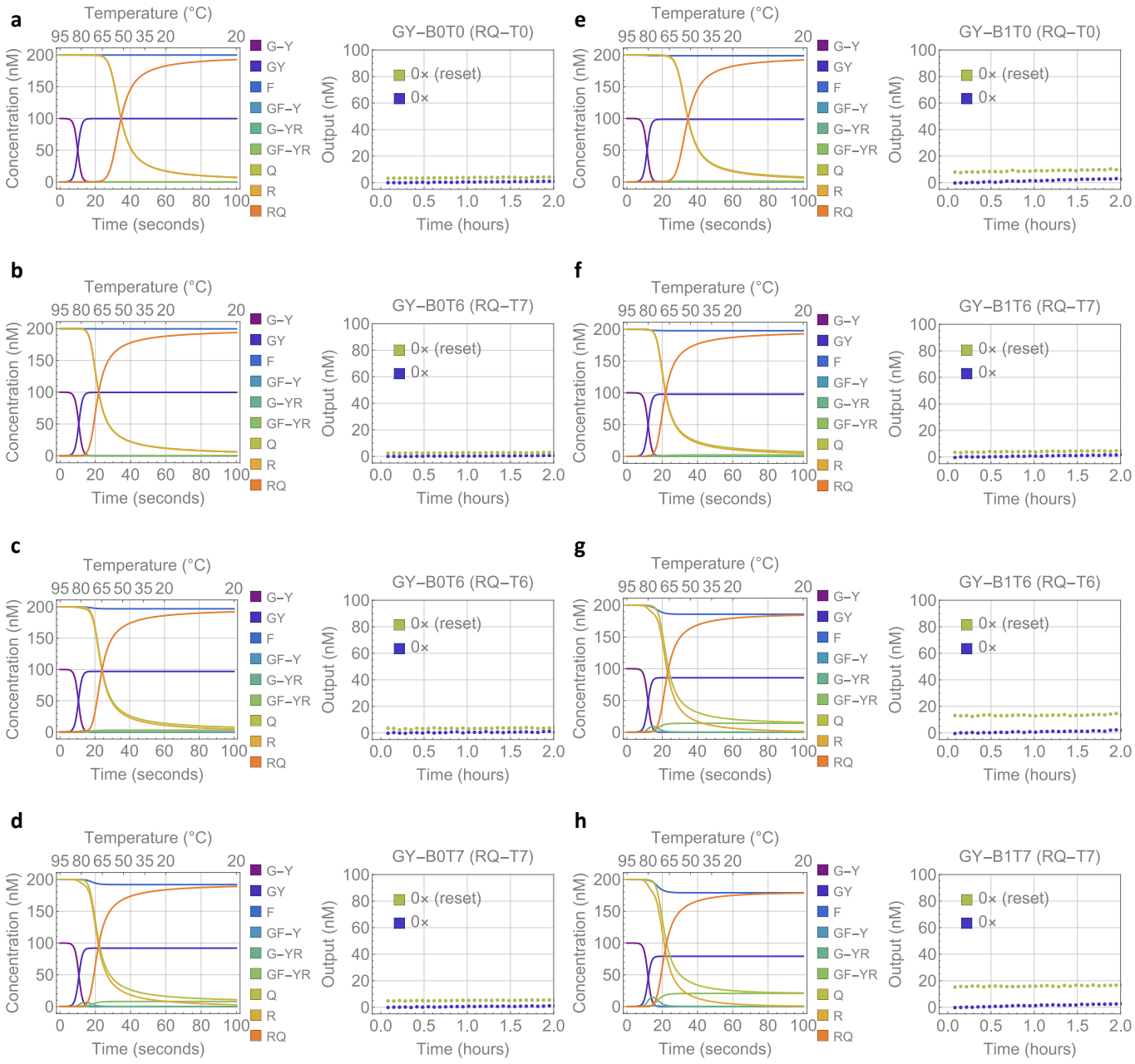

Fig. S15 | Simulations and fluorescence data of resetting eight distinct designs of a DNA catalyst. The catalytic circuit (1× GY, 2× F, and 2× RQ, 1× = 100 nM) without any input (0× S) was heated to 95 °C for five minutes, cooled to 20 °C in one minute, and then stayed at 20 °C for three minutes. Simulations show the one-minute cooling process plus the first 40 seconds of staying at 20 °C. The concentration of fluorescent complex GF-YR after heating and cooling indicates the reset success rate ([GY] ≈ 100 nM − [GF-YR]). Other fluorescent molecules, G-YR and R, are expected to be depleted by the end of cooling, because fuel F (that converts G-YR to GF-YR) and quencher Q (that converts R to RQ) were in excess.

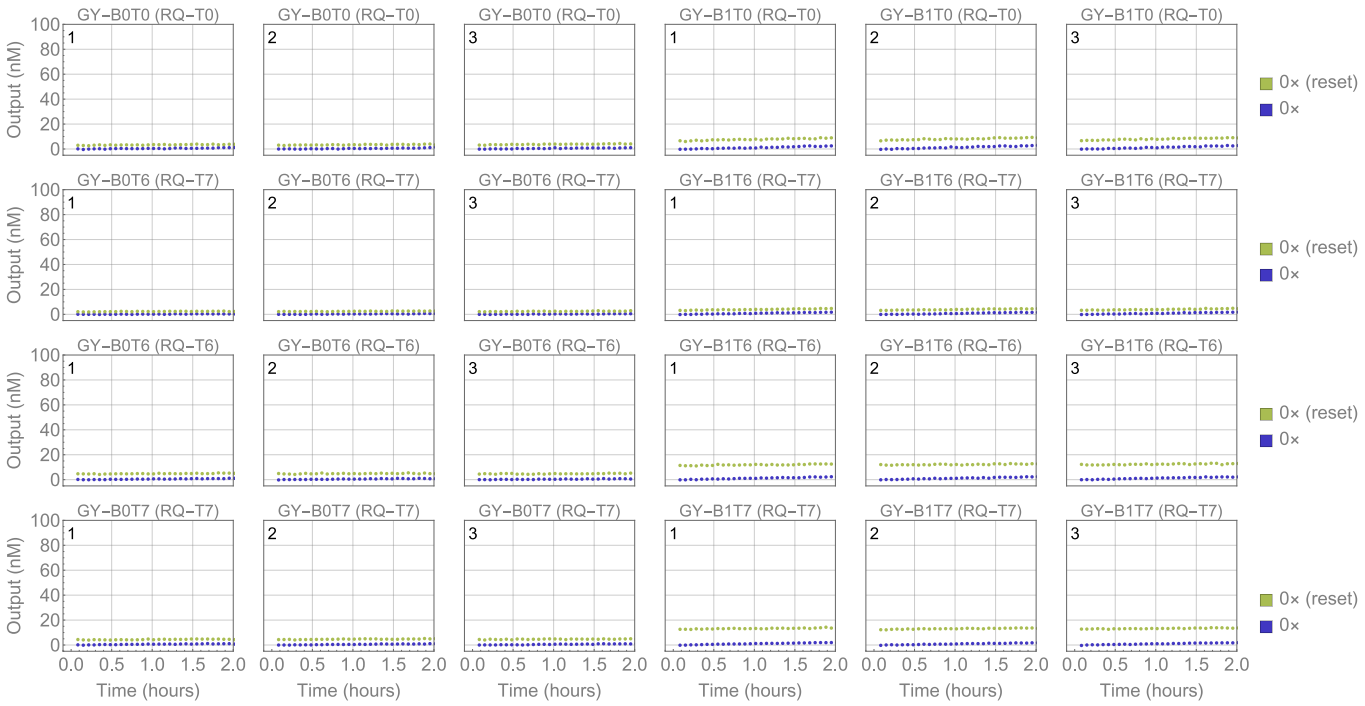

Fig. S16 | Reproducibility of reset of the DNA catalyst. Each of the experiments shown in Fig. S15 was repeated three times.

3.3 Impact of a nucleotide deletion in the loop toehold on reset success rate

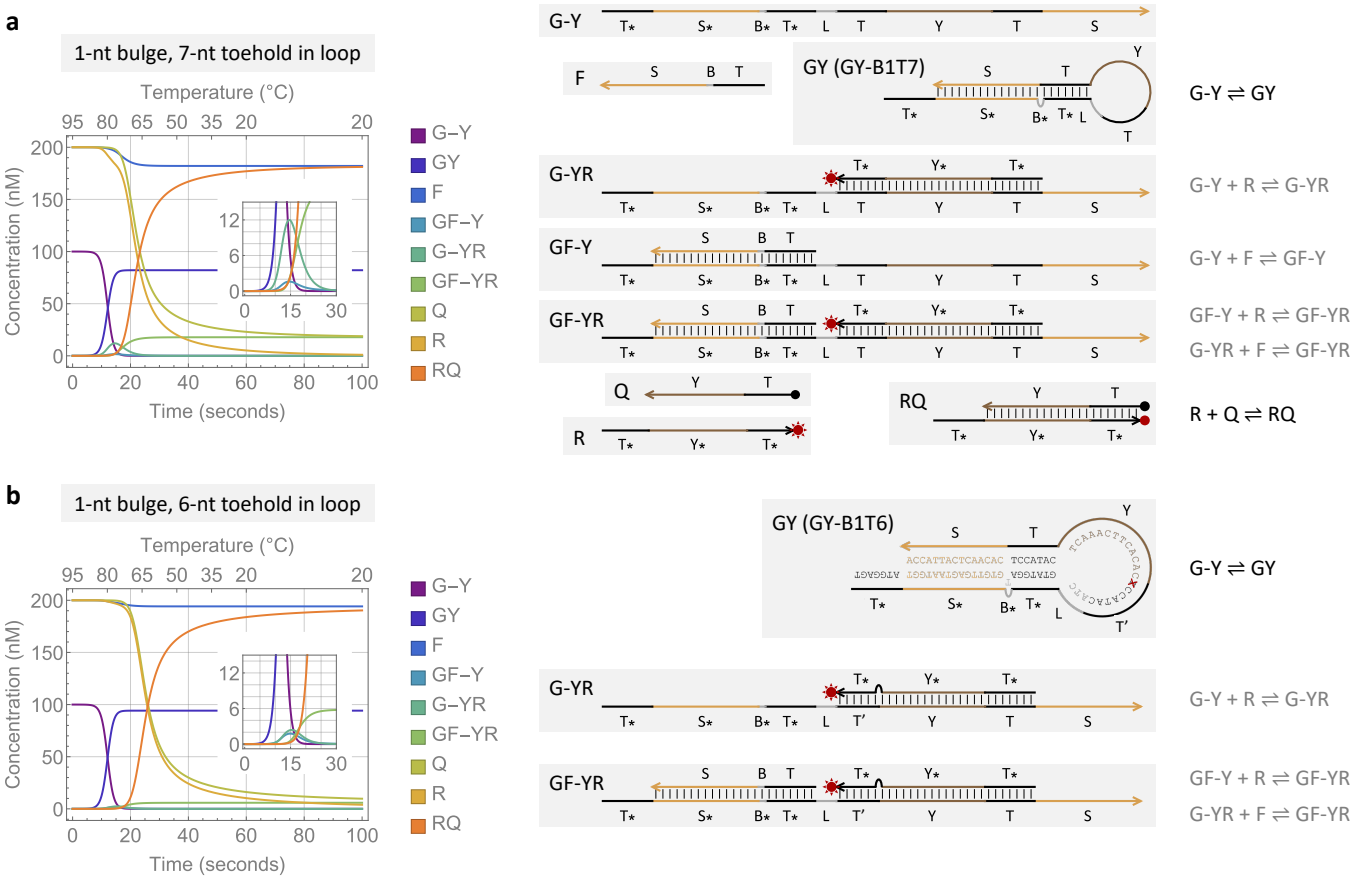

Fig. S17 | Impact of a one-nucleotide deletion in the loop toehold on reset success rate. a,b, Reactions and simulation of resetting a catalytic circuit with a 1-nt bulge and a 7-nt (**a**) or 6-nt (**b**) additional toehold in the hairpin loop. Reactions in black and gray indicate desired and undesired reactions, respectively.

In a catalytic circuit containing a hairpin gate (GY), fuel (F), and reporter (RQ), there are two competing reactions that could prevent the hairpin gate from restoring properly during heating and cooling (Fig. S17a). First, the fluorophore-labeled reporter strand (R) could bind to the single-stranded gate:output (G-Y) at a sufficiently high temperature (G-Y + R ⇌ G-YR). Second, the fuel strand could also bind to the single-stranded gate:output (G-Y + F ⇌ GF-Y), which occurs at a lower temperature because the number of base pairs in GF-Y is fewer than that in G-YR. Without the reporter strand, it would be unlikely for the fuel to bind to the gate because the additional base pair in GF-Y than GY and the entropic cost of forming a bulge in GY are insignificant compared to the entropic cost of bringing together two molecules in GF-Y at a high temperature. However, G-YR has 7 more base pairs than GY. Accordingly, simulation suggested that the reporter strand would start binding to the single-stranded gate:output before all hairpins have fully closed (G-Y + R ⇌ G-YR). With the reporter strand bound, hairpin closing would be inhibited because the S and S∗ domains are now on the two sides of a relatively rigid double-stranded domain and unable to reach well. The fuel strand would then bind to G-YR and form a stable three-stranded complex

(GF-YR) by the end of cooling. Zooming in around 15 seconds (76 °C) in the simulation, we see that the concentration of G-YR increases and then decreases, illustrating the two reactions G-Y + R $\rightleftharpoons$ G-YR and G-YR + F $\rightleftharpoons$ GF-YR that take place sequentially in a temperature ramp. Quantitatively, simulation suggested that roughly 18 nM of the hairpin gate would not be restored, which corresponds to a 82% success rate of reset.

To reduce the impact of the competing reactions, we deleted one nucleotide from the toehold in the hairpin loop (Fig. S17b). This deletion creates a bulge when the reporter strand is bound to the output, which in turn reduces the binding energy and decreases the temperature for which the reaction G-Y + R $\rightleftharpoons$ G-YR could take place. Again zooming in around 15 seconds in the simulation, we now see that the amplitude of the bump in G-YR concentration becomes much smaller, indicating reduced amount of undesired reactions. Because hairpin formation occurs quickly at this temperature, the concentration of single-stranded G-Y drops quickly. Thus even a small (1 to 2 °C) shift in the melting temperature of G-YR already has a significant impact on how much of it could form during heating and cooling. With the one-nucleotide deletion, simulation suggested that roughly 4 nM of the hairpin gate would not be restored, which corresponds to an improved 96% success rate of reset.

3.4 Robustness of reusability

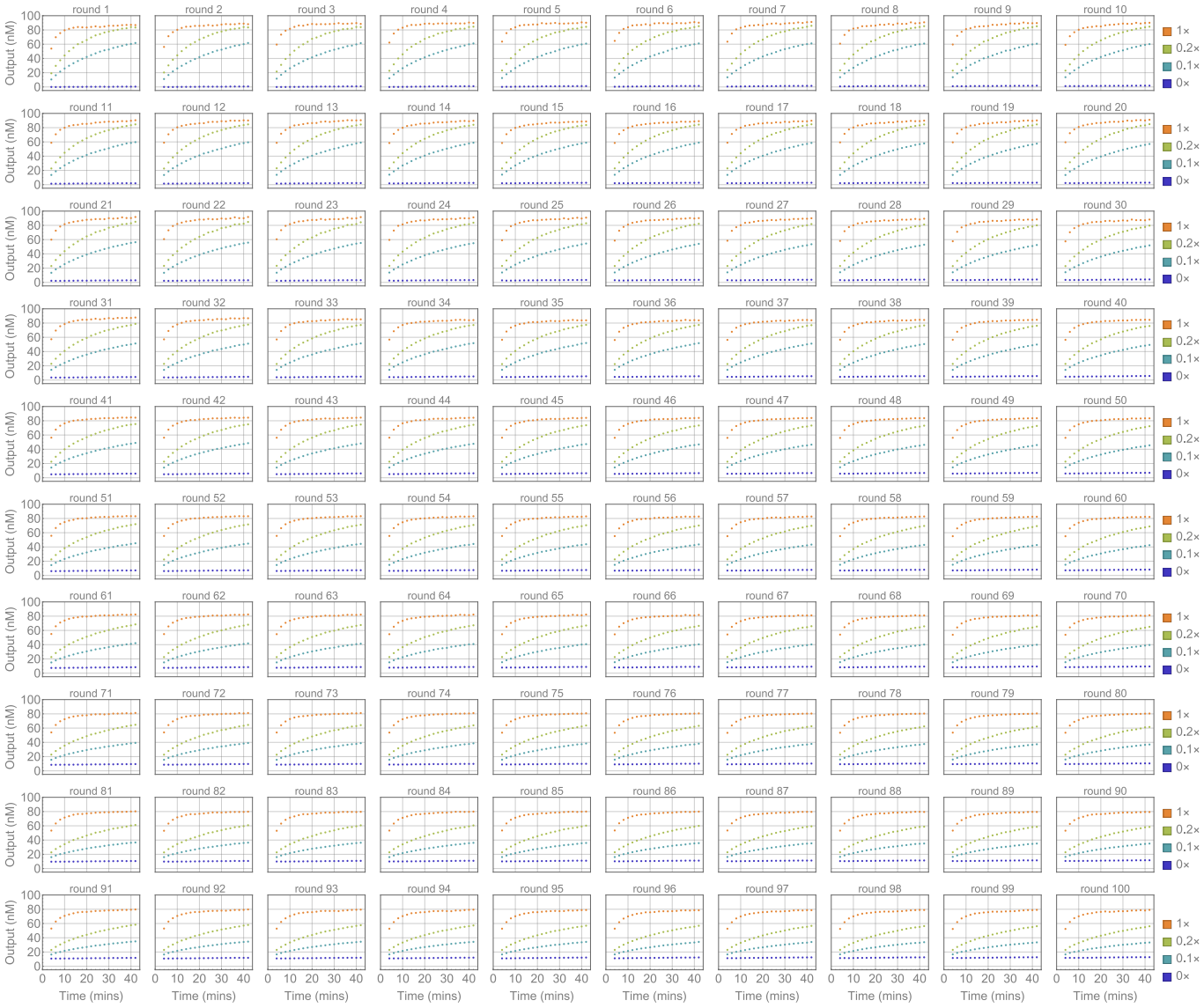

Fig. S18 | Robustness of reusability with a shorter heating time. Fluorescence kinetics experiments of a reusable catalytic DNA circuit with 100 rounds of reset using a protocol that heats for 2 minutes at 95 °C before cooling to 25 °C in 1 minute. Experiments were performed on a quantitative PCR machine and a single sample was used for all data shown in here. Standard concentration $1\times = 100$ nM.

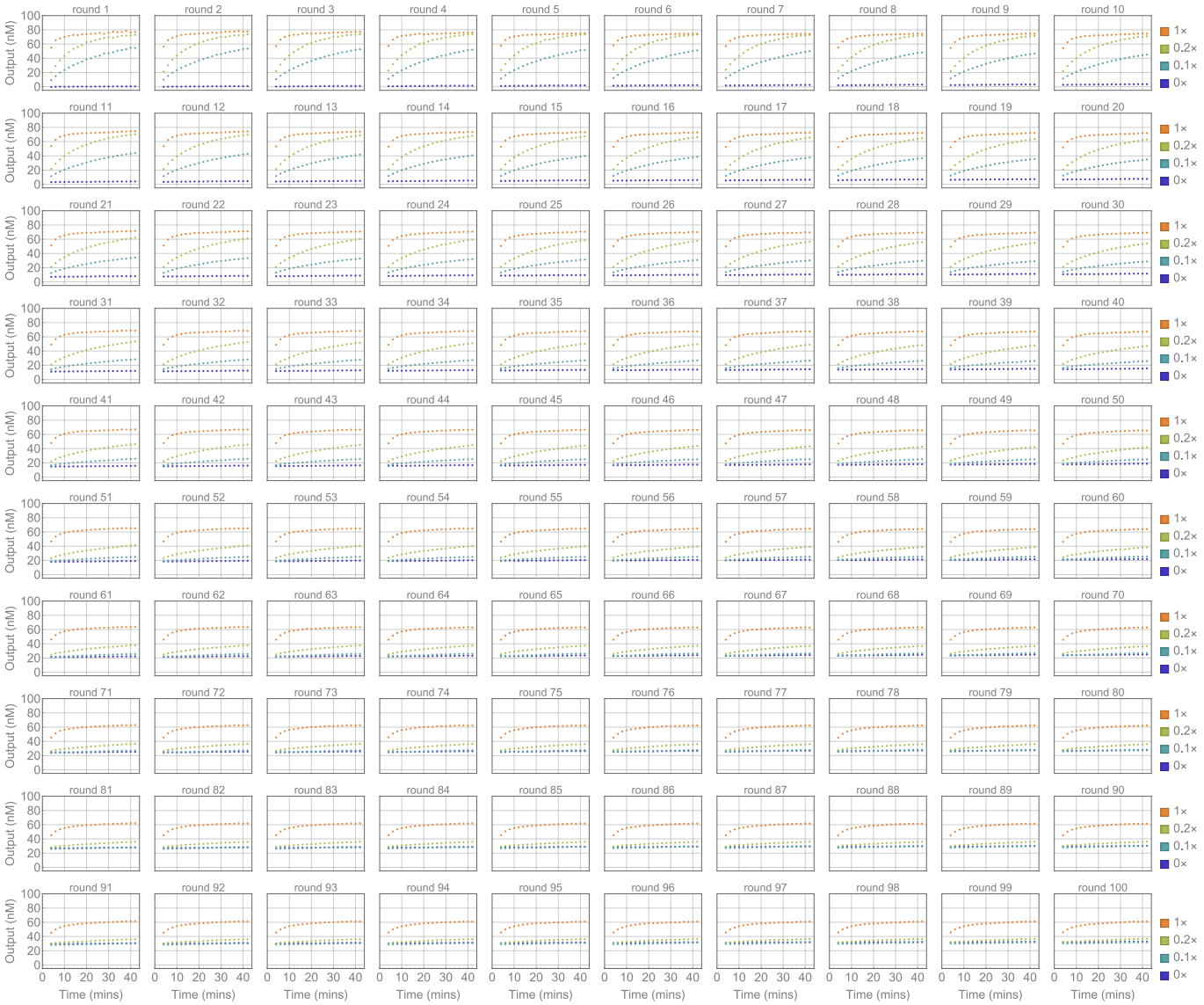

Fig. S19 | Robustness of reusability with a longer heating time. Fluorescence kinetics experiments of a reusable catalytic DNA circuit with 100 rounds of reset using a protocol that heats for 5 minutes at 95 °C before cooling to 25 °C in 1 minute. Experiments were performed on a quantitative PCR machine and a single sample was used for all data shown in here. Standard concentration $1\times = 100$ nM.

3.5 Kinetics problem in a winner-take-all circuit

In a two-input winner-take-all function (Fig. S20a), binary outputs $y_1 = 1$ and $y_2 = 0$ if analog inputs $s_1 > s_2$, whereas $y_1 = 0$ and $y_2 = 1$ if $s_1 < s_2$ ($0 \leq s_1, s_2 \leq 1$). This function can be implemented with three reactions, where the concentration of a species (S_1, Y_1, etc.) indicates the value of a variable (s_1, y_1, etc.):

$$\begin{aligned} S_1 + S_2 + Anh_{1,2} &\xrightarrow{k_f} \emptyset \\ S_1 + GY_1 + F_1 &\xrightarrow{k_s} S_1 + Y_1 \\ S_2 + GY_2 + F_2 &\xrightarrow{k_s} S_2 + Y_2 \end{aligned}$$

An annihilator ($Anh_{1,2}$) facilitates the competition between inputs. Restoration gates (GY_1 and GY_2) and fuels (F_1 and F_2) enable the amplification of the winner. Importantly, annihilation should

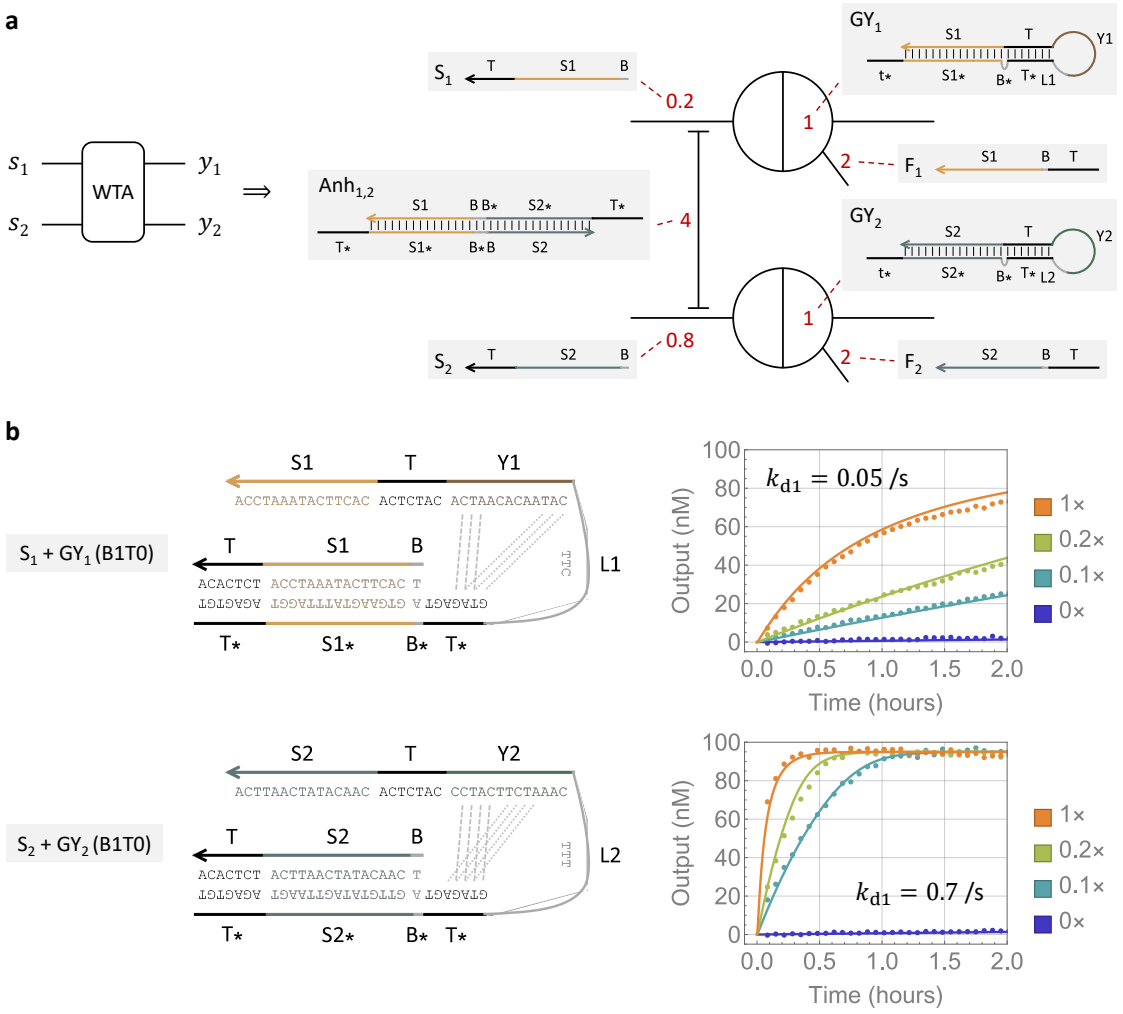

Fig. S20 | Kinetics problem in a winner-take-all circuit. a, Implementation of a two-input winner-take-all function. **b,** Sequence-level diagrams, simulations, and fluorescence kinetics experiments of a pair of DNA catalysts without a loop toehold. In each set of experiments, a single hairpin gate (GY_1 or GY_2), fuel (F_1 or F_2), and reporter (RQ_1 or RQ_2) were present with varying input (S_1 or S_2) concentrations. Two distinct values of k_{d1} were used in simulations for comparing with experiments using the two hairpin gates.

be much faster than signal amplification ($k_f \gg k_s$) so that the loser (lower-concentration input) will be effectively consumed whereas the winner (higher-concentration input) will effectively trigger output production only after it has survived the competition. Moreover, the two amplification reactions should have equal rates, otherwise the input with a higher k_s/k_f ratio will have an advantage for bypassing the annihilator to produce the output, leading to biased competition that is no longer solely determined by input concentrations.

Like in previous work,[4] the rate difference between annihilation and signal amplification was realized by longer toeholds (7-nt T∗) on the annihilator and shorter toeholds (5-nt t∗) on the restoration gates (Fig. S20a). Unlike in previous work, we found that a common toehold was

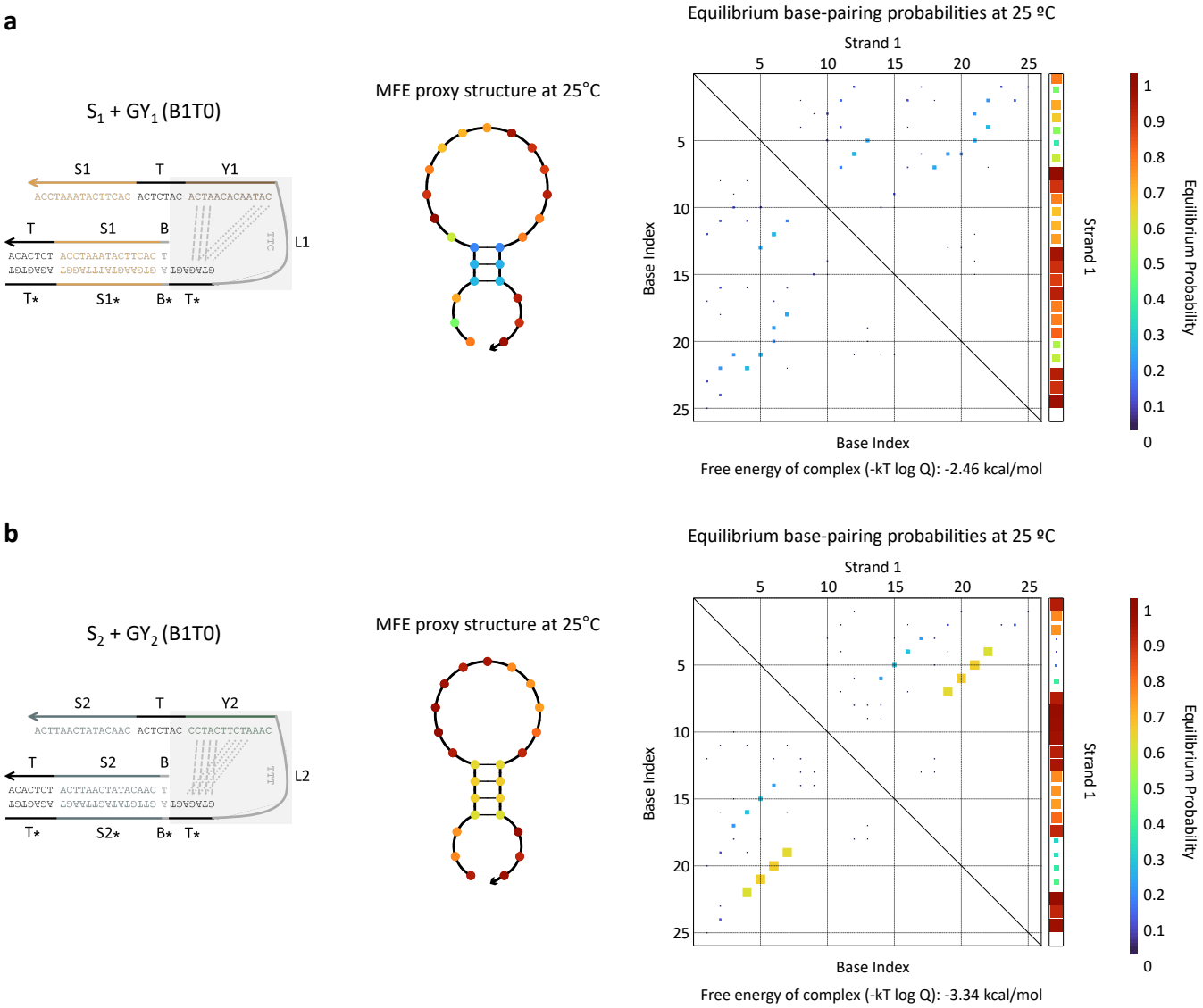

Fig. S21 | NUPACK analysis of two hairpin gates with distinct sequences. Gray box highlights the portion of sequence analyzed, whose minimum free energy (MFE) structure and equilibrium base-paring probabilities at 25°C are shown. Dashed lines in sequence diagrams indicate the strongest group of spurious base pairs shown in the MFE structure whereas dotted lines indicate the second strongest group of spurious base pairs revealed by the equilibrium base-paring probabilities.

insufficient for achieving approximately equal reaction rates in reusable hairpin gates: two gates with the same toehold but distinct long domains resulted in an over 10-fold difference in kinetics (Fig. S20b).

The experimental results were further supported by NUPACK[5,6] analysis (Fig. S21): the two output domains (Y_1 and Y_2) in the hairpin loop both had some interactions with the open toehold ($T*$) when the input is bound to the gate, although the energies of the interactions differed by roughly one weak base pair (-2.46 versus -3.34 kcal/mol). We approximated the effect of the spurious interactions by altering the dissociation rate (k_{d1} and k_{d2}) of the toehold for output release in simulations, which agreed well with the experimental data (Fig. S20b).

3.6 Impact of strand purity on reaction kinetics

To evaluate whether the kinetics difference between the two DNA catalysts (Fig. S20b) was caused by synthesis errors which could have resulted in different effective concentrations of the two hairpin gates, we performed experiments with HPLC purified strands purchased from IDT DNA. No noticeable difference was observed comparing unpurified (Figs. S22c,d) and purified strands (Figs. S22e,f), suggesting that the kinetics problem was not caused by strand purity.

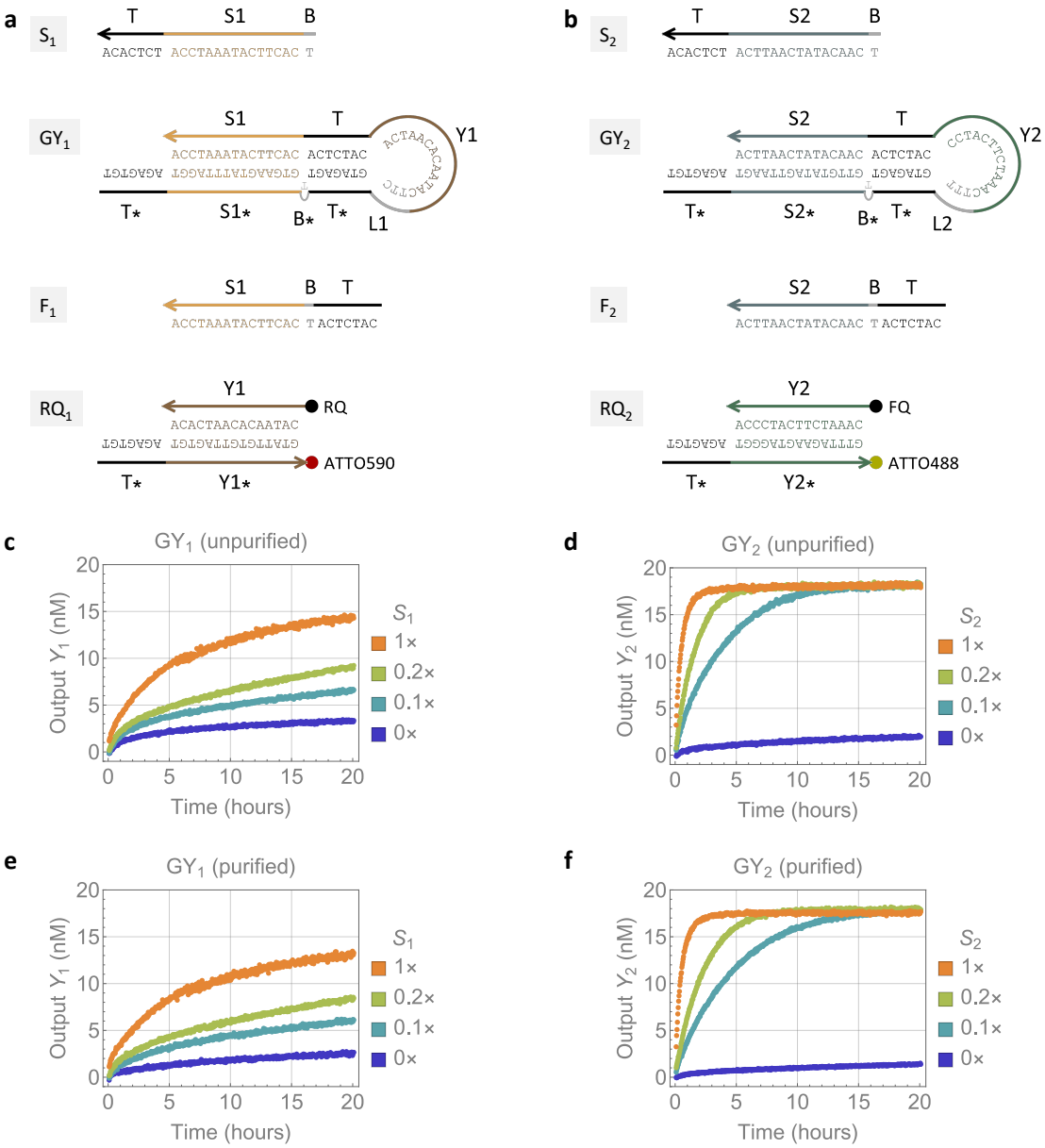

Fig. S22 | Evaluating the impact of strand purity on reaction kinetics. a,b, Sequence diagrams of two catalytic circuits. **c,d,** Fluorescence kinetics data for the two circuits shown in (a) and (b) with unpurified strands (excepted for reporter strands) purchased from IDT DNA. **e,f,** Fluorescence kinetics data for the two circuits shown in (a) and (b) with HPLC purified strands purchased from IDT DNA. Standard concentration $1\times = 20$ nM. Relative concentrations of the input (S_1 or S_2) are shown in the legend. Hairpin gate (GY_1 or GY_2), fuel (F_1 or F_2), and reporter (RQ_1 or RQ_2) were at $1\times$, $2\times$, and $1.5\times$, respectively.

3.7 Impact of reporter reversibility on reaction kinetics

It is known that fluorophore-quencher interaction could provide a binding energy as strong as three base pairs, and it various across distinct fluorophore-quencher pairs. Thus it is more accurate to consider the reporting reaction as a reversible reaction, where the reverse strand displacement is initiated by the fluorophore-quencher interaction (Fig. S23a). Because distinct fluorophore-quencher pairs were used in the two reporters (ATTO590 and RQ versus ATTO488 and FQ), they could result in different reverse rates of the two reporting reactions. This difference would most likely change reaction completion rather than overall kinetics, but we still wanted to verify whether the kinetics difference between the two DNA catalysts (Fig. S20b) was caused by the difference between the two fluorophore-quencher pairs. Thus we performed experiments with varying concentrations of the quencher strand—if the reversibility of the reporter played a significant role here, a large excess (e.g. 5×) of the quencher strand would further slow down the overall reaction kinetics. Our results confirmed that the impact of the reporter reversibility was insignificant (Fig. S23b).

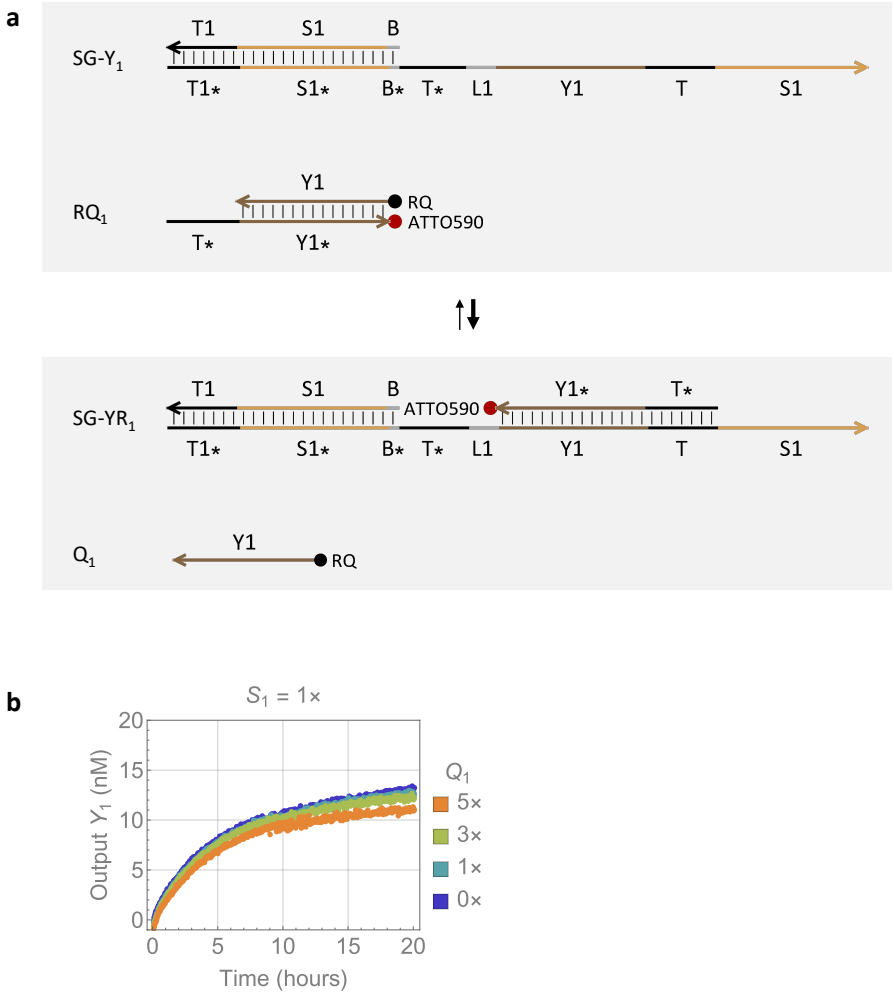

Fig. S23 | Evaluating the impact of reporter reversibility on reaction kinetics. a, Reporting reaction shown as a reversible reaction. Thickness of the arrows indicates relative forward and reverse rates; thicker means faster. **b,** Fluorescence kinetics data for the circuit shown in Fig. S22a with varying concentrations of the quencher strand. Standard concentration 1× = 20 nM. Relative concentrations of the quencher strand (Q_1) are shown in the legend. Input (S_1), hairpin gate (GY_1), fuel (F_1), and reporter (RQ_1) were at 1×, 1×, 2×, and 1.5×, respectively.

3.8 Impact of linker sequence on reaction kinetics

To evaluate whether the kinetics difference between the two DNA catalysts (Fig. S20b) was caused by different sequences of the linker domain within the hairpin loop, we repeated the experiments with revised linker sequences: the L1 sequence (TTC) previously used in GY_1 was replaced by a new linker sequence L3 (AAA), and the L2 sequence (TTT) previously used in GY_2 was replace by the L1 sequence (Figs. S24a and S24b). We did not simply swap the L1 and L2 sequences because L2 sequence in GY_1 would cause the two nucleotides at the 5' and 3' ends of the loop to form a base pair, which would slow down the toehold dissociation rate for opening the hairpin; this is also the reason that the two linker sequences were designed to be different. Compared to Fig. S20b, the change in linker sequences did not result in any noticeable difference in the experimental data (Figs. S24c,d), suggesting that the linker sequence was not responsible for the kinetics problem.

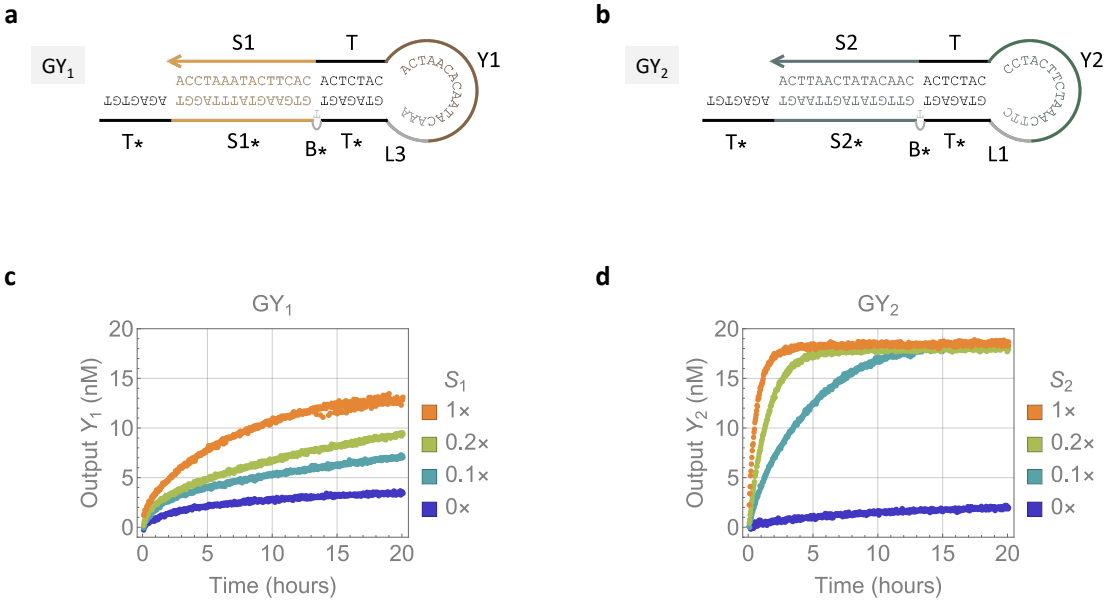

Fig. S24 | Evaluating the impact of linker sequence on reaction kinetics. a,b, Hairpin gates with revised linker sequences. **c,d,** Fluorescence kinetics data for the two circuits shown in Figs. S22a,b with the hairpin gates replaced by those shown here in (a) and (b). Standard concentration $1\times = 20$ nM. Relative concentrations of the input (S_1 or S_2) are shown in the legend. Hairpin gate (GY_1 or GY_2), fuel (F_1 or F_2), and reporter (RQ_1 or RQ_2) were at $1\times$, $2\times$, and $1.5\times$, respectively.

3.9 Impact of branch migration sequence on reaction kinetics

To evaluate whether the kinetics difference between the two DNA catalysts (Fig. S20b) was caused by different sequences of the branch migration domain for opening the hairpin, we repeated the experiments with swapped S_1 and S_2 domains on the two hairpin gates (Figs. S25a,b). Compared to Fig. S20b, this change did not result in any noticeable difference in the experimental data (Figs. S25c,d), suggesting that the branch migration sequence was not responsible for the kinetics problem. At this point, we were able to conclude that the Y_1 and Y_2 domain sequences composing the majority of the hairpin loop in the two gates must be the reason for the kinetics difference.

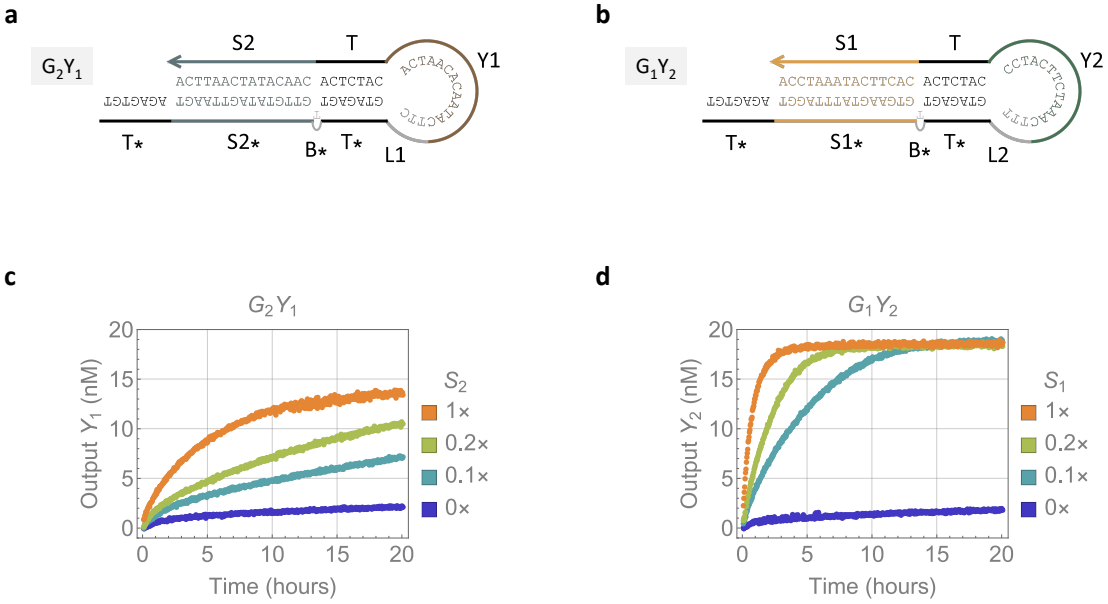

Fig. S25 | Evaluating the impact of branch migration sequence on reaction kinetics. a,b, Hairpin gates with swapped branch migration sequences. **c,d,** Fluorescence kinetics data for the two circuits shown in Figs. S22a,b with the hairpin gates replaced by those shown here in (a) and (b) along with swapped input and fuel strands. Standard concentration $1\times = 20$ nM. Relative concentrations of the input (S_1 or S_2) are shown in the legend. Hairpin gate (GY_1 or GY_2), fuel (F_1 or F_2), and reporter (RQ_1 or RQ_2) were at $1\times$, $2\times$, and $1.5\times$, respectively.

3.10 Impact of loop sequence on reaction kinetics

The next question is: how does the loop sequence affect the overall reaction kinetics? It could affect the reverse rate of output production (i.e. the rate of input release) or the forward rate of reporting, or both. To simplify the system, we removed the open toehold and branch migration domain on the hairpin gate and just kept the hairpin loop with adjacent toeholds, which is essentially the output signal itself (Y_1 or Y_2) plus a linker and toehold T∗ (Figs. S26a,b). Slower kinetics and lower reaction completion level were observed for Y_1 than Y_2 (comparing Fig. S26c to Fig. S26d), suggesting that stronger spurious interactions between the output sequence and toehold T∗ (Fig. S21) increased the rate of reporting.

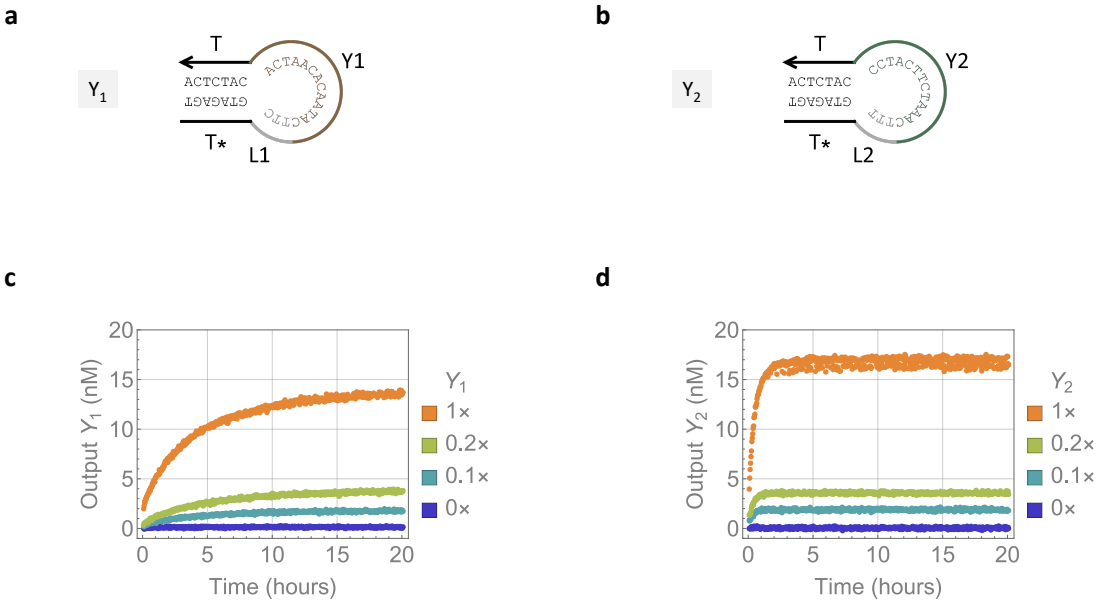

Fig. S26 | Evaluating the impact of loop sequence on reaction kinetics. a,b, Output strands with a linker and T∗ toehold. **c,d,** Fluorescence kinetics data for a single reporting reaction where the reporter RQ_1 or RQ_2 was present with varying concentrations of the output strand shown in (a) or (b). Standard concentration $1\times = 20$ nM. Relative concentrations of the output (Y_1 or Y_2) are shown in the legend. Reporter (RQ_1 or RQ_2) was at $1.5\times$.

This was at first surprising, because stronger secondary structure within the branch migration domain should slow down rather than speed up the reporting reaction. However, it is known that the availability of the toehold plays a much more important role than the availability of the branch migration domain in strand displacement kinetics. In this case, the stronger secondary structure within the branch migration domain could more effectively compete with the toehold for binding to T∗, and thus making the toehold more available for downstream reactions.

To further verify the above hypothesis, we modified the output sequence in hairpin gate GY_2 to reduce the spurious binding predicted by NUPACK: two As were replaced by two Ts to interrupt two A-T base pairs (Fig. S27b). With this modification, slower reaction kinetics was observed in Fig. S27d compared to Fig. S27c, providing direct evidence for the role of the spurious binding.

To achieve better kinetic control, we could introduce more stringent sequence design criteria to minimize spurious binding. However, as shown above, the spurious binding here actually led to faster reaction kinetics. Minimizing spurious binding would allow for similar reaction rates across distinct

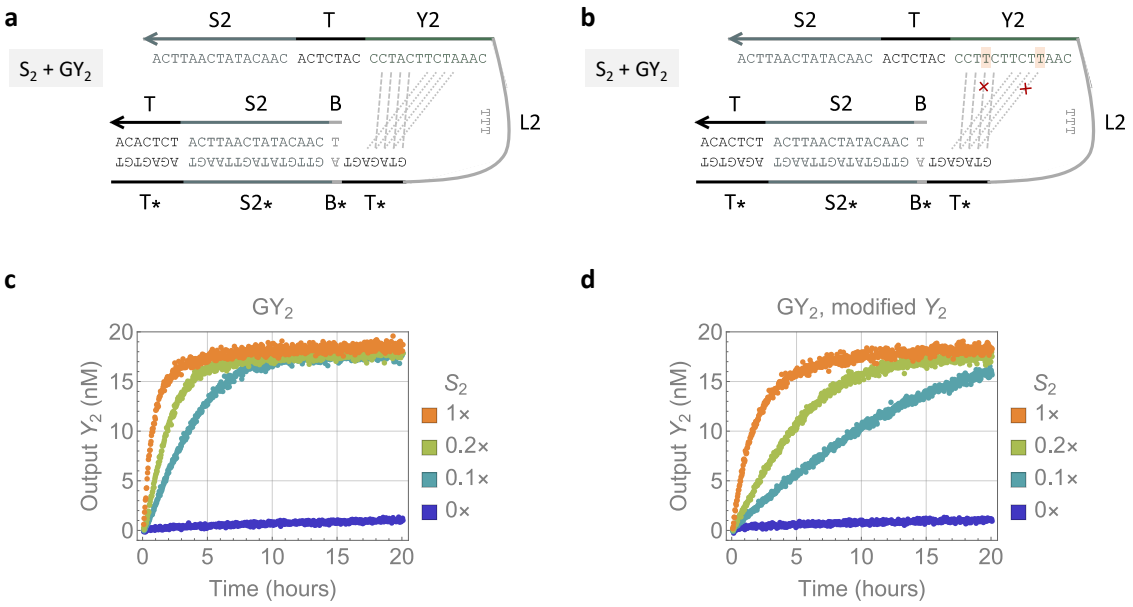

Fig. S27 | Verifying the impact of loop sequence on reaction kinetics using a modified sequence. a,b, Hairpin gates with the original and modified output sequence. **c,d,** Fluorescence kinetics data for the circuit shown in Fig. S22b with the original sequence of the hairpin gate GY_2 shown here in (a) or with the modified sequence shown here in (b). In each set of experiments, a two-stranded translator $TR_{2,1}$ was used to react with output Y_2 and produce output Y_1 for reacting with reporter RQ_1. The purpose of the translator was to avoid ordering new fluorophore and quencher modified strands yet still achieve a direct comparison of the kinetics between the original and modified output sequences. Standard concentration $1\times = 20$ nM. Relative concentrations of the input (S_2) are shown in the legend. Hairpin gate (GY_2), fuel (F_2), translator ($TR_{2,1}$), and reporter (RQ_1) were at $1\times$, $2\times$, $2\times$, and $1.5\times$, respectively.

DNA catalysts, but at the cost of slower kinetics. Instead, we sought to provide a solution that allows for better kinetic control and faster kinetics, by introducing a designed binding to compete with the toehold for binding to T∗, which in turn makes the toehold more available for downstream reactions. This led to the introduction of an additional toehold in the hairpin loop, which is both simple and effective. This toehold not only has more base pairs but also results in a shorter loop, replacing any possible spurious binding. With the same output sequences that previously caused a 10-fold kinetics difference (Fig. 3b) but now with a loop toehold, the two hairpin gates exhibited similar kinetics (Fig. 3c).

3.11 Intramolecular toehold occlusion in a cascade of hairpin gates

Implementing the weighted sum function in a winner-take-all neural network requires composing upstream gates that compute weight multiplication with downstream gates that compute summation (Fig. S28a). Weight multiplication $p_{ij} = w_{ij} \times x_i$, in which $x_i \in \{0, 1\}$ and $w_{ij} \in \mathbb{R}^+$, is carried out by a catalytic reaction $\mathrm{X}_i + \mathrm{GP}_{ij} + \mathrm{XF}_i \rightarrow \mathrm{X}_i + \mathrm{P}_{ij}$, in which the concentration of product P_{ij} corresponds to the initial concentration of weight gate $[\mathrm{GP}_{ij}]_0 = w_{ij}$ when input X_i is present and fuel XF_i is in excess. Summation $s_j = \sum_i p_{ij}$ is carried out by a stoichiometric reaction $\mathrm{P}_{ij} + \mathrm{GS}_j \rightarrow \mathrm{S}_j$, in which all products P_{ij} for the same neuron j are converted to a common weighted sum signal S_j when the summation gate GS_j is in excess. The weight multiplication reaction can be implemented using the hairpin gate design shown above, and the summation reaction could also be implemented with a hairpin gate but with no fuel. Because the loop toehold in the weight gate will become double-stranded when the product is fully bound to the summation gate, the summation reaction is already driven forward, eliminating the need for a bulge and an additional toehold in the hairpin loop. However, unexpected experimental results were observed for this two-layer circuit: the output only reached ~60% reaction completion when the input concentration was high (Fig. 3f).

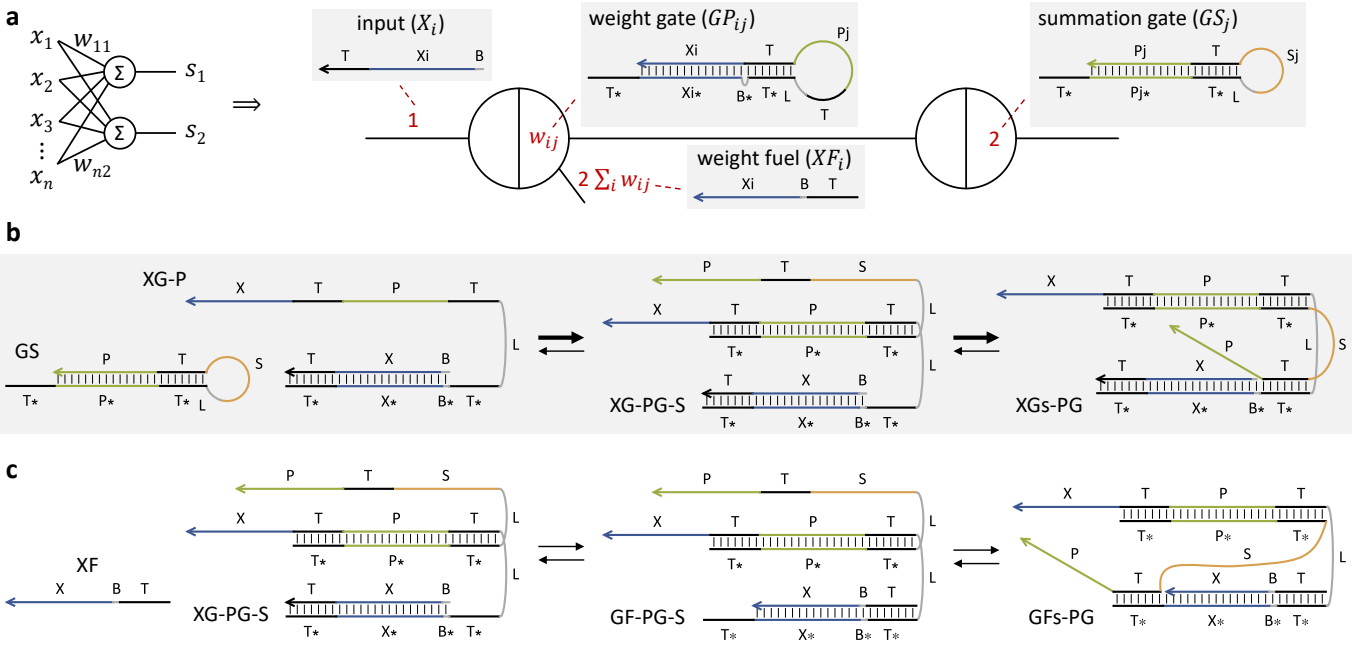

Fig. S28 | Intramolecular toehold occlusion in a cascade of hairpin gates. a, Implementation of a weighted-sum function. **b,** Mechanism of intramolecular toehold occlusion. Thickness of the arrows indicates relative forward and reverse rates; thicker means faster. **c,** Fuel-bound gate (GF-PG-S) has a larger entropic penalty for intramolecular toehold occlusion than the input-bound gate (XG-PG-S).

To explain the reaction completion problem observed in the cascade, we proposed a hypothesis of intramolecular toehold occlusion. It is known that using a common toehold in DNA circuits provides a simple method for kinetic control and a natural proof-of-concept for scalability, but with a tradeoff that all signal and fuel strands can temporarily bind to all gates that they are not designed to react with and thus slow down the desired reactions.[1,7] This phenomenon of toehold occlusion can cause more serious problems here as it occurs within the same molecule (Fig. S28b). When the weighted sum signal is activated, it remains linked to the product-bound gate; when the product itself is

linked to the input-bound gate, the three components are constrained within one molecule (XG-PG-S). The toehold on the weighted sum signal now binds to the open toehold on the input-bound gate, inhibiting it from participating in downstream reactions (such as the reporting reaction). This occlusion is biased forward because unimolecular hybridization is faster than toehold dissociation. When we included the occlusion in modeling the two-layer circuit, simulations agreed with the experimental data (Fig. 3f), supporting the hypothesis that the reaction completion problem was caused by intramolecular toehold occlusion. The problem was less significant with lower input concentrations (0.1 and 0.2×), because more weighted sum signal would be linked to the fuel-bound gate, which has a larger entropic penalty for unimolecular hybridization of the toehold than the input-bound gate (Fig. S28c).

3.12 A reusable logic gate with a hairpin threshold

Like the annihilator, a threshold produces only wastes and no cascadable products, and thus it can be either two-stranded or a hairpin. In the logic circuit design, a threshold is downstream of a summation gate that carries out a stoichiometric reaction.[1] Because stoichiometric reactions are implemented with two-stranded gates that reset at a relatively low temperature, thresholds need to reset at a higher temperature in order to avoid interfering with the reset of the upstream gates. Given these considerations, we explored two reusable threshold designs: a hairpin design that naturally resets at a relatively high temperature (Fig. S29) and a two-stranded design similar to an annihilator but with a single-stranded fuel that represents an always-active signal (Fig. S30). In both cases, the performance of the threshold was somewhat compromised after reset, indicated by the higher off states of an AND gate when one of the two inputs were present.

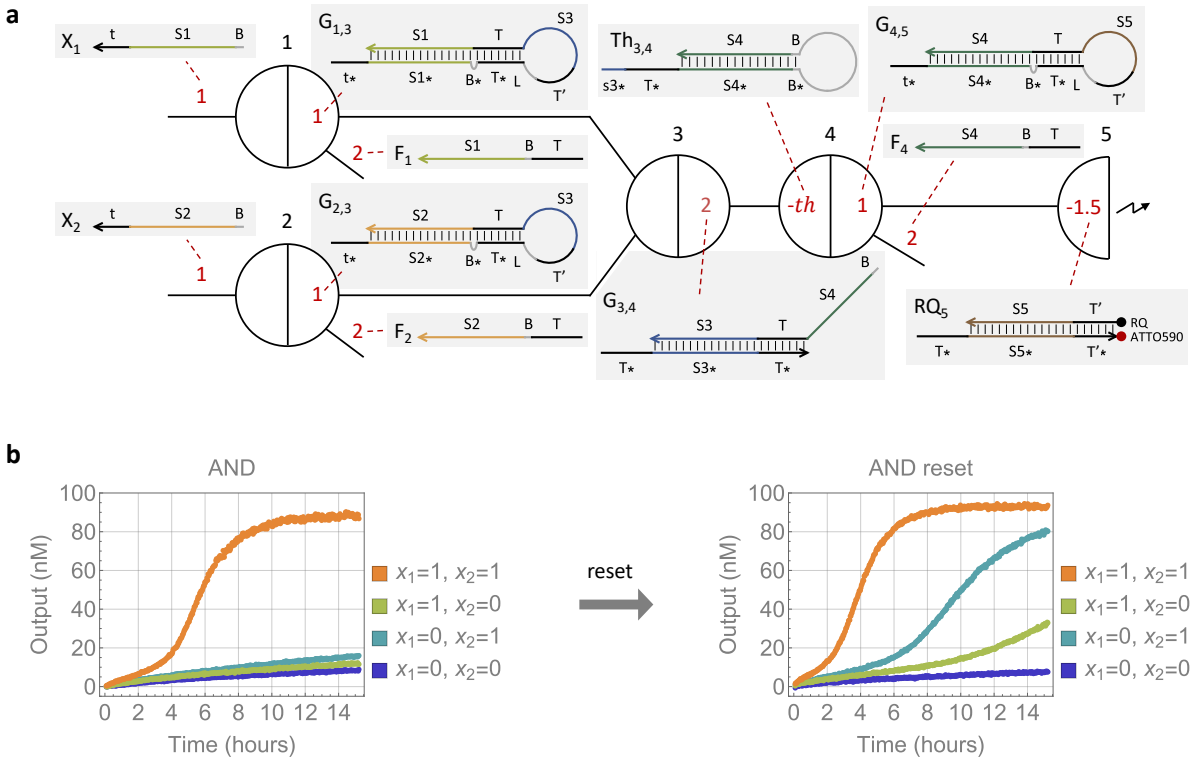

Fig. S29 | A reusable logic gate with a hairpin threshold. a, Implementation of a two-input logic gate with signal restoration. **b,** Fluorescence kinetics experiments of an AND gate before and after rest. All hairpin gates have a 1-nt bulge and 6-nt loop toehold.

3.13 A reusable logic gate with a two-stranded threshold

Compared to the hairpin threshold (Fig. S29), the two-stranded threshold exhibited a better performance after reset, although at the cost of longer strands and more molecules (Fig. S30). The kinetics difference between two input combinations ($x_1 = 0$ and $x_2 = 1$, $x_1 = 1$ and $x_2 = 0$) became more noticeable after reset, likely because the two hairpin gates associated with the two inputs had restored to slightly different concentrations due to their sequences and melting temperatures.

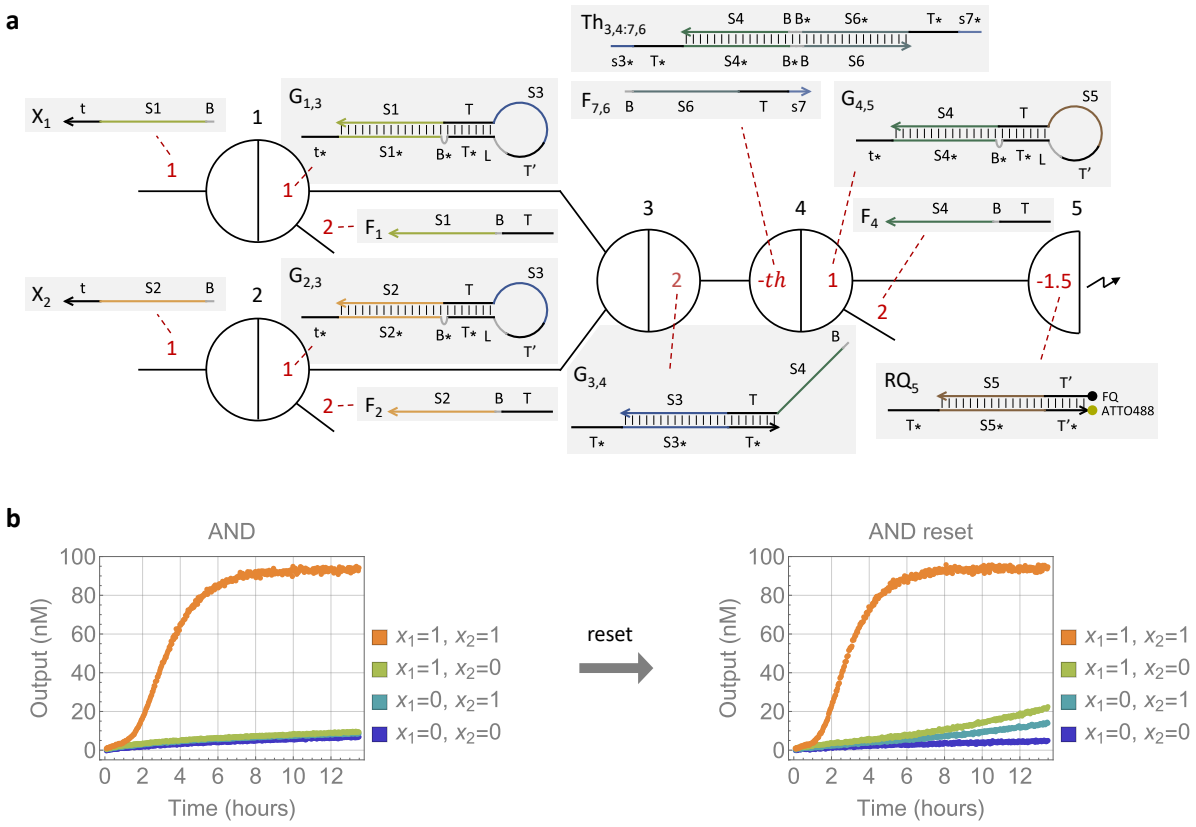

Fig. S30 | A reusable logic gate with a two-stranded threshold. a, Implementation of a two-input logic gate with signal restoration. The fuel strand $F_{7,6}$ represents an always-active signal, reacting with the annihilator $Th_{3,4:7,6}$ and converting it to a threshold $Th_{3,4}$ ($Th_{3,4:7,6} + F_{7,6} \rightleftharpoons Th_{3,4}$) for the summation signal $S_{3,4}$. **b,** Fluorescence kinetics experiments of an AND gate before and after rest. All hairpin gates have a 1-nt bulge and 6-nt loop toehold.

4 DNA sequences

4.1 Sequences for the quantification of effective concentration

Table S1: Sequences for the quantification of effective concentration (Fig. S6).

Name	Sequence
S	ACCACTATAATTCCA TACCT CATTCCTACATTTCA
SI	TGAAATGTAGGAATG AGGTA TGGAATTATAGTGGT
Translator-t	CACACTTCAAACTCA TACCT ACCACTATAATTCCA
Translator-b	TG AGGTA TGGAATTATAGTGGT AGGTA TG
Q	/5IAbRQ/ ACACTTCAAACTCA
R	GT AGGTA TGAGTTTGAAGTGTG /3ATTO590N/

4.2 Sequences of a reusable DNA catalyst

Table S2: Sequences of a reusable DNA catalyst (Figs. 2c, 2d, 2f, S13–S16).

Name	Sequence
S-B0	ACCAACTCATTACCA TACCT CATCTTCTAACATCA
S-B1	A ACCAACTCATTACCA TACCT CATCTTCTAACATCA
SI-B1	TGATGTTAGAAGATG AGGTA TGGTAATGAGTTGGT T
GY-B0T0	TG AGGTA TGGTAATGAGTTGGT AGGTA TG CTA CACACTTCAAACTCA TACCT ACCAACTCATTACCA
GY-B0T6	TG AGGTA TGGTAATGAGTTGGT AGGTA TG CTA CATACC CACACTTCAAACTCA TACCT ACCAACTCATTACCA
GY-B0T7	TG AGGTA TGGTAATGAGTTGGT AGGTA TG CTA CATACCT CACACTTCAAACTCA TACCT ACCAACTCATTACCA
GY-B1T0	TG AGGTA TGGTAATGAGTTGGT T AGGTA TG CTA CACACTTCAAACTCA TACCT ACCAACTCATTACCA
GY-B1T6	TG AGGTA TGGTAATGAGTTGGT T AGGTA TG CTA CATACC CACACTTCAAACTCA TACCT ACCAACTCATTACCA
GY-B1T7	TG AGGTA TGGTAATGAGTTGGT T AGGTA TG CTA CATACCT CACACTTCAAACTCA TACCT ACCAACTCATTACCA
F-B0	CA TACCT ACCAACTCATTACCA
F-B1	CA TACCT A ACCAACTCATTACCA
Q-T0	/5IAbRQ/ ACACTTCAAACTCA
R-T0	GT AGGTA TGAGTTTGAAGTGTG /3ATTO590N/
Q-T6	/5IAbRQ/ ATACC CACACTTCAAACTCA
R-T6	GT AGGTA TGAGTTTGAAGTGTG GGTATG /3ATTO590N/
Q-T7	/5IAbRQ/ ATACCT CACACTTCAAACTCA
R-T7	GT AGGTA TGAGTTTGAAGTGTG AGGTATG /3ATTO590N/
TriggerGY-B0	CA TACCT ACCAACTCATTACCA TACCT CA
TriggerGY-B1	CA TACCT A ACCAACTCATTACCA TACCT CA

4.3 Sequences of a pair of catalysts

Table S3: Sequences of a pair of catalysts (Figs. 3b and 3c).

Name	Sequence
S1	T CACTTCATAAATCCA TCTCA CACTATAATTCCA
S2	T CAACATATCAATTCA TCTCA CACAACAACCACA
GY1-B1T0	TG TGAGA TGGATTTATGAAGTG A TGAGA TG CTT CATAACACAATCACA TCTCA CACTTCATAAATCCA
GY2-B1T0	TG TGAGA TGAATTGATATGTTG A TGAGA TG TTT CAAATCTTCATCCCA TCTCA CAACATATCAATTCA
GY1-B1T7	TG TGAGA TGGATTTATGAAGTG A TGAGA TG CTT CATCTCA CATAACACAATCACA TCTCA CACTTCATAAATCCA
GY2-B1T7	TG TGAGA TGAATTGATATGTTG A TGAGA TG TTT CATCTCA CAAATCTTCATCCCA TCTCA CAACATATCAATTCA
F1	CA TCTCA T CACTTCATAAATCCA
F2	CA TCTCA T CAACATATCAATTCA
TR1t	CAAATCTTCATCCCA TCTCA CATAACACAATCACA
TR1b	TG TGAGA TGTGATTGTGTTATG TGAGA TG
TR2t	CATAACACAATCACA TCTCA CAAATCTTCATCCCA
TR2b	TG TGAGA TGGGATGAAGATTTG TGAGA TG
Q1	/5IAbRQ/ CATAACACAATCACA
R1	TG TGAGA TGTGATTGTGTTATG /3ATTO590N/
Q2	/5IABkFQ/ CAAATCTTCATCCCA
R2	TG TGAGA TGGGATGAAGATTTG /3ATTO488N/
TriggerGY1	CA TCTCA T CACTTCATAAATCCA TCTCA CA
TriggerGY2	CA TCTCA T CAACATATCAATTCA TCTCA CA

4.4 Sequences of a two-layer cascade

Table S4: Sequences of a two-layer cascade (Figs. 3f and 3g).

Name	Sequence
X	T CACTTCATAAATCCA TCTCA CACTATAATTCCA
GP	TG TGAGA TGGATTTATGAAGTG A TGAGA TG CTT CATCTCA ATTCTACCTCCACCA TCTCA CACTTCATAAATCCA
XF	CA TCTCA T CACTTCATAAATCCA
GS	TG TGAGA TGGTGGAGGTAGAAT TGAGA TG CTT CATAACACAATCACA TCTCA ATTCTACCTCCACCA
S	CATAACACAATCACA TCTCA ATTCTACCTCCACCA
G	TG TGAGA TGGTGGAGGTAGAAT TGAGA TG
Q	/5IAbRQ/ CATAACACAATCACA
R	TG TGAGA TGTGATTGTGTTATG /3ATTO590N/
TriggerGS	CA TCTCA T CACTTCATAAATCCA TCTCA CA

4.5 Sequences of a reusable winner-take-tall neural network

Table S5: Sequences of a reusable winner-take-tall neural network (Fig. 4).

Name	Sequence
X1	A CAAACAATTCACACCTTCCA TACCT CA
X2	A CAATCCATACACCTTTTCCA TACCT CA
X3	A CAAATCCTCCACTCTTTCCA TACCT CA
X4	A CACACCATCCAACCTTACCA TACCT CA
X5	A CAAACCTCCCAACCCTTACA TACCT CA
X6	A CACTCCACCCAACTCCTCCA TACCT CA
X7	A CACTCCATCTACCCTCTACA TACCT CA
X8	A CAAACCATCCTCCTCCTACA TACCT CA
X9	A CAACCAATCCACCAATACCA TACCT CA
X10	A CACATCCCACAACCCTATCA TACCT CA
X11	A CACATCATCCTAACCCTCCA TACCT CA
X12	A CACACAACCCTCCACTTCCA TACCT CA
X13	A CACTCAATACATCCCATCCA TACCT CA
X14	A CACTTCACCTAAACCTTACA TACCT CA
X15	A CACACCCTCTACACCTTTCA TACCT CA
X16	A CACACAATCACCACCCTACA TACCT CA
X17	A CACTTCCTCCATCTCTTACA TACCT CA
X18	A CACCTCACCCACACCAACCA TACCT CA
X19	A CACACTATCCTTACTTTACA TACCT CA
X20	A CAAACAACACACCCTTAACA TACCT CA
X21	A CAAACCCTCCTACTTACCCA TACCT CA
X22	A CACTTCTTACACACCCTTCA TACCT CA
X23	A CACTCTATACTCTCCCTACA TACCT CA
X24	A CAAACACTCTTCCCTCTCCA TACCT CA
X25	A CACTAAACCCAATCCTACCA TACCT CA
X26	A CACACACTACTAACCATACA TACCT CA
X27	A CACTCAACCCTACCTTCACA TACCT CA
X28	A CACTCATCCCACCTCTAACA TACCT CA
X29	A CAATCCACCTACACCCATCA TACCT CA
X30	A CACTCCCTATACTCAATCCA TACCT CA
X31	A CAACCCACCCTTCCCATTCA TACCT CA
X32	A CAATCACTACTCCCTACACA TACCT CA
X33	A CACACACCCTTATCCCTTCA TACCT CA
X34	A CAATCAATCTACATACTCCA TACCT CA
X35	A CACACATTCCATACATATCA TACCT CA
X36	A CAAACCCACCACCCTCCACA TACCT CA
X37	A CATACCCTACACCACCTCCA TACCT CA
X38	A CACACACACCACACCCACCA TACCT CA
X39	A CACTCACCTCACCCTTTCCA TACCT CA
X40	A CACTTCATCTTCTCCTCCCA TACCT CA
X41	A CAAATCACCTATCCTCACCA TACCT CA
X42	A CAAATCCCACTCACCATCCA TACCT CA
X43	A CACCCACTCCCACCCTTCCA TACCT CA
X44	A CAATCAAACCACTCTCTTCA TACCT CA
X45	A CAATTCACCCTCTTCCACCA TACCT CA
X46	A CACACCTCATACCCTTCCCA TACCT CA
X47	A CACATACCCTACTCCACCCA TACCT CA
X48	A CAAACACCACTCATTCTACA TACCT CA
X49	A CACCCTATCCTACCACTTCA TACCT CA

Name	Sequence
X50	A CACTTAACCCTTACCCAACA TACCT CA
X51	A CATATCATACAACCATTACA TACCT CA
X52	A CATTCCCAACACCTCTCACA TACCT CA
X53	A CACATACTCCAACTTCTCCA TACCT CA
X54	A CACCCAACACAAATCTTACA TACCT CA
X55	A CATACCATCTCACACTTACA TACCT CA
X56	A CACACCTTACTCACCTACCA TACCT CA
X57	A CACCTATCACAAACTTACCA TACCT CA
X58	A CACATCTTCTACCTCTACCA TACCT CA
X59	A CACACTTTCCCTCTCTTTCA TACCT CA
X60	A CAAAACATCTATACCTCCCA TACCT CA
X61	A CAACCCATCTTCAACTTCCA TACCT CA
X62	A CACTTCAACAACCTCCAACA TACCT CA
X63	A CACATCACACATCTCCCACA TACCT CA
X64	A CACACCCAACCAACTTTCCA TACCT CA
X65	A CACTCCTTCTTACTTCACCA TACCT CA
X66	A CAAACCAAACTCTCCTCACA TACCT CA
X67	A CAATCTATCCAACACTCACA TACCT CA
X68	A CACACCACTTACCACTAACA TACCT CA
X69	A CACAAAACCTACCCACTCCA TACCT CA
X70	A CACTCACTCTCCCTTTCACA TACCT CA
X71	A CATACCACACTCCTCTATCA TACCT CA
X72	A CACTCTAACCACATCTTTCA TACCT CA
X73	A CACACTACCACACCATTCCA TACCT CA
X74	A CATTCCATTCACTCATACCA TACCT CA
X75	A CAATCCCTCCACATCAACCA TACCT CA
X76	A CAATCCTACTACCCATTTCA TACCT CA
X77	A CACCCACCCATCCTACTCCA TACCT CA
X78	A CATTCCACACAACCTACCCA TACCT CA
X79	A CAAACATTACCACTCATCCA TACCT CA
X80	A CACCTCATATCCCATTTCCA TACCT CA
X81	A CAAAACCTCTAACTACACCA TACCT CA
X82	A CACACTCTCTCCTCTTACCA TACCT CA
X83	A CACCCAAACCAACCCAAACA TACCT CA
X84	A CACAAACTATTCCACTACCA TACCT CA
X85	A CAACCCTCCCTAATCTACCA TACCT CA
X86	A CACATTCACCTACCCAACCA TACCT CA
X87	A CAACTCACATACCTTCTACA TACCT CA
X88	A CAAACCACCATCACTTTTCA TACCT CA
X89	A CAATACTCCCACACTCTCCA TACCT CA
X90	A CATATCCTCATCCCATACCA TACCT CA
X91	A CACCACCTCCAAAACTACCA TACCT CA
X92	A CACACTTACCAAAACCTACA TACCT CA
X93	A CACACTTCCTTCATCCTCCA TACCT CA
X94	A CATACATTCTCCCACCACCA TACCT CA
X95	A CACATTCTCCACCACCAACA TACCT CA
X96	A CACAACAAACACCACTTTCA TACCT CA
X97	A CACTACCACCTCAACCTCCA TACCT CA
X98	A CAACTTCTCCAACCATCCCA TACCT CA
X99	A CAATCTAAACAACTCAACCA TACCT CA
X100	A CACATTACACACTACCTCCA TACCT CA
XI1	TG AGGTA TGGAAGGTGTGAATTGTTTG T
XI2	TG AGGTA TGGAAAAGGTGTATGGATTG T

Name	Sequence
XI3	TG AGGTA TGGAAAGAGTGGAGGATTTG T
XI4	TG AGGTA TGGTAAGGTTGGATGGTGTG T
XI5	TG AGGTA TGTAAGGGTTGGGAGGTTTG T
XI6	TG AGGTA TGGAGGAGTTGGGTGGAGTG T
XI7	TG AGGTA TGTAGAGGGTAGATGGAGTG T
XI8	TG AGGTA TGTAGGAGGAGGATGGTTTG T
XI9	TG AGGTA TGGTATTGGTGGATTGGTTG T
XI10	TG AGGTA TGATAGGGTTGTGGGATGTG T
XI11	TG AGGTA TGGAGGGTTAGGATGATGTG T
XI12	TG AGGTA TGGAAGTGGAGGGTTGTGTG T
XI13	TG AGGTA TGGATGGGATGTATTGAGTG T
XI14	TG AGGTA TGTAAGGTTTAGGTGAAGTG T
XI15	TG AGGTA TGAAAGGTGTAGAGGGTGTG T
XI16	TG AGGTA TGTAGGGTGGTGATTGTGTG T
XI17	TG AGGTA TGTAAGAGATGGAGGAAGTG T
XI18	TG AGGTA TGGTTGGTGTGGGTGAGGTG T
XI19	TG AGGTA TGTAAAGTAAGGATAGTGTG T
XI20	TG AGGTA TGTTAAGGGTGTGTTGTTTG T
XI21	TG AGGTA TGGGTAAGTAGGAGGGTTTG T
XI22	TG AGGTA TGAAGGGTGTGTAAGAAGTG T
XI23	TG AGGTA TGTAGGGAGAGTATAGAGTG T
XI24	TG AGGTA TGGAGAGGGAAGAGTGTTTG T
XI25	TG AGGTA TGGTAGGATTGGGTTTAGTG T
XI26	TG AGGTA TGTATGGTTAGTAGTGTGTG T
XI27	TG AGGTA TGTGAAGGTAGGGTTGAGTG T
XI28	TG AGGTA TGTTAGAGGTGGGATGAGTG T
XI29	TG AGGTA TGATGGGTGTAGGTGGATTG T
XI30	TG AGGTA TGGATTGAGTATAGGGAGTG T
XI31	TG AGGTA TGAATGGGAAGGGTGGGTTG T
XI32	TG AGGTA TGTGTAGGGAGTAGTGATTG T
XI33	TG AGGTA TGAAGGGATAAGGGTGTGTG T
XI34	TG AGGTA TGGAGTATGTAGATTGATTG T
XI35	TG AGGTA TGATATGTATGGAATGTGTG T
XI36	TG AGGTA TGTGGAGGGTGGTGGGTTTG T
XI37	TG AGGTA TGGAGGTGGTGTAGGGTATG T
XI38	TG AGGTA TGGTGGGTGTGGTGTGTGTG T
XI39	TG AGGTA TGGAAAGGGTGAGGTGAGTG T
XI40	TG AGGTA TGGGAGGAGAAGATGAAGTG T
XI41	TG AGGTA TGGTGAGGATAGGTGATTTG T
XI42	TG AGGTA TGGATGGTGAGTGGGATTTG T
XI43	TG AGGTA TGGAAGGGTGGGAGTGGGTG T
XI44	TG AGGTA TGAAGAGAGTGGTTTGATTG T
XI45	TG AGGTA TGGTGGAAGAGGGTGAATTG T
XI46	TG AGGTA TGGGAAGGGTATGAGGTGTG T
XI47	TG AGGTA TGGGTGGAGTAGGGTATGTG T
XI48	TG AGGTA TGTAGAATGAGTGGTGTTTG T
XI49	TG AGGTA TGAAGTGGTAGGATAGGGTG T
XI50	TG AGGTA TGTTGGGTAAGGGTTAAGTG T
XI51	TG AGGTA TGTAATGGTTGTATGATATG T
XI52	TG AGGTA TGTGAGAGGTGTTGGGAATG T
XI53	TG AGGTA TGGAGAAGTTGGAGTATGTG T
XI54	TG AGGTA TGTAAGATTTGTGTTGGGTG T
XI55	TG AGGTA TGTAAGTGTGAGATGGTATG T

Name	Sequence
XI56	TG AGGTA TGGTAGGTGAGTAAGGTGTG T
XI57	TG AGGTA TGGTAAGTTTGTGATAGGTG T
XI58	TG AGGTA TGGTAGAGGTAGAAGATGTG T
XI59	TG AGGTA TGAAAGAGAGGGAAAGTGTG T
XI60	TG AGGTA TGGGAGGTATAGATGTTTTG T
XI61	TG AGGTA TGGAAGTTGAAGATGGGTTG T
XI62	TG AGGTA TGTTGGAGGTTGTTGAAGTG T
XI63	TG AGGTA TGTGGGAGATGTGTGATGTG T
XI64	TG AGGTA TGGAAAGTTGGTTGGGTGTG T
XI65	TG AGGTA TGGTGAAGTAAGAAGGAGTG T
XI66	TG AGGTA TGTGAGGAGAGTTTGGTTTG T
XI67	TG AGGTA TGTGAGTGTTGGATAGATTG T
XI68	TG AGGTA TGTTAGTGGTAAGTGGTGTG T
XI69	TG AGGTA TGGAGTGGGTAGGTTTTGTG T
XI70	TG AGGTA TGTGAAAGGGAGAGTGAGTG T
XI71	TG AGGTA TGATAGAGGAGTGTGGTATG T
XI72	TG AGGTA TGAAAGATGTGGTTAGAGTG T
XI73	TG AGGTA TGGAATGGTGTGGTAGTGTG T
XI74	TG AGGTA TGGTATGAGTGAATGGAATG T
XI75	TG AGGTA TGGTTGATGTGGAGGGATTG T
XI76	TG AGGTA TGAAATGGGTAGTAGGATTG T
XI77	TG AGGTA TGGAGTAGGATGGGTGGGTG T
XI78	TG AGGTA TGGGTAGGTTGTGTGGAATG T
XI79	TG AGGTA TGGATGAGTGGTAATGTTTG T
XI80	TG AGGTA TGGAAATGGGATATGAGGTG T
XI81	TG AGGTA TGGTGTAGTTAGAGGTTTTG T
XI82	TG AGGTA TGGTAAGAGGAGAGAGTGTG T
XI83	TG AGGTA TGTTTGGGTTGGTTTGGGTG T
XI84	TG AGGTA TGGTAGTGGAATAGTTTGTG T
XI85	TG AGGTA TGGTAGATTAGGGAGGGTTG T
XI86	TG AGGTA TGGTTGGGTAGGTGAATGTG T
XI87	TG AGGTA TGTAGAAGGTATGTGAGTTG T
XI88	TG AGGTA TGAAAAGTGATGGTGGTTTG T
XI89	TG AGGTA TGGAGAGTGTGGGAGTATTG T
XI90	TG AGGTA TGGTATGGGATGAGGATATG T
XI91	TG AGGTA TGGTAGTTTTGGAGGTGGTG T
XI92	TG AGGTA TGTAGGTTTTGGTAAGTGTG T
XI93	TG AGGTA TGGAGGATGAAGGAAGTGTG T
XI94	TG AGGTA TGGTGGTGGGAGAATGTATG T
XI95	TG AGGTA TGTTGGTGGTGGAGAATGTG T
XI96	TG AGGTA TGAAAGTGGTGTTTGTTGTG T
XI97	TG AGGTA TGGAGGTTGAGGTGGTAGTG T
XI98	TG AGGTA TGGGATGGTTGGAGAAGTTG T
XI99	TG AGGTA TGGTTGAGTTGTTTAGATTG T
XI100	TG AGGTA TGGAGGTAGTGTGTAATGTG T
GP35-1	TG AGGTA TGATATGTATGGAATGTGTG T AGGTA TG CTA CATACC CAATCTAACACTCCA TACCT CACACATTCCATACATATCA
GP44-1	TG AGGTA TGAAGAGAGTGGTTTGATTG T AGGTA TG CTA CATACC CAATCTAACACTCCA TACCT CAATCAAACCACTCTCTTCA
GP53-1	TG AGGTA TGGAGAAGTTGGAGTATGTG T AGGTA TG CTA CATACC CAATCTAACACTCCA TACCT CACATACTCCAACTTCTCCA
GP54-1	TG AGGTA TGTAAGATTTGTGTTGGGTG T AGGTA TG CTA CATACC CAATCTAACACTCCA TACCT CACCCAACACAAATCTTACA

Name	Sequence
GP55-1	TG AGGTA TGTAAGTGTGAGATGGTATG T AGGTA TG CTA CATACC CAATCTAACACTCCA TACCT CATACCATCTCACACTTACA
GP56-1	TG AGGTA TGGTAGGTGAGTAAGGTGTG T AGGTA TG CTA CATACC CAATCTAACACTCCA TACCT CACACCTTACTCACCTACCA
GP63-1	TG AGGTA TGTGGGAGATGTGTGATGTG T AGGTA TG CTA CATACC CAATCTAACACTCCA TACCT CACATCACACATCTCCCACA
GP64-1	TG AGGTA TGGAAAGTTGGTTGGGTGTG T AGGTA TG CTA CATACC CAATCTAACACTCCA TACCT CACACCCAACCAACTTTCCA
GP65-1	TG AGGTA TGGTGAAGTAAGAAGGAGTG T AGGTA TG CTA CATACC CAATCTAACACTCCA TACCT CACTCCTTCTTACTTCACCA
GP66-1	TG AGGTA TGTGAGGAGAGTTTGGTTTG T AGGTA TG CTA CATACC CAATCTAACACTCCA TACCT CAAACCAAACTCTCCTCACA
GP67-1	TG AGGTA TGTGAGTGTTGGATAGATTG T AGGTA TG CTA CATACC CAATCTAACACTCCA TACCT CAATCTATCCAACACTCACA
GP73-1	TG AGGTA TGGAATGGTGTGGTAGTGTG T AGGTA TG CTA CATACC CAATCTAACACTCCA TACCT CACACTACCACACCATTCCA
GP74-1	TG AGGTA TGGTATGAGTGAATGGAATG T AGGTA TG CTA CATACC CAATCTAACACTCCA TACCT CATTCCATTCACTCATACCA
GP75-1	TG AGGTA TGGTTGATGTGGAGGGATTG T AGGTA TG CTA CATACC CAATCTAACACTCCA TACCT CAATCCCTCCACATCAACCA
GP76-1	TG AGGTA TGAAATGGGTAGTAGGATTG T AGGTA TG CTA CATACC CAATCTAACACTCCA TACCT CAATCCTACTACCCATTTCA
GP77-1	TG AGGTA TGGAGTAGGATGGGTGGGTG T AGGTA TG CTA CATACC CAATCTAACACTCCA TACCT CACCCACCCATCCTACTCCA
GP83-1	TG AGGTA TGTTTGGGTTGGTTTGGGTG T AGGTA TG CTA CATACC CAATCTAACACTCCA TACCT CACCCAAACCAACCCAAACA
GP84-1	TG AGGTA TGGTAGTGGAATAGTTTGTG T AGGTA TG CTA CATACC CAATCTAACACTCCA TACCT CACAAACTATTCCACTACCA
GP85-1	TG AGGTA TGGTAGATTAGGGAGGGTTG T AGGTA TG CTA CATACC CAATCTAACACTCCA TACCT CAACCCTCCCTAATCTACCA
GP86-1	TG AGGTA TGGTTGGGTAGGTGAATGTG T AGGTA TG CTA CATACC CAATCTAACACTCCA TACCT CACATTCACCTACCCAACCA
GP14-2	TG AGGTA TGTAAGGTTTAGGTGAAGTG T AGGTA TG CTA CATACC CAATTCACTCAATCA TACCT CACTTCACCTAAACCTTACA
GP15-2	TG AGGTA TGAAAGGTGTAGAGGGTGTG T AGGTA TG CTA CATACC CAATTCACTCAATCA TACCT CACACCCTCTACACCTTTCA
GP16-2	TG AGGTA TGTAGGGTGGTGATTGTGTG T AGGTA TG CTA CATACC CAATTCACTCAATCA TACCT CACACAATCACCACCCTACA
GP17-2	TG AGGTA TGTAAGAGATGGAGGAAGTG T AGGTA TG CTA CATACC CAATTCACTCAATCA TACCT CACTTCCTCCATCTCTTACA
GP23-2	TG AGGTA TGTAGGGAGAGTATAGAGTG T AGGTA TG CTA CATACC CAATTCACTCAATCA TACCT CACTCTATACTCTCCCTACA
GP24-2	TG AGGTA TGGAGAGGGAAGAGTGTTTG T AGGTA TG CTA CATACC CAATTCACTCAATCA TACCT CAAACACTCTTCCCTCTCCA
GP25-2	TG AGGTA TGGTAGGATTGGGTTTAGTG T AGGTA TG CTA CATACC CAATTCACTCAATCA TACCT CACTAAACCCAATCCTACCA
GP26-2	TG AGGTA TGTATGGTTAGTAGTGTGTG T AGGTA TG CTA CATACC CAATTCACTCAATCA TACCT CACACACTACTAACCATACA
GP27-2	TG AGGTA TGTGAAGGTAGGGTTGAGTG T AGGTA TG CTA CATACC CAATTCACTCAATCA TACCT CACTCAACCCTACCTTCACA
GP28-2	TG AGGTA TGTTAGAGGTGGGATGAGTG T AGGTA TG CTA CATACC CAATTCACTCAATCA TACCT CACTCATCCCACCTCTAACA
GP37-2	TG AGGTA TGGAGGTGGTGTAGGGTATG T AGGTA TG CTA CATACC

Name	Sequence
	CAATTCACTCAATCA TACCT CATACCCTACACCACCTCCA
GP38-2	TG AGGTA TGGTGGGTGTGGTGTGTGTG T AGGTA TG CTA CATACC
	CAATTCACTCAATCA TACCT CACACACACCACACCCACCA
GP46-2	TG AGGTA TGGGAAGGGTATGAGGTGTG T AGGTA TG CTA CATACC
	CAATTCACTCAATCA TACCT CACACCTCATACCCTTCCCA
GP47-2	TG AGGTA TGGGTGGAGTAGGGTATGTG T AGGTA TG CTA CATACC
	CAATTCACTCAATCA TACCT CACATACCCTACTCCACCCA
GP56-2	TG AGGTA TGGTAGGTGAGTAAGGTGTG T AGGTA TG CTA CATACC
	CAATTCACTCAATCA TACCT CACACCTTACTCACCTACCA
GP57-2	TG AGGTA TGGTAAGTTTGTGATAGGTG T AGGTA TG CTA CATACC
	CAATTCACTCAATCA TACCT CACCTATCACAAACTTACCA
GP65-2	TG AGGTA TGGTGAAGTAAGAAGGAGTG T AGGTA TG CTA CATACC
	CAATTCACTCAATCA TACCT CACTCCTTCTTACTTCACCA
GP66-2	TG AGGTA TGTGAGGAGAGTTTGGTTTG T AGGTA TG CTA CATACC
	CAATTCACTCAATCA TACCT CAAACCAAACTCTCCTCACA
GP74-2	TG AGGTA TGGTATGAGTGAATGGAATG T AGGTA TG CTA CATACC
	CAATTCACTCAATCA TACCT CATTCCATTCACTCATACCA
GP75-2	TG AGGTA TGGTTGATGTGGAGGGATTG T AGGTA TG CTA CATACC
	CAATTCACTCAATCA TACCT CAATCCCTCCACATCAACCA
XF14	CA TACCT A CACTTCACCTAAACCTTACA
XF15	CA TACCT A CACACCCTCTACACCTTTCA
XF16	CA TACCT A CACACAATCACCACCCTACA
XF17	CA TACCT A CACTTCCTCCATCTCTTACA
XF23	CA TACCT A CACTCTATACTCTCCCTACA
XF24	CA TACCT A CAAACACTCTTCCCTCTCCA
XF25	CA TACCT A CACTAAACCCAATCCTACCA
XF26	CA TACCT A CACACACTACTAACCATACA
XF27	CA TACCT A CACTCAACCCTACCTTCACA
XF28	CA TACCT A CACTCATCCCACCTCTAACA
XF35	CA TACCT A CACACATTCCATACATATCA
XF37	CA TACCT A CATACCCTACACCACCTCCA
XF38	CA TACCT A CACACACACCACACCCACCA
XF44	CA TACCT A CAATCAAACCACTCTCTTCA
XF46	CA TACCT A CACACCTCATACCCTTCCCA
XF47	CA TACCT A CACATACCCTACTCCACCCA
XF53	CA TACCT A CACATACTCCAACTTCTCCA
XF54	CA TACCT A CACCCAACACAAATCTTACA
XF55	CA TACCT A CATACCATCTCACACTTACA
XF56	CA TACCT A CACACCTTACTCACCTACCA
XF57	CA TACCT A CACCTATCACAAACTTACCA
XF63	CA TACCT A CACATCACACATCTCCCACA
XF64	CA TACCT A CACACCCAACCAACTTTCCA
XF65	CA TACCT A CACTCCTTCTTACTTCACCA
XF66	CA TACCT A CAAACCAAACTCTCCTCACA
XF67	CA TACCT A CAATCTATCCAACACTCACA
XF73	CA TACCT A CACACTACCACACCATTCCA
XF74	CA TACCT A CATTCCATTCACTCATACCA
XF75	CA TACCT A CAATCCCTCCACATCAACCA
XF76	CA TACCT A CAATCCTACTACCCATTTCA
XF77	CA TACCT A CACCCACCCATCCTACTCCA
XF83	CA TACCT A CACCCAAACCAACCCAAACA
XF84	CA TACCT A CACAAACTATTCCACTACCA
XF85	CA TACCT A CAACCCTCCCTAATCTACCA

Name	Sequence
XF86	CA TACCT A CACATTCACCTACCCAACCA
S1	A CACCCTAAAATCTCA TACCT CAATCTAACACTCCA
S2	A CAATACAAATCCACA TACCT CAATTCACTCAATCA
G1	TG AGGTA TGGAGTGTTAGATTG AGGTA TG
G2	TG AGGTA TGATTGAGTGAATTG AGGTA TG
Anh1	TG AGGTA TGTGGATTTGTATTG T A CACCCTAAAATCTCA
Anh2	TG AGGTA TGAGATTTTAGGGTG T A CAATACAAATCCACA
GY1	AGGTA TGAGATTTTAGGGTG T AGGTA TG CTT CATACC CACTTTTCACTATCA TACCT CACCCTAAAATCTCA
GY2	AGGTA TGTGGATTTGTATTG T AGGTA TG CTA CATACC CACACTTCAAACTCA TACCT CAATACAAATCCACA
SF1	CA TACCT A CACCCTAAAATCTCA
SF2	CA TACCT A CAATACAAATCCACA
Q1	/5IABkFQ/ CATACC CACTTTTCACTATCA
R1	TG AGGTA TGATAGTGAAAAGTG GGTATG /3ATTO488N/
Q2	/5IAbRQ/ CATACC CACACTTCAAACTCA
R2	TG AGGTA TGAGTTTGAAGTGTG GGTATG /3ATTO590N/
TriggerGY1	CA TACCT A CACCCTAAAATCTCA TACCT
TriggerGY2	CA TACCT A CAATACAAATCCACA TACCT

4.6 Sequences of a reusable AND gate with a hairpin threshold

Table S6: Sequences of a reusable AND gate with a hairpin threshold (Fig. S29).

Name	Sequence
X1	A CAATCTAACACTCCA TACCT
X2	A CAACCATACTAAACA TACCT
G1-3	AGGTA TGGAGTGTTAGATTG T AGGTATG CTA CATACC
	CAATATCCATAACCA TACCT CAATCTAACACTCCA
G2-3	AGGTA TGTTTAGTATGGTTG T AGGTATG CTA CATACC
	CAATATCCATAACCA TACCT CAACCATACTAAACA
F1	CA TACCT A CAATCTAACACTCCA
F2	CA TACCT A CAACCATACTAAACA
S3-4	A CAATACAAATCCACA TACCT CAATATCCATAACCA
G3	TG AGGTA TGGTTATGGATATTG AGGTA TG
Th3-4	TATTG AGGTA TGTGGATTTGTATTG T TTTTTTTTTTTTTTTTTTTTT
	A CAATACAAATCCACA
G4-5	AGGTA TGTGGATTTGTATTG T AGGTA TG CTA CATACC
	CACACTTCAAACTCA TACCT CAATACAAATCCACA
F4	CA TACCT A CAATACAAATCCACA
Q5	/5IAbRQ/ CATACC CACACTTCAAACTCA
R5	TG AGGTA TGAGTTTGAAGTGTG GGTATG /3ATTO590N/
TriggerG4	CA TACCT A CAATACAAATCCACA TACCT

4.7 Sequences of a reusable AND gate with a two-stranded threshold

Table S7: Sequences of a reusable AND gate with a two-stranded threshold (Fig. S30).

Name	Sequence
X1	A CACATAACAACCACA TACCT
X2	A CATCCATTCCACTCA TACCT
G1-3	AGGTA TGTGGTTGTTATGTG T AGGTA TG CTT CATACC CAATTCACTCAATCA TACCT CACATAACAACCACA
G2-3	AGGTA TGAGTGGAATGGATG T AGGTA TG CTT CATACC CAATTCACTCAATCA TACCT CATCCATTCCACTCA
F1	CA TACCT A CACATAACAACCACA
F2	CA TACCT A CATCCATTCCACTCA
S3-4	A CACCCTAAAATCTCA TACCT CAATTCACTCAATCA
G3	TG AGGTA TGATTGAGTGAATTG AGGTA TG
Th3-4	AATTG AGGTA TGAGATTTTAGGGTG T A CATCCTTAACTCCCA
Th7-6	ATATG AGGTA TGGGAGTTAAGGATG T A CACCCTAAAATCTCA
F7-6	A CATCCTTAACTCCCA TACCT CATAT
G4-5	AGGTA TGAGATTTTAGGGTG T AGGTA TG CTT CATACC CACTTTTCACTATCA TACCT CACCCTAAAATCTCA
F4	CA TACCT A CACCCTAAAATCTCA
Q5	/5IABkFQ/ CATACC CACTTTTCACTATCA
R5	TG AGGTA TGATAGTGAAAAGTG GGTATG /3ATTO488N/
TriggerG4	CA TACCT A CACCCTAAAATCTCA TACCT

4.8 Sequences of a reusable logic gate

Table S8: Sequences of a reusable logic gate (Fig. 5).

Name	Sequence
X1	ACCACTATAATTCCA TACCT CATTCCTACATTTCA
X2	ACCTTCACAACTACA TACCT CATACAACATCTACA
G1-3	TG AGGTA TGGAATTATAGTGGT AGGTA TG CTA CA TACCT CATCTTCTAACATCA TACCT ACCACTATAATTCCA
G2-3	TG AGGTA TGTAGTTGTGAAGGT AGGTA TG CTA CA TACCT CATCTTCTAACATCA TACCT ACCTTCACAACTACA
F1	CA TACCT ACCACTATAATTCCA
F2	CA TACCT ACCTTCACAACTACA
S3-4	ACCAACTCATTACCA TACCT CATCTTCTAACATCA
G3	GT AGGTA TGATGTTAGAAGATG AGGTA TG
Th3-4	AGA TG AGGTA TGGTAATGAGTTGGT TTT TTTTTT TTTTTTTTTTTT ACCAACTCATTACCA
G4-5	TG AGGTA TGGTAATGAGTTGGT AGGTA TG CTA CA TACCT CACACTTCAAACTCA TACCT ACCAACTCATTACCA
F4	CA TACCT ACCAACTCATTACCA
Q5	/5IAbRQ/ ATACCT CACACTTCAAACTCA
R5	GT AGGTA TGAGTTTGAAGTGTG AGGTATG /3ATTO590N/
TriggerG4	CA TACCT ACCAACTCATTACCA TACCT CA

4.9 Sequences of a reusable Fibonacci logic circuit

Table S9: Sequences of a reusable Fibonacci logic circuit (Fig. 6).

Name	Sequence
S1 (X1-0)	ACTTCTCCCATTTCA ACATC ACAAA
S2 (X1-1)	ACAACCCAACTCACA ACATC ACTTT
S3 (X2-0)	ACCTTATCCTTTACA ACATC ATATA
S4 (X2-1)	ACACATCAAATCACA ACATC AATAA
S5 (X3-0)	ACCTATACACACCCA ACATC TTAAA
S6 (X3-1)	ACTTCTCCATCACCA ACATC TATTT
S7 (X4-0)	ACCCTCTTCCCTTCA ACATC TAACA
S8 (X4-1)	ACCAAACTACATCCA ACATC TACAT
SI1	TTTGT GATGT TGAAATGGGAGAAGT
SI2	AAAGT GATGT TGTGAGTTGGGTTGT
SI3	TATAT GATGT TGTAAAGGATAAGGT
SI4	TTATT GATGT TGTGATTTGATGTGT
SI5	TTTAA GATGT TGGGTGTGTATAGGT
SI6	AAATA GATGT TGGTGATGGAGAAGT
SI7	TGTTA GATGT TGAAGGGAAGAGGGT
SI8	ATGTA GATGT TGGATGTAGTTTGGT
G3-11	AT GATGT TGTAAAGGATAAGGT AGGTA TG CTT CA TACCT CAACTCCTAATATCA TACCT ACCTTATCCTTTACA
G3-15	AT GATGT TGTAAAGGATAAGGT AGGTA TG CTA CA TACCT CATTCCTACATTTCA TACCT ACCTTATCCTTTACA
F3	CA TACCT ACCTTATCCTTTACA
G4-9	TT GATGT TGTGATTTGATGTGT AGGTA TG CTA CA TACCT CAAAACAAAACCTCA TACCT ACACATCAAATCACA
G4-13	TT GATGT TGTGATTTGATGTGT AGGTA TG CTA CA TACCT CATACAACATCTACA TACCT ACACATCAAATCACA
F4	CA TACCT ACACATCAAATCACA
G5-11	AA GATGT TGGGTGTGTATAGGT AGGTA TG CTT CA TACCT CAACTCCTAATATCA TACCT ACCTATACACACCCA
F5	CA TACCT ACCTATACACACCCA
G6-13	TA GATGT TGGTGATGGAGAAGT AGGTA TG CTA CA TACCT CATACAACATCTACA TACCT ACTTCTCCATCACCA
F6	CA TACCT ACTTCTCCATCACCA
G7-9	TA GATGT TGAAGGGAAGAGGGT AGGTA TG CTA CA TACCT CAAAACAAAACCTCA TACCT ACCCTCTTCCCTTCA
G7-13	TA GATGT TGAAGGGAAGAGGGT AGGTA TG CTA CA TACCT CATACAACATCTACA TACCT ACCCTCTTCCCTTCA
F7	CA TACCT ACCCTCTTCCCTTCA
G8-11	TA GATGT TGGATGTAGTTTGGT AGGTA TG CTT CA TACCT CAACTCCTAATATCA TACCT ACCAAACTACATCCA
G8-15	TA GATGT TGGATGTAGTTTGGT AGGTA TG CTA CA TACCT CATTCCTACATTTCA TACCT ACCAAACTACATCCA
F8	CA TACCT ACCAAACTACATCCA
S9-10	ACCATAACAACCACA TACCT CAAAACAAAACCTCA
G9	GT AGGTA TGAGGTTTTGTTTTG AGGTA TG
Th9-10	TTT TG AGGTA TGTGGTTGTTATGGT TTT TTTTTT TTTTTTTTTTTTT ACCATAACAACCACA
G10-17	TG AGGTA TGTGGTTGTTATGGT AGGTA TG CTA CA TACCT CAATTCACTCAATCA TACCT ACCATAACAACCACA
F10	CA TACCT ACCATAACAACCACA

Name	Sequence
S11-12	ACCTAACATACAACA TACCT CAACTCCTAATATCA
G11	GT AGGTA TGATATTAGGAGTTG AGGTA TG
Th11-12	AGT TG AGGTA TGTTGTATGTTAGGT TTT TTTTTT TTTTTTTTTTTTT ACCTAACATACAACA
G12-17	TG AGGTA TGTTGTATGTTAGGT AGGTA TG CTA CA TACCT CAATTCACTCAATCA TACCT ACCTAACATACAACA
F12	CA TACCT ACCTAACATACAACA
S13-14	ACCTTCACAACTACA TACCT CATACAACATCTACA
G13	GT AGGTA TGTAGATGTTGTATG AGGTA TG
Th13-14	GTA TG AGGTA TGTAGTTGTGAAGGT TTT TTTTTT TTTTTTTTTTTTT ACCTTCACAACTACA
G14-19	TG AGGTA TGTAGTTGTGAAGGT AGGTA TG CTA CA TACCT CATCTTCTAACATCA TACCT ACCTTCACAACTACA
F14	CA TACCT ACCTTCACAACTACA
S15-16	ACCACTATAATTCCA TACCT CATTCCTACATTTCA
G15	GT AGGTA TGAAATGTAGGAATG AGGTA TG
Th15-16	GAA TG AGGTA TGGAATTATAGTGGT TTT TTTTTT TTTTTTTTTTTTT ACCACTATAATTCCA
G16-19	TG AGGTA TGGAATTATAGTGGT AGGTA TG CTA CA TACCT CATCTTCTAACATCA TACCT ACCACTATAATTCCA
F16	CA TACCT ACCACTATAATTCCA
S17-18	ACCCCTAAAATCTCA TACCT CAATTCACTCAATCA
G17	GT AGGTA TGATTGAGTGAATTG AGGTA TG
Th17-18	AAT TG AGGTA TGAGATTTTAGGGGT TTT TTTTTT TTTTTTTTTTTTT ACCCCTAAAATCTCA
G18-21	TG AGGTA TGAGATTTTAGGGGT AGGTA TG CTT CA TACCT CACTTTTCACTATCA TACCT ACCCCTAAAATCTCA
F18	CA TACCT ACCCCTAAAATCTCA
S19-20	ACCAACTCATTACCA TACCT CATCTTCTAACATCA
G19	GT AGGTA TGATGTTAGAAGATG AGGTA TG
Th19-20	AGA TG AGGTA TGGTAATGAGTTGGT TTT TTTTTT TTTTTTTTTTTTT ACCAACTCATTACCA
G20-22	TG AGGTA TGGTAATGAGTTGGT AGGTA TG CTA CA TACCT CACACTTCAAACTCA TACCT ACCAACTCATTACCA
F20	CA TACCT ACCAACTCATTACCA
Q21	/5IABkFQ/ ATACCT CACTTTTCACTATCA
F21 (Y-1)	GT AGGTA TGATAGTGAAAAGTG AGGTATG /3ATTO488N/
Q22	/5IAbRQ/ ATACCT CACACTTCAAACTCA
F22 (Y-0)	GT AGGTA TGAGTTTGAAGTGTG AGGTATG /3ATTO590N/
TriggerG18	CA TACCT ACCCCTAAAATCTCA TACCT CA
TriggerG20	CA TACCT ACCAACTCATTACCA TACCT CA

References

[1] Lulu Qian and Erik Winfree. Scaling up digital circuit computation with DNA strand displacement cascades. *Science*, 332(6034):1196–1201, 2011.

[2] John SantaLucia Jr and Donald Hicks. The thermodynamics of DNA structural motifs. *Annu. Rev. Biophys. Biomol. Struct.*, 33:415–440, 2004.

[3] Stefan Badelt, Casey Grun, Karthik V Sarma, Brian Wolfe, Seung Woo Shin, and Erik Winfree. A domain-level DNA strand displacement reaction enumerator allowing arbitrary non-pseudoknotted secondary structures. *Journal of the Royal Society Interface*, 17(167):20190866, 2020.

[4] Kevin M Cherry and Lulu Qian. Scaling up molecular pattern recognition with DNA-based winner-take-all neural networks. *Nature*, 559(7714):370–376, 2018.

[5] Joseph N Zadeh, Conrad D Steenberg, Justin S Bois, Brian R Wolfe, Marshall B Pierce, Asif R Khan, Robert M Dirks, and Niles A Pierce. NUPACK: Analysis and design of nucleic acid systems. *Journal of Computational Chemistry*, 32(1):170–173, 2011.

[6] Mark E Fornace, Jining Huang, Cody T Newman, Nicholas J Porubsky, Marshall B Pierce, and Niles A Pierce. NUPACK: analysis and design of nucleic acid structures, devices, and systems. *ChemRxiv preprint DOI:10.26434/chemrxiv-2022-xv98l*, 2022.

[7] Niranjan Srinivas, James Parkin, Georg Seelig, Erik Winfree, and David Soloveichik. Enzyme-free nucleic acid dynamical systems. *Science*, 358(6369):eaal2052, 2017.